2014

EXPERIMENTAL INVESTIGATION OF LOW MODE NUMBER CYLINDERS SUBJECTED TO VORTEXINDUCED VIBRATIONS

Ersegun Deniz Gedikli
University of Rhode Island, ersegundeniz@gmail.com

EXPERIMENTAL INVESTIGATION OF LOW MODE NUMBER CYLINDERS SUBJECTED TO VORTEX-INDUCED VIBRATIONS

BY

ERSEGUN DENIZ GEDIKLI

A THESIS SUBMITTED IN PARTIAL FULFILLMENT OF THE

REQUIREMENTS FOR THE DEGREE OF

MASTER OF SCIENCE

IN

OCEAN ENGINEERING

UNIVERSITY OF RHODE ISLAND

2014

MASTER OF OCEAN ENGINEERING

OF

ERSEGUN DENIZ GEDIKLI

APPROVED:

Thesis Committee:

Major Professor Jason M. Dahl

James Hu

Arun Shukla

Nasser H. Zawia
DEAN OF THE GRADUATE SCHOOL

UNIVERSITY OF RHODE ISLAND
2014

ABSTRACT

The excitation of three low-mode number, flexible cylinders in uniform-flow is investigated to determine effects of structural mode shape on vortex-induced vibrations. Experiments are performed in a re-circulating flow channel and in a small flow visualization tank using object tracking and digital particle image velocimetry (DPIV) to measure the excitation of the cylinder, to estimate forces acting on the structure, and to observe the wake of the structure under the observed body motions. Previous research has focused on understanding the effect of in-line to cross-flow natural frequency ratio on the excitation of the structure in an attempt to model the excitation of multiple structural modes on long, flexible bodies. The current research investigates the impact of structural mode shape on this relationship by holding the in-line to cross-flow natural frequency constant and attempting to excite a specific structural mode shape. Understanding the effects of mode excitation will improve the ability to predict fatigue life in structures which may exhibit combined irregular and regular oscillations by understanding how mode shape affects the vibrating response. In this series of experiments, three cylinders are tested. The in-line to cross-flow natural frequency is kept constant with a ratio of 2:1, while the modes associated with these frequencies are varied: first mode inline to first mode cross-flow, second mode in-line to first mode cross-flow, and third mode in-line to first mode cross-flow.

It is found that it is difficult to isolate the effect of mode shape on the vibration of the structure as the cylinder can easily be excited with different combinations of modes. It is shown that for the low-mode number beams tested, there are three

primary responses possible for the cylinder when trying to excite the first mode in the cross-flow direction and first mode in the in-line direction (cylinder 1), the first mode in the cross-flow direction and the second mode in the in-line direction (cylinder 2); and the first mode in the cross-flow direction and third mode in the in-line direction (cylinder 3).

Cylinder 1 response consists of an expected excitation of the first mode cross-flow with an excitation of the first mode frequency in in-line direction. Regular and periodic cylinder oscillations obtained along the length of the cylinder. Cylinder 2 response consists of an expected excitation of the first mode cross-flow with an excitation of the second mode frequency in in-line direction; however, the structural shape resembles the first mode shape. This response is attributed to the structural mode being an insufficient description of the phenomenon as the wake must be included as part of the mode shape. This response is characteristic of a figure eight response of the cylinder. In cylinder 3 experiments, two different responses as crescent and figure eight patterns were obtained. In this case, higher flow speeds could not be reached so third mode shape in the in-line direction could not be obtained.

The wake is observed using DPIV on a rigid cylinder with forced motions equivalent to the flexible body. A case of mode switching is also observed where the even in-line mode exhibits an excitation at twice the cross-flow frequency; however, the spatial mode shape in-line appears similar to the first structural mode shape. It is hypothesized that this situation is possible due to variation in the effective added mass along the length of the cylinder. Odd mode shapes in both in-line and cross-flow directions show similar motions to those observed for rigid cylinders.

ACKNOWLEDGMENTS

I would like to express my deep gratitude to Professor Jason Dahl, my thesis supervisor, for his patient guidance, enthusiastic encouragement and useful critiques of this thesis work. I also wish to acknowledge Professor James Hu and Professor Arun Shukla for their advice and assistance in keeping my progress on schedule. I am grateful to Amin Mivehchi for his friendship and our valuable discussions. In addition, I thank Gail Paolino for her assistance with procurement and paperwork.

Most importantly, I must acknowledge my wife Hazel for supporting me through my research, providing moral support during my experiments, reading and re-reading my thesis. Also, I would like to extend my greatest appreciation to my parents who have always supported me in my academic pursuits.

TABLE OF CONTENTS

LIST OF TABLES

TABLE **PAGE**

LIST OF FIGURES

FIGURE **PAGE**

APPENDIX B.1

APPENDIX B.2

APPENDIX B.3

CHAPTER 1

INTRODUCTION

Vortex-induced vibration (VIV) has long been a problem in offshore structures including risers, mooring lines as well as in other structures such as chimneys, bridges, and buildings. When an incoming fluid flow interacts with a bluff body, it creates vortices behind it causing the bluff body to oscillate. This basic phenomenon is called vortex-induced vibration. Vortex induced vibration is specifically amplitude-limited motions caused by vortex shedding.

Vibrations of a flexible structure due to VIV are related to the natural frequency of the structure, which is time dependent, and mode shape, which is spatially dependent. Previous studies examined different frequency ratios (Dahl et al. (2006), Jauvtis and Williamson (2004), Kang et al. (2013)) to explain VIV phenomena; however, in this thesis the effect of different mode ratios were examined while attempting to keep the frequency characteristics constant.

Vortex-induced vibration may occur when vortices are shed alternately from opposite sides of a structure. Figure 1 shows a cylinder placed horizontal to the incoming fluid flow. As fluid flow hits the cylinder, it oscillates with the shedding frequency in cross-flow direction and twice shedding frequency in in-line direction because of the nature of the vortex shedding.

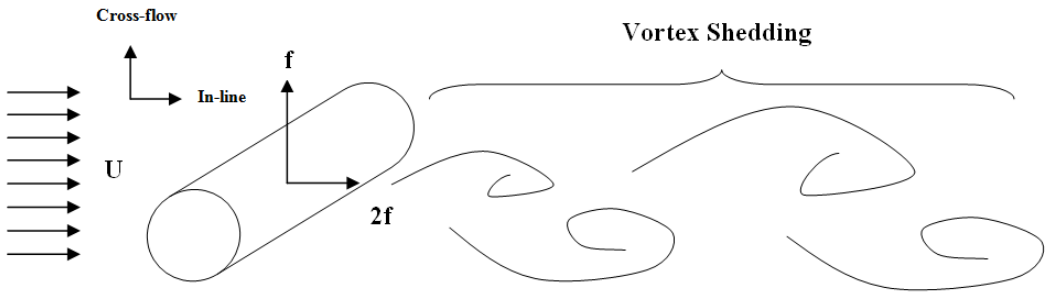

Figure 1 Vortex shedding behind the cylinder

Over the large Reynolds numbers which are greater than 40 (Re>40), unsteady separation of the fluid flow around the cylinder cause a repeating pattern of vortices which is known as Karman vortex street in literature. The Karman vortex street created by a cylindrical object is shown in Figure 2.

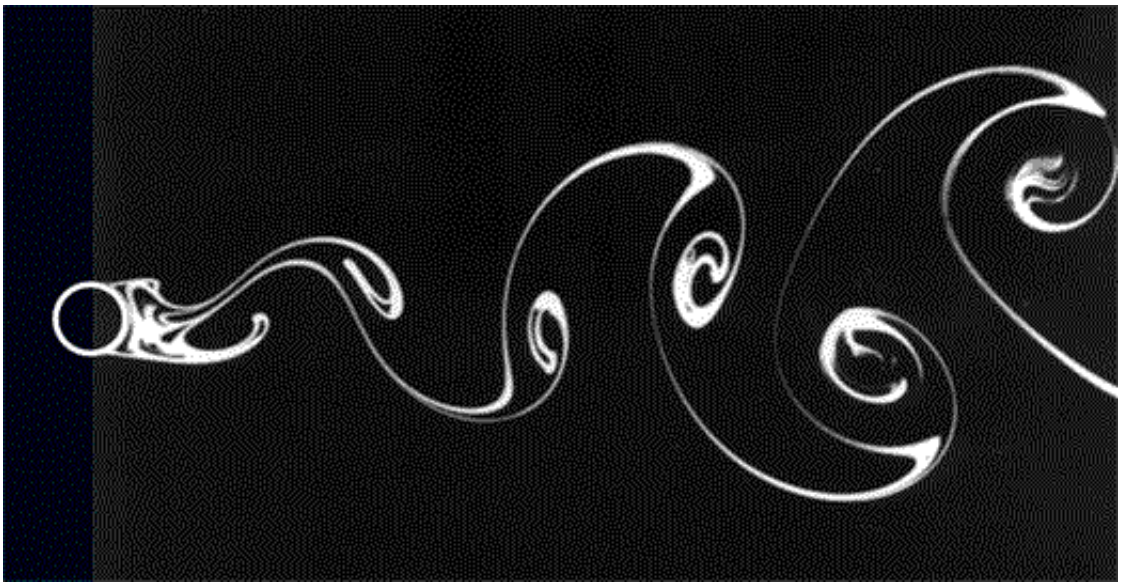

Figure 2 Karman Vortex Street (Van Dyke, 2002)

For a smooth bluff body; vortex shedding is defined as a function of Reynolds number and Strouhal number;

$$Re = \frac{UD}{\upsilon} \tag{1.1}$$

where U is the current velocity, D is the cylinder diameter, υ is the kinematic viscosity of the fluid. Lienhard (1966) categorized the vortex shedding regimes (Figure 3) depending on different Reynolds number ranges such that; the flow regime between $300<Re<1.5X10^5$ is called subcritical Reynolds number range, flow regime between $1.5x10^5<Re<3.5x10^6$ is called transitional Reynolds number range, and finally the flow regime for $Re>3.5x10^6$ is called supercritical Reynolds number range. Our flexible cylinder experiments falls into the subcritical Reynolds number range with a range of reduced velocity between 2,000 and 10,000.

Vortex shedding frequency can be defined depending on Strouhal number;

$$f_s = \frac{StU}{D} \tag{1.2}$$

where fs is vortex shedding frequency in Hertz, St is the Strouhal number, U is the free stream flow velocity, and D is the cylinder diameter. The Strouhal number of a stationary circular cylinder is a function of Reynolds number and surface roughness. Achenback and Heinecke (1981) found that Reynolds numbers between $5x10^2$ and 10^5 Strouhal number has a constant value of ~0.2. After the Reynolds number value of 10^5, for smooth surface cylinders Strouhal number reached the value as high as 0.5. Hammache and Gharib (1991) have shown Strouhal number change based on increasing Reynolds number values in Figure 4.

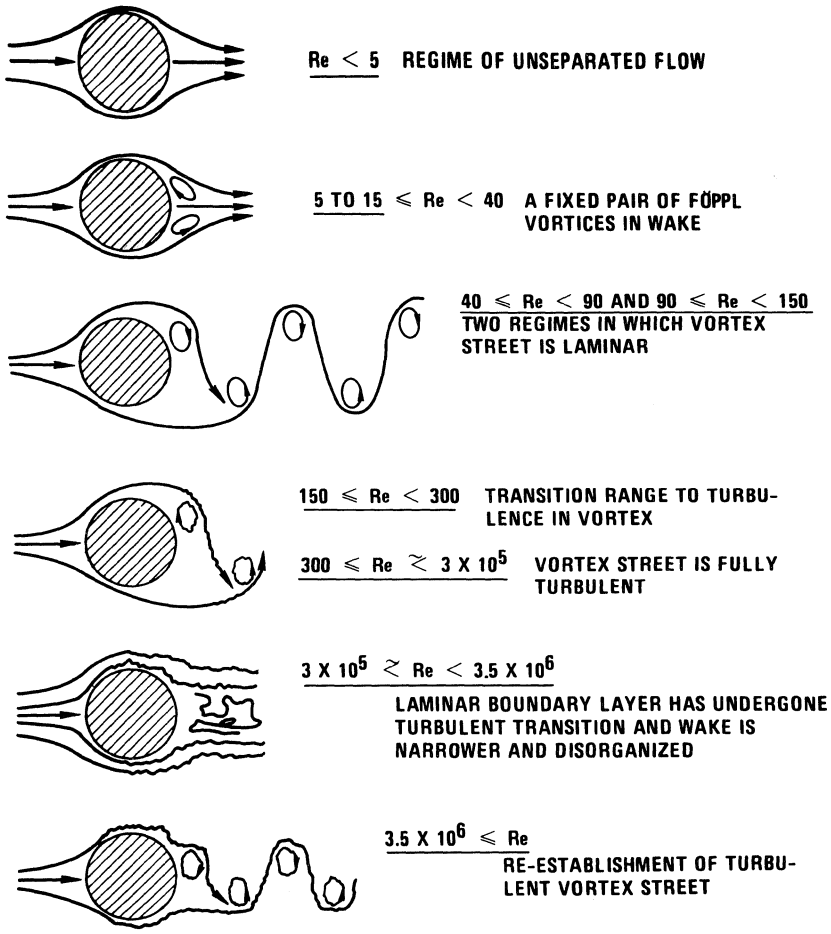

Figure 3 Regimes of fluid flow across smooth circular cylinders (Leinhard 1966)

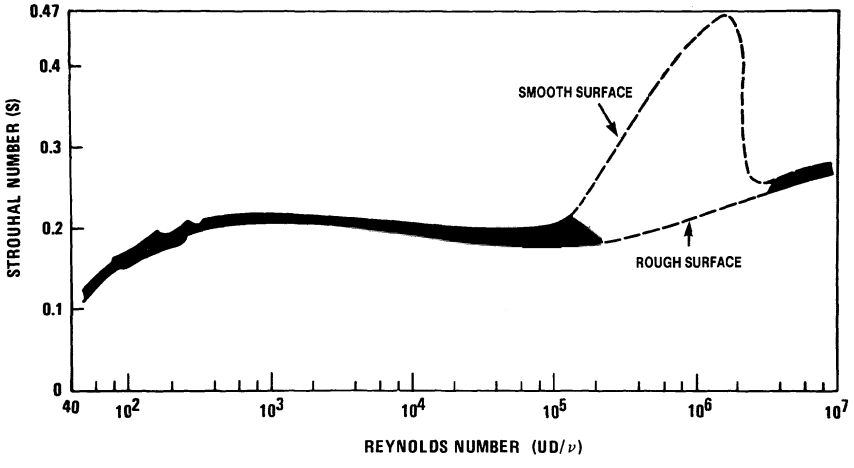

Figure 4 Strouhal Number (St) vs. Reynolds number for circular cylinders (Hammache and Gharib 1991)

CHAPTER 2

REVIEW OF LITERATURE

Long slender marine structures such as risers or towed cables tend to behave in a manner similar to a tensioned beam or tensioned string. Depending on the length of the structure, the structure may have large number of natural frequencies as well as mode shapes. Under these conditions, vibration of the structure due to vortex shedding is inevitable as the vortex shedding frequency will always be near one of the structural natural frequencies.

The motions of long, slender structures undergoing vortex-induced vibrations are complex, potentially consisting of traveling waves (Marcollo et al, 2011), large amplitude standing waves, chaotic motions (Modarres-Sadeghi et al., 2011), and six degree of freedom vibration of the structure. Until 2000's, mostly simpler one degree-of-freedom structural system had been studied to understand the nature of the vortex-induced vibration where cylinder is allowed to oscillate only in cross-flow direction and very less studies had been done about two degrees-of-freedom vortex-induced vibrations (Moe and Wu (1990), Sarpkaya (1995), others). Several reviews helped to explain the basic fluid-structure interactions for a single degree of freedom spring mass system (Williamson and Govardhan (2004), Sarpkaya (2004), Bearman (2011), others).

Most of the past research on VIV has been conducted with flexibly mounted rigid bodies where cylinder is allowed to oscillate only in cross-flow direction (one degree of freedom system). Jauvtis and Williamson (2004) have shown that when a cylinder

with mass ratios below 6 (low mass ratio) is allowed to move both in cross-flow and in-line directions, it oscillates differently in terms of resulting hydrodynamic forces and amplitude responses than the simpler one-degree-of-freedom systems where cylinder is allowed to oscillate only in cross-flow direction. They conducted their experiments with a cylinder having equal natural frequencies and oscillating masses both in in-line and cross-flow directions. They introduced the new amplitude response branch which is called 'super-upper' branch, where the amplitude response reached up to ~1.5 exceeding the typical peak amplitudes (A_y*~1) obtained previously for just cross-flow vibration experiments. They also introduced in-line vortex modes carrying out DPIV method at the low normalized velocities and found '2T' mode which is a triplet of vortices being shed in each half cycle downstream of the cylinder. It is also shown in the paper that most of the features documented for one degree of freedom VIV experiments are still valid for two degree of freedom systems for mass ratios higher than 6. However, it is known that real structures has mass ratio (m*) near to 3 or less, which is why it is very important to consider in-line motion to the cylinder motion.

Vortex-induced vibration experiments showed that the forcing frequency in in-line (drag) direction tends to be almost always twice the forcing frequency in cross-flow (lift) direction. In other words, due to the fact that vortex wake behind the cylinder follows one after the other, cylinder oscillates at vortex shedding frequency in cross-flow direction, and oscillates twice vortex shedding frequency in in-line direction. Lie et al. (1997), Chaplin et al. (2005b), Trim et al. (2005), and Vandiver et al. (2009) and several other research groups made full scale observation of marine risers. Field

experiments on VIV (Vandiver et al, 2005, Vandiver and Jong, 1987), and laboratory experiments (Passano et al, 2010,Huera-Huerte et al, 2014), showed that for long flexible bodies subjected to vortex-induced vibrations, it is possible to excite different modes separately in the in-line and cross-flow directions. Huera-Huerta et al. (2014) conducted their experiments for very low mass ratios ~1 since there was no publicly known research on flexible cylinders having multi-modal behavior for that mass ratios and they observed a large increase in cross-flow and in-line response amplitudes.

Dahl et al. (2006) investigated the effect of the natural frequency ratios (in-line to cross-flow) on a vibrating cylinder. The cylinder was allowed to oscillate both in cross-flow and in-line directions in an attempt to model a long structure that may have different modes and different frequency ratios. Dahl et al. (2006) also wanted to answer the traditional question: How do different frequency ratios affect the cylinder motion and forces exerted on the body? In their experiments they showed that by increasing the in-line to cross-flow frequency ratio from 1 to 1.9, higher amplitudes obtained in the in-line motion response, and lower amplitudes obtained in cross-flow response. When the natural frequency ratios get closer to 2, the effective natural frequency ratio adjusted for the effective added mass of the system will almost always take a value of 2. Similar experiments were performed for different frequency ratios by Srinil et al. (2013) for sub-critical Reynolds range (Re ~ 2 x 10^3-5 x 10^4) resulting one peak in the amplitude response figures for the natural frequency ratios 2:1 (in-line to cross-flow), and longer lock-in region. Reported lock-in region in Dahl et al. (2006) was between ~4 to ~12, but Srinil et al. (2013) obtained longer lock-in region, reaching up to ~20, possibly because of the difference in mass-ratios (m*) between the

experiments which itself shows the importance of the mass ratio in VIV. Dahl et al. (2006) performed their experiments for the mass ratios between 3-6 with $m_x \neq m_y$; however, for Srinil et al. (2013) the mass ratio range was between 1-3 and $m_x = m_y$. Later, Dahl et al. (2010) carried out another set of experiments, and observed the same phenomenon for supercritical Reynolds numbers. Kang et al. (2013) performed similar experiments for natural frequency ratios lower than 1 and showed that the vibration of the cylinder in the in-line direction seem to have multi-frequency component causing different cylinder motions rather than traditional figure 8 shape with slanted circle, egg shaped or teardrop orbital motions.

In the studies of Dahl et al (2006) and Kang et al (2013), the effect of natural frequency ratio is modeled by tuning natural frequencies on a rigid cylinder, hence the mode shape of the cylinder does not play a role in the excitation of the body. A problem persists; however, for a cylinder that may be excited with an odd mode cross-flow and an even mode in-line. For example, consider a tensioned infinitely long string, where the natural frequencies are multiples of a fundamental frequency. If the first mode of the structure is excited in the cross-flow direction and the second mode with twice the fundamental frequency is excited in the in-line direction, the anti-nodes of the second mode may move with a figure eight orbital pattern under the right flow conditions. However, since the mode shape in the in-line direction is a sine curve, the two anti-nodes must move in opposite directions, with one figure eight moving downstream at the top and bottom of the orbit (referred to as clockwise motion in the literature) and the other moving upstream at the top and bottom of the orbit (counter-clockwise motion). The observations from Dahl et al (2007), indicate that there is a

natural preference for the figure eight to move upstream (counter-clockwise) at the top and bottom of the orbit, so if these frequencies of the structure are truly excited, which anti-node, if any, will move with this motion? Figure 5 shows a schematic of first mode excitation of a beam in cross-flow with second mode excitation on in-line direction.

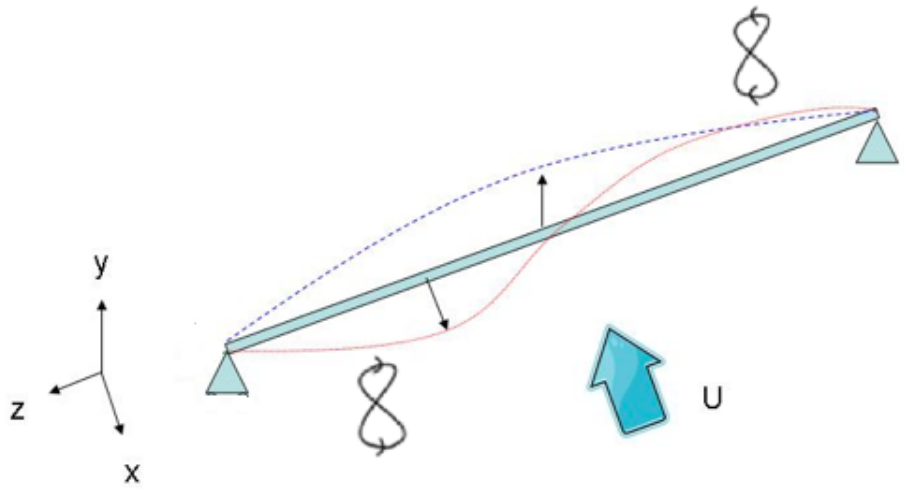

Figure 5 Example first mode excitation of beam in cross-flow with second mode excitation in in-line direction. Vibration of the cross-section at the in-line antinodes will result in figure eight motions that move in opposite directions.

The present study aims to clarify,

1. The effect of mode shape on the vibration of a flexible structure with multiple modes and

2. The effects of mode shape on wake modes.

In this study, the test cylinder is not tensioned, which gives a bending dominated system.

In contrast to the studies of Dahl et al (2006) and Yang et al (2013), the present study attempts to excite the natural frequencies of a flexible structure where the natural frequency ratio of particular modes is set to a ratio on 2:1 (in-line: cross-flow), but the structure has a particular chosen in-vacuum mode shape.

2.1 Non-Dimensional Parameters

In order to examine the vortex-induced vibration phenomenon, particular non-dimensional parameters are widely used. Therefore, descriptions of these non-dimensional parameters are very important. In this thesis, the following non-dimensional parameters have been used.

Reynolds Number (Re): This parameter can be defined as the ratio between the inertia forces to viscous forces. This parameter is mostly used to determine the fluid flow regimes as shown in Figure 3. In addition, vortex formation and the resulting forces exerted on the cylinder are known to be a function of Reynolds number (Morse and Williamson, 2009). Reynolds number can be written as:

$$Re = \frac{\rho UD}{\mu} = \frac{UD}{\upsilon} \tag{2.1}$$

where ρ is the fluid density, U is the flow speed, D is the cylinder diameter and μ is fluid viscosity.

True Reduced Velocity (Vr): Different than nominal reduced velocity; frequency component is equal to oscillation frequency of the cylinder in the cross-flow direction. It can also be defined as the ratio of free stream velocity to transverse cylinder velocity. Tru reduced velocity (Vr) can be written as:

$$Vr = \frac{U}{f_y D} \tag{2.2}$$

where U is the flow speed, f_y is the oscillation frequency of the cylinder and D is the cylinder diameter. This parameter is especially very important because Moe and Wu (1990) showed that the true reduced velocity value must be matched in order to compare the free vibration of a cylinder with forced cylinder vibrations.

Nominal Reduced Velocity (Vr_n): This parameter can be defined similar to an inverse Strouhal number. In nominal reduced velocity, frequency is equal to natural frequency of the cylinder in the cross-flow direction. Nominal reduced velocity can be written as:

$$Vr_n = \frac{U}{f_n D} = \frac{U\,T}{D} \tag{2.3}$$

where U is the flow speed, f_n is the natural frequency of cylinder, D is the cylinder diameter, and T is the oscillation period.

Reduced velocity can also be defined as the ratio between the path length in flow direction per cycle and the cylinder diameter since oscillation frequency is equal to cylinder oscillation per cycle by definition.

Most of the non-dimensional VIV parameters are non-unique when they are compared to reduced velocity (i.e. A/D vs. Vr) since the ratio of velocity over oscillation frequency may remain constant in the reduced velocity equation in a free vibration cylinder experiment due to interactions between the structure and the fluid. Instead, it is common to use the nominal reduced velocity for a unique representation of the non-dimensional VIV parameters because natural frequency of the structure is used to calculate the nominal reduced velocity and this frequency is constant. Therefore one can obtain a unique mapping of measured parameters for a given flow speed.

Non-dimensional Cross-Flow Amplitude: This parameter is defined as the amplitude in cross-flow direction normalized by the cylinder diameter.

$$A_y^* = \frac{A_y}{D} \tag{2.4}$$

Non-dimensional In-Line Amplitude: This parameter is defined as the amplitude in in-line direction normalized by the cylinder diameter.

$$A_x^* = \frac{A_x}{D} \tag{2.5}$$

Mass Ratio: This parameter can be defined as the ratio of cylinder mass to displaced fluid mass.

$$m^* = \frac{m}{\rho \pi L \frac{D^2}{4}} \tag{2.6}$$

Non-dimensional Frequency Ratio: The non-dimensional frequency is defined as the ratio of cylinder oscillation frequency to the cylinder natural frequency. The subscript indicates the direction of the oscillation. (y= cross-flow, x=in-line)

$$\frac{f_y}{f_{ny}}, \quad \frac{f_x}{f_{nx}} \tag{2.7}$$

Aspect Ratio: This parameter is defined as the ratio of cylinder length to the cylinder diameter.

$$\frac{L}{D} \tag{2.8}$$

CHAPTER 3

METHODOLOGY

Experiments were conducted in two different locations at the University of Rhode Island, Narragansett Bay Campus. The reason of performing two different experiments is flexible cylinder experiments could not give force measurements or visualization of wake, hence rigid cylinder experiments were performed to approximate these measurements.

Flexible cylinder experiments were carried out in a re-circulating flow channel, and forced cylinder experiments were performed in a small flow visualization tank by replicating the motions obtained from the re-circulating flow channel.

In flexible cylinder experiments three different cylinders were tested in order to clarify the effect of mode shape on the vibration of a flexible structure with multiple modes. Therefore, in contrast to the previous studies (Dahl et al. (2006), Kang et al. (2013), Huera-Huerta et al. (2014), others) mode shape was varied keeping the frequency ratio to 2:1. Mode shapes were calculated so that first cylinder would oscillate with the first mode shape (half sine curve) in in-line and first mode shape in cross-flow direction, second cylinder would oscillate with the second mode shape (full sine curve) in in-line and first mode shape in cross-flow direction; and third cylinder would oscillate with the third mode shape (one and half sine curve) in in-line and first mode shape in cross-flow direction.

3.1 Cylinders

In order to examine the different mode shapes of the structure and their effect on the vibration; a particular in-vacuum mode shape was chosen. Natural frequency ratio was set to 2:1 for each mode for the cylinders. Since there is an n^2 relation between the mode number and the frequency associated with the mode for simply supported beams, in order to obtain desired structural characteristics, aluminum beams were molded through the center of the each cylinder, which is based on the assumption that short risers naturally oscillates like a beam. Cylinders were assumed to vibrate in a vacuum, therefore, equation of motion for an un-tensioned beam with simply supported ends was solved in order to obtain the specific mode shapes. From that perspective, frequency of shedding (f_s) for each cylinder was equated to the natural frequency of beam (f_{nbeam}) in vacuum for sizing the beam as shown below:

$$f_s = \frac{U\,St}{D} \tag{3.1}$$

$$f_{nbeam} = \frac{n^2\pi}{2}\sqrt{\frac{EI}{L^4 M}} \tag{3.2}$$

$$I = \frac{bh^3}{12} \tag{3.3}$$

where U is the fluid velocity, St is the Strouhal Number (St=0.2 for circular cylinders), D is the cylinder diameter, n is the mode number, E is the elastic modulus, I is the area moment of inertia, L is the beam length and M is the mass per unit length. After equating those two formulas, beam characteristics "b and h" were determined from elastic modulus formula where b is the cross-sectional width of the beam and h is the

cross-sectional height of the beam. Using the calculated beam characteristics, cylinder 1 motion was tuned to have first mode in cross-flow direction and first mode in in-line direction, cylinder 2 was tuned to have first mode shape in cross-flow and second mode shape in in-line direction and cylinder 3 was tuned to have first mode shape in cross-flow and third mode shape in in-line direction.

Cylinders were desired to have mode shapes sketched in Figure 6, Figure 7 and Figure 8 where aluminum beam was placed horizontal to the incoming fluid flow for cylinder 1 case, and vertical to the incoming fluid flow for cylinder 2 and 3 cases. In those sketches black lines illustrate the cross-flow direction motion trajectory and dotted lines illustrate the in-line motion trajectories.

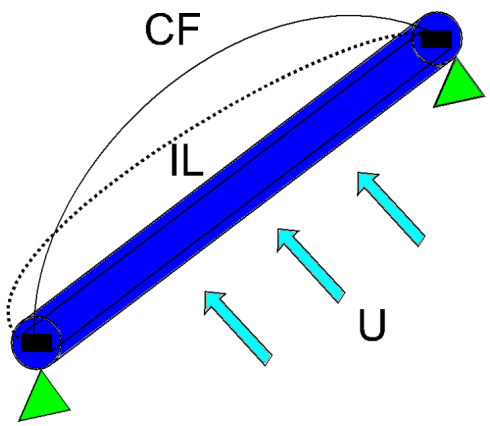

Figure 6 Cylinder 1 Case- First mode excitation both in Cross Flow (CF) and In-Line (IL) direction

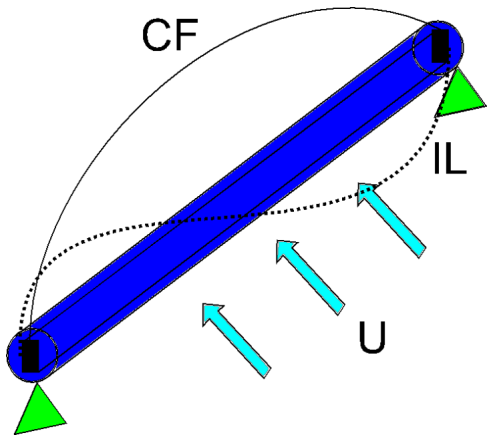

Figure 7 Cylinder 2 Case- First mode excitation in Cross Flow (CF) and second mode excitation in In-Line (IL) direction

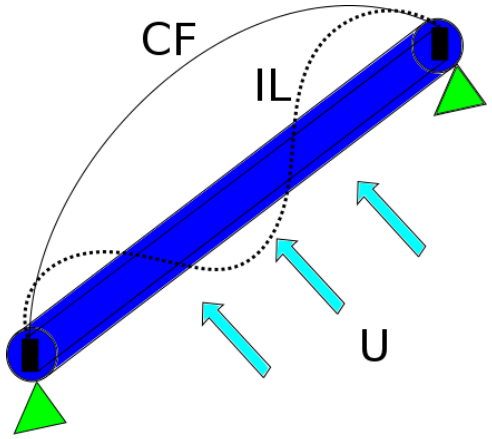

Figure 8 Cylinder 3 Case- First mode excitation in Cross Flow (CF) and third mode excitation in In-Line (IL) direction

Each cylinder was molded using PMC-744 type Urethane Rubber material with aluminum beam inside it. The present study shows that specific mode shape set under vacuum conditions are not held in underwater because of the fact that added mass forces and in-line frequency change in time can alter the mode shape. This can be explained as the structural mode being an insufficient description of the phenomenon as the wake must be included as part of the mode shape.

Table 1 shows the physical dimensions and frequency characteristics for the first three modes of the three test cylinders: cylinder 1, cylinder 2 and cylinder 3. Cylinders need to reach the calculated frequencies for desired mode shapes. It should also be noted that all three cylinders have very close aspect ratios, and have the same cross section areas but different beam sizes and orientations.

Table 1 Physical dimensions and frequency characteristics of the flexible test cylinders.

		Cylinder 1	Cylinder 2	Cylinder 3
Diameter (mm)		6.35	6.35	6.35
In-line beam width (mm)		1.016	1.6	1.82
Cross-flow beam width (mm)		2.032	0.8	0.4
Beam material		Aluminum	Aluminum	Aluminum
Reynolds number		2,000-8,500	3,500-10,000	2,000-10,000
Aspect Ratio		40	38	37
Mass Ratio		1.1	1.3	1
Span wise tracking points		25	25	25
In-line natural frequency (Hz)	**Mode 1**	28.8	9.4	3.91
	Mode 2	116	37.5	15.6
	Mode 3	260	84.4	35.2
Cross-flow natural frequency (Hz)	**Mode 1**	14.2	18.8	17.6
	Mode 2	57	75.0	70.5
	Mode 3	128	169	158.6

3.2 Flexible Cylinder Experiments

Flexible cylinder experiments were conducted in a re-circulating flow channel. Re-circulating flow channel has a working section of 152.4cm l x 50.8cm h x 38.1cm w with two glass viewing walls in both sides of the tank as well as at the bottom side. It

has an additional cross sectional glass-viewing wall with the test portion of 38 cm x 48 cm. The flow channel is capable of producing steady velocities in a range from 0.1 to 1.3 m/s.

Test cylinders were marked with 25 white dots along the length of the cylinder, placing 1 cm difference between each dot. Two high-speed Vision Research Phantom V10 cameras were used to capture the motion of the white dots on the cylinder. One camera was placed underneath the water tunnel to capture the amplitude response motion in in-line direction, and second camera was placed right in front of the tank to capture the motion response in cross-flow direction. Cameras have maximum resolution of 2400x1800 pixels, but maximum resolution was not used in these tests. Instead, 2400x560 pixels were used as a resolution while keeping the full length of the cylinder in the frame in order to increase the length of the time history. In the image measurements, the sum of the all pixel intensities in the cylinder area (a rectangular area was selected keeping the entire cylinder length in the frame to measure the pixel characteristics) was 306000 pixels, which is equivalent to 1,29e+007 counts specified in the Davis 8 software. The average value of all pixel intensities was found to be equal to 42 counts with +/- rms value of 134 counts. Since the length of all three cylinders was around ~250 mm, the scale of the camera was found to be ~0.125 mm/pixels. Converting the units of the rms value to the pixels reveals that we are incapable of measuring dot sizes smaller than 0.4 mm.

A schematic view of the test apparatus used in the flexible cylinder experiments is shown in Figure 9. Top view in Figure 9 represents the isometric view of the test system showing the locations of the cameras with the flexible cylinder. Bottom

scheme in Figure 9 represents the top view of the test system. False walls were placed each side of the tank to minimize three-dimensional effects at the flexible cylinder end supports, and cylinder was attached to the false walls with universal joints. Four fairings were used to reduce the flow separation inside the tank. Cylinder was placed 50 diameters downstream and 50 diameters upstream from the fairings so it was not affected by the flow since fairings redirected the flow through false walls.

The high-speed cameras recorded the motion of white dots in time with a frame rate of 250 Hz, ensuring that frequencies as high as the third mode could be captured. The number of dots was sufficient to capture the spatial response of the structure up to the third mode.

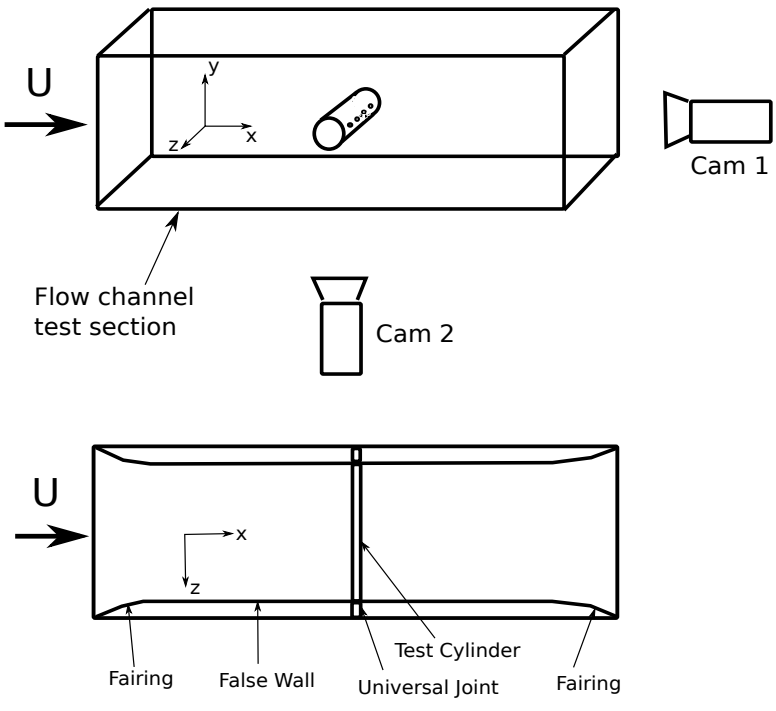

Figure 9 Schematic of freely vibrating flexible cylinder test apparatus in re-circulating flow channel, isometric view and top view.

Since the presence of the support structure and fairings within the flow channel would alter the flow velocity in the water channel, it was necessary to calibrate the impeller motor speed for the channel with the measured flow speed in the test section. With the support structure installed in the test section and without the test cylinder in place, the flow speed was measured in the tunnel as a function of motor RPM using a Marsh-McBirney Flo-Mate2000 electro-magnetic flow meter. Measurement of the speed was repeated 10 times for each speed to determine a calibrated relation between the tunnel motor speed and water speed. This calibration was performed over depth and over the entire range of flow velocities capable in the tunnel with a constant water level. The current profiles were uniform over depth. Error in the reported flow velocity was estimated to be +/- 1-2%.

Cylinder 1, 2 and 3 were tested for 30, 27 and 30 different flow speeds respectively where flow speeds range from 0.20 to 1.58 m/s. When the flow speed reached to the desired flow velocity, approximately 1 minute passed to reach the stabilized velocity. Same approach was used during the measurement of the calibration process.

3.2.1 Motion Tracking

ProAnalyst motion tracking software was used to track all 25 points on the cylinder. The tracking algorithm utilizes an interpolation scheme so that particles could be tracked to sub-pixel accuracy. With the high-resolution cameras, each dot was composed of approximately 4-8 pixels, ensuring unique tracking for each marker. Each dot was selected in a rectangle region of pixels in the initial frame, and automatic tracking option automatically analyzed the displacement of this particular point for

subsequent frames. Figure 10 shows an example image of the test cylinder with markings.

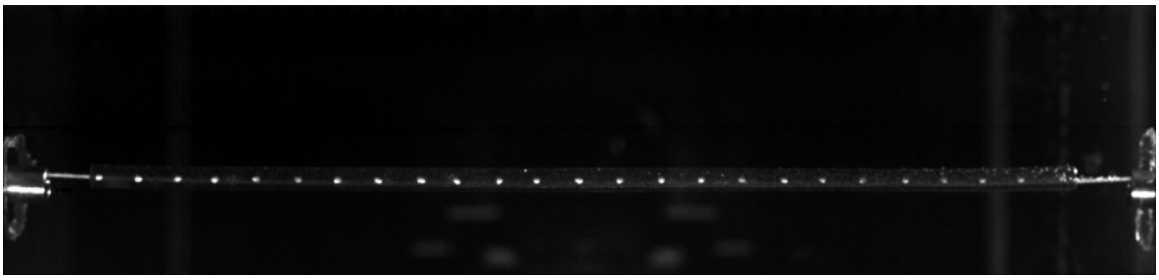

Figure 10 Example image of test cylinder with markers for position tracking

The modules of the ProAnalyst software used in this study can be explained as follows. It is important to note that some specified modules needed to be adjusted separately for each video that was processed.

Important modules used to analyze the motion (ProAnalyst User Manual);

1. **Image processing module**: controls the color balance, brightness, contrast, and gamma correction. This module helps user to adjust the brightness and contrast of an individual image. User should adjust the brightness and contrast of the image until he gets necessary resolution for further processing. One can save the settings and restore them for later use.
2. **Image filtering module**: helps to filter the image. In this module user can apply a sequence of image filters to the video images. Used filters and their definitions:
    a. Common Filters
        i. Threshold (Binary): This filter performs a threshold operation on the image meaning all image pixels below the threshold will be

set to black (0), and all image pixels above the threshold will be set to white (255).

ii. Fill center of objects: This filter helps to fill the interior of a circle.

b. Convolution Filters

i. Edge Detector (5 x 5 Laplacian High Pass): This filter helps to make the edges more thicker and visible by convolving the image with a Laplacian high-pass filter. Depending on the image, other similar methods can be used (i.e. 3 x 3 Laplacian High Pass).

ii. Smoothing (5 x 5 Gaussian): This filter helps to smooth the image by convolving the image with a Gaussian low-pass filter

iii. Sharpening (3 x 3 Center): This filter helps sharpening the image by convolving the image with a basic sharpening filter

c. Morphological Operations

i. Make Thinner (Erode): This operation helps the image edges make thinner by performing erosion on the input image.

ii. Make Thicker (Dilate): This operation helps the image edges make thicker by performing dilation on the input image.

d. Neighborhood Operations

i. Median: This method replaces each pixel in the output image with the median of pixels in the neighborhood of each pixel.

ii. Average: This method replaces each pixel in the output image with the average of pixels in the neighborhood of each pixel. (ProAnalyst User Manual)

3. **Image calibration module:** helps to convert the experiment coordinates to real word coordinates. In other words, this window helps user to convert and scale the recorded video image to real world dimensions (i.e. meters used in the present study). In software interface, calibration settings panel helps to achieve this goal. For instance, if user specifies a known frame of reference object, calibration can be achieved by selecting two points with a known distance between those points. This process can also be applied to the scale for later use.
4. **Feature (2D) tracking module:** helps to track the distinct features along with all the video frames. In the present study, previously marked dots were selected in the initial frame, and it was desired to track the displacement of those dots in –XY plane. For this purpose, automatic tracking option was used.

In order to have advanced motion tracking, auto-tracking settings can be changed in 'Track Settings' dialog. Sometimes, a point can be lost during the auto process. If the information on lost point is needed, virtual point parameter can be chosen. With this option, one can have the relative information of the selected point to other features. One important thing to remember is that a virtual point cannot be created automatically because in reality they do not exist.

In the present study, 'Midpoint' style virtual point was used to define the loss parameters. This virtual point created a new point as the midpoint of two other features, so the method is not applicable if two near points both loss at the same

time. Since, all of the dots are evenly spaced on the cylinder with 1 cm intervals, this method can be applied to those points cannot be tracked in time.

3.2.2 Time Dependent Frequency Analyses (Scalogram)

Boashash (2003) has defined scalogram as the squared magnitude of a continuous wavelet transform as a function of frequency and time. In comparison with other traditional methods such as time dependant signal and single sided amplitude spectrum, a scalogram gives more information. For example, in a time dependent signal one cannot observe the frequency content (Figure 11, a) and in a single sided amplitude spectrum one can only observe the frequency content for an instantaneous time (Figure 11, b). But, scalogram (Figure 11, c) helps us to see how a specific signal varies in time without losing the frequency content of this signal; therefore it gives much more information about the nature of the system.

In the present study, MATLAB time-frequency toolbox was used to compute the scalogram plot. In the contour plots, the regions of high intensity correspond to the dominant frequency component excited over time as seen in Figure 11.

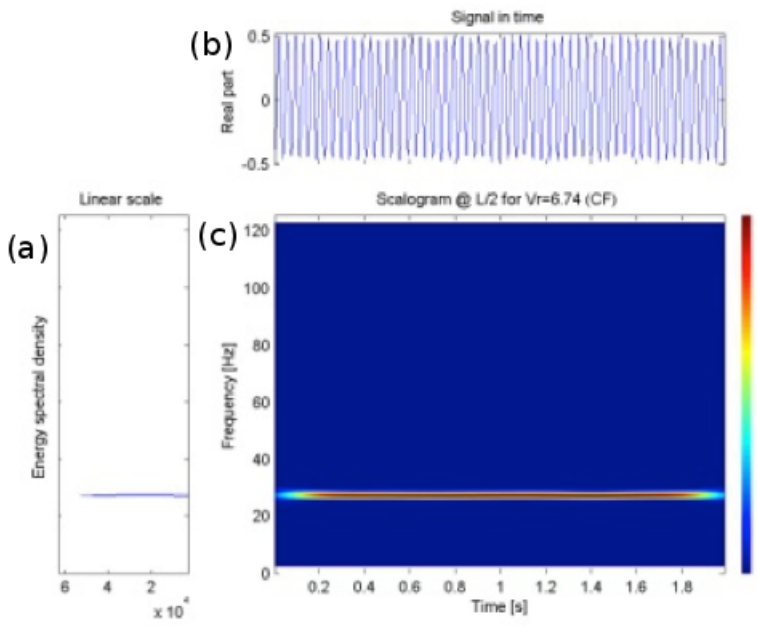

Figure 11 Example scalogram(c) with energy spectral density (a) and time dependant signal (b). Colors indicate the magnitude of the dominant frequency.

In this study, the frequency content of the motion at specific locations along the length of the cylinder for both cross-flow and in-line direction is shown. Locations on the cylinder have chosen to be at L/4, L/2 and 3L/4.

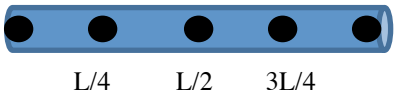

Figure 12 Locations selected on the cylinder

Scalograms help to compare VIV signals. In order to compare two VIV signals, those signals need to be statistically stationary. From VIV perspective, fluid excitation is stationary for an oscillating cylinder. In other words, the energy content in the signal corresponding to each frequency remains constant.

3.2.3 Orbital Pattern Analysis

Cylinder motions subjected to vortex-induced vibration can be examined by looking their orbital patterns. Depending on the cross flow amplitude (A_y), in-line amplitude (A_x) and phase angle between in-line and cross-flow motion (θ); possible cylinder trajectories can be represented as harmonic function.

$$\frac{y}{D} = \frac{A_y}{D} cos(\omega t) \tag{3.4}$$

$$\frac{x}{D} = \frac{A_x}{D} \cos(2\omega t + \theta) \tag{3.5}$$

In the two-degree freedom system, resulting orbital pattern will be combination of these two functions along with the phase angle. The orbitals show the motion of the cylinder in a fixed coordinate system as seen in Figure 13. In this study it should be noted that there is 90-degree phase difference between a sine and cosine function. Therefore, resulting cylinder motions are shifted 90 degree depending on the definition of motion (sine or cosine).

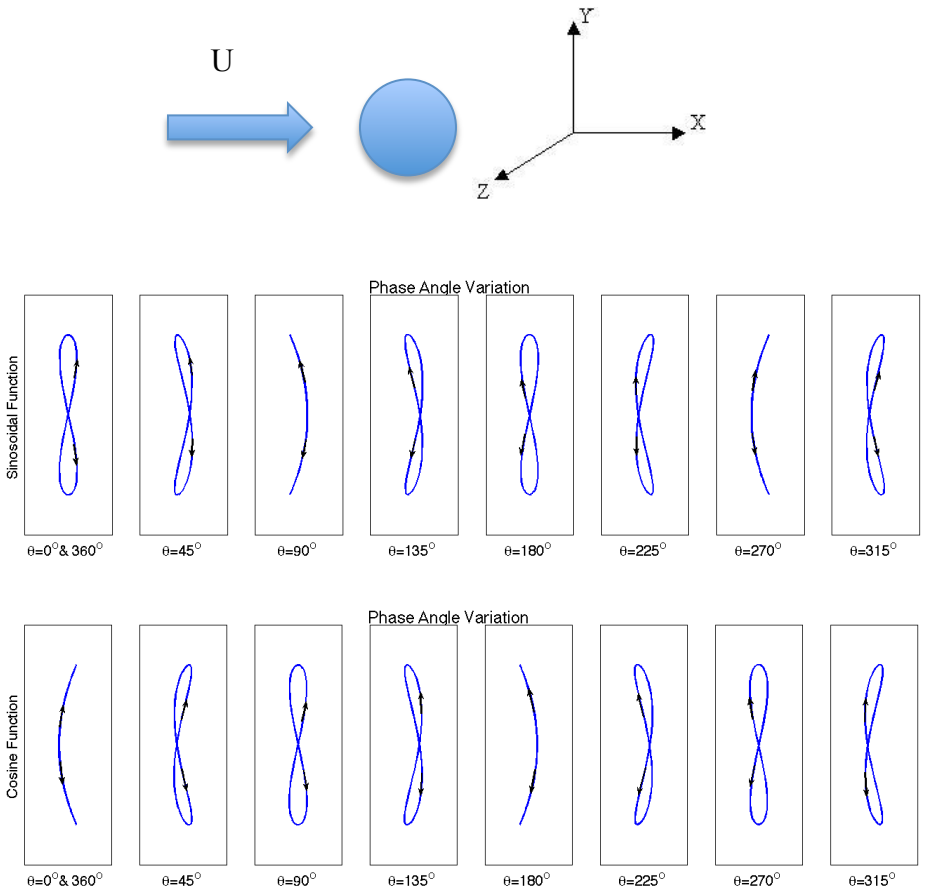

Figure 13 Orbital patterns of a two-degree of freedom cylinder

Figure 13 shows the orbital pattern variation for a given sinusoidal and cosine function at incremented phase angle values.

3.3 Forced Rigid Cylinder Experiments

Since it was not possible to directly measure forces along the length of the flexible cylinder, additional tests were conducted to estimate the hydrodynamic forces exerted on the cylinder under the various observed motions.

The cylinder has a large aspect ratio, such that the diameter of the flexible cylinder is much smaller than the length of the cylinder and the curvature of the cylinder under dynamic motion is small, therefore we can apply a strip theory assumption about the forces acting on the cylinder (Newman, 1977). With this assumption, we can model the forces acting on a particular cross-section location along the span of the flexible cylinder as being equivalent to the force exerted on a rigid cylinder moving with the same motion as the flexible cylinder cross-section.

Forced motion experiments were performed in a small flow visualization tank using an ATI Gamma SI-130-10 six-axis force transducer to measure the hydrodynamic forces exerted on the cylinder. Flow visualization tank has a working section of 420cm l x 80 h x 90cm w.

Figure 14 and Figure 15 show the rigid cylinder test set up and it's schematic view respectively. The test cylinder, a 32 mm diameter delrin tube, was cantilevered from a two-axis linear actuator system, capable of having forced motions in both the in-line and cross-flow directions. The linear actuators were mounted to a carriage, which was driven forward at constant speed. The speed of the carriage was monitored using both the encoder position of the servo drive motor and using an external spring potentiometer. The force transducer was mounted between the test cylinder and the

linear actuators, measuring both the inertial force on the cylinder and the hydrodynamic forces exerted on the cylinder. For data processing, the inertial force was subtracted from the total measured force in order to isolate the hydrodynamic force exerted on the cylinder. Accelerations were calculated from the measured position of the cylinder based on the encoder readings of the actuator servomotors. Position was accurate to within 0.1 mm.

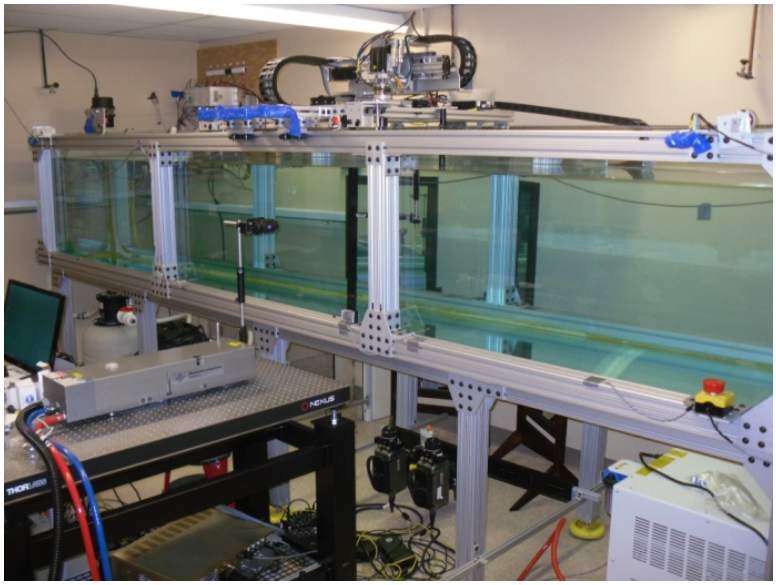

Figure 14 View of rigid cylinder test system

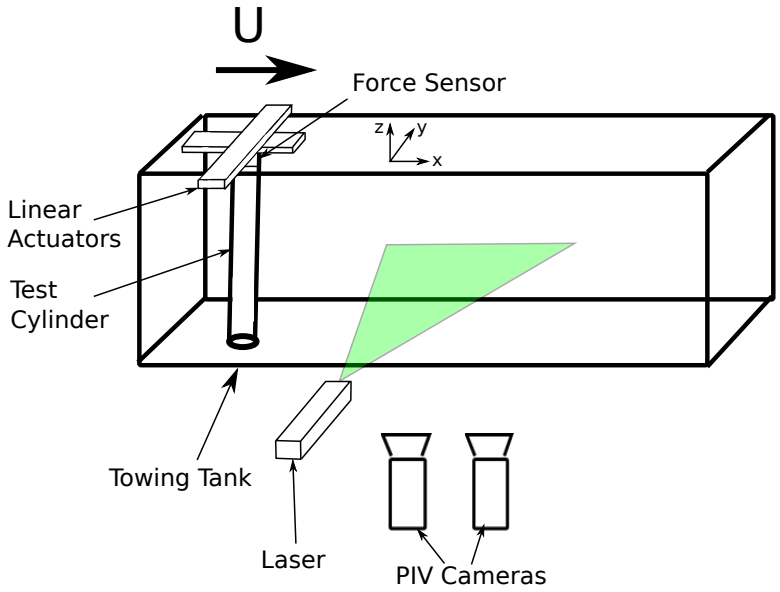

Figure 15 Schematic of rigid cylinder test apparatus in a small towing tank for force measurement and flow visualization.

In the towing tank experiments, the rigid cylinder was forced to move with the same motions measured from the flexible cylinder experiments. In the reported measurements, all forced motions are those for the midpoint motions of cylinder 1 and 2 for various reduced velocities.

3.3.1 Modeling: Equation of Motions, Force and Added Mass Calculations

In order to measure the hydrodynamic forces exerted on the body and wake modes associated with the motions, flexible cylinder experiments were replicated through forced motion experiments such that the cylinder oscillates at the same amplitude with the same motion. The measured hydrodynamic lift force on the moving cylinder was treated as a phase shifted sinusoid.

In the present study, a cross-section of the structure vibrates in two-degrees-of-freedom. Assuming our motion is approximated by a cosine function, the motion can be represented by:

$$y(t) = A_y^* cos(\omega t) \tag{3.6}$$

$$x(t) = A_x^* \cos(2\omega t + \theta) \tag{3.7}$$

where A* is the non-dimensional oscillation amplitude (normalized with the cylinder diameter), θ represents the phase difference between in-line and cross-flow motions, and f (where f = $\frac{\omega}{2\pi}$) is the oscillation frequency of the cylinder. Total force is sum of fluid force and inertial force. In the experiment since the model cylinder has mass, the total force was measured. However, we are interested in calculating the fluid force. Fluid force can be rewritten by subtracting the inertial force from total force:

$$\text{Fluid Force (Lift)=Total Force - Inertial Force} \tag{3.8}$$

$$F(t) = m\ddot{y} + b\dot{y} + ky \tag{3.9}$$

Of special interest in this study are periodic external forces, and therefore we can assume the forcing function F (lift force) in the form:

$$F_y(t) = |F| \cos(\omega t + \theta) \tag{3.10}$$

The force then can be decomposed into two components, a non-dimensional force in phase with velocity, C_{Lv}, which governs the excitation of the structure and a force in

phase with acceleration, C_{La}, which governs the effective mass of the system (Sarpkaya, 1979).

$$F_y(t) = \underbrace{|F|\cos\theta\cos(\omega t)}_{1^{st}\text{ term}} - \underbrace{|F|sin\theta\sin(\omega t)}_{2^{nd}\text{ term}} \tag{3.11}$$

First term can be equated to the acceleration term of the second order differential equation. By equating:

$$|F|\cos\theta\cos(\omega t) = m_{a_y}\ddot{y} = m_{a_y} * (-A_y\omega^2 cos(\omega t)) \tag{3.12}$$

where $\ddot{y}$ can be find from,

$$y(t) = A_y cos(\omega t) \tag{3.13}$$

$$\dot{y}(t) = -A_y\omega sin(\omega t) \tag{3.14}$$

$$\ddot{y}(t) = -A_y\omega^2 cos(\omega t) \tag{3.15}$$

The added mass (m_a) of the cylinder can be defined as the sum of fluid forces acting in phase with acceleration (3.16) and added mass coefficient (C_m) can be defined as the ratio of added mass to the displaced fluid mass of the cylinder (3.17):

$$m_a = \frac{F_a}{a} \tag{3.16}$$

$$C_m = \frac{m_{a_y}}{\rho\pi\frac{D^2}{4}L} \tag{3.17}$$

where m_{ay} is effective added mass, L is the cylinder length, ρ is density of water and D is cylinder diameter.

Assigning the lift in phase with acceleration to be equal to an effective added mass times the acceleration of the body (3.12), an added mass coefficient, C_m, can be defined for a particular amplitude normalized with cylinder diameter, A* at a particular reduced velocity, Vr.

$$C_m = \frac{-2C_{L_a}Vr^2}{2\pi^3 A_y^*} \tag{3.18}$$

The time dependent lift coefficient can be written dimensionless as:

$$C_L(t) = \frac{F_y(t)}{\frac{1}{2}\rho U^2 DS} \tag{3.19}$$

The force coefficients can be computed based on the inner product of the lift coefficient and velocity/acceleration of the body as in Smogeli (2002):

$$C_{L_V} = \sqrt{\frac{2}{T}}\frac{C_L(t)\cdot\dot{y}(t)}{\sqrt{\dot{y}(t)\cdot\dot{y}(t)}} \tag{3.20}$$

$$C_{L_a} = \sqrt{\frac{2}{T}}\frac{C_L(t)\cdot\ddot{y}(t)}{\sqrt{\ddot{y}(t)\cdot\ddot{y}(t)}} \tag{3.21}$$

C_{L_V} can be defined as the excitation component of the fluid force . C_{L_a} can be defined as the force in phase with acceleration, which has the effect of altering the frequency of oscillation (effective natural frequency).

The relationship between C_{L_v} and C_{L_a}:

$$C_L = \sqrt{C_{L_v}^2 + C_{L_a}^2} \tag{3.22}$$

where $C_L(t)$ is the time dependent lift force coefficient and T is the window length for the inner product. C_{L_V} refers to the cross-flow motion. The same form of equations may be applied for determining force coefficients associated with in-line motions using the total force in in-line direction. In in-line direction, C_{D_V} means drag coefficient in phase with velocity and C_{D_a} means drag coefficient in phase with acceleration.

$$C_{D_v} = \sqrt{\frac{2}{T}} \frac{C_D(t) \cdot \dot{x}(t)}{\sqrt{\dot{x}(t) \cdot \dot{x}(t)}} \tag{3.23}$$

$$C_{D_a} = \sqrt{\frac{2}{T}} \frac{C_D(t) \cdot \ddot{x}(t)}{\sqrt{\ddot{x}(t) \cdot \ddot{x}(t)}} \tag{3.24}$$

The same relationship with (3.19) holds for drag coefficient:

$$C_D = \sqrt{C_{D_v}^2 + C_{D_a}^2} \tag{3.25}$$

In vortex-induced vibration, fluid forces will cause excitation or dissipation of motion depending on the flow of power in the system. If the system has very little damping and if the structure neutrally buoyant; an equilibrium condition can be written.

$$C_{D_v} \approx 0 \tag{3.26}$$

and for a continuous structure;

$$\int C_{L_v}\, dx = 0 \tag{3.27}$$

$$C_{L_v} \approx 0 \tag{3.28}$$

This situation means that the energy through fluid forcing must balance energy due to damping, resulting in a steady-amplitude periodic oscillation (Dahl et al. 2008).

3.3.1.1 Finding the Motion Amplitude

The energy spectrum from the measured data of the flexible cylinder was used to determine the frequencies and amplitudes for the modeled motion equations.

It is known that the power spectrum of a given signal illustrates the power as the mean squared amplitude at each frequency component. In other words, it is the distribution of power per unit frequency. As an example, the figures 16 and 17 were generated using Welch's method to estimate the power spectral density of the signal in cross-flow direction.

Amplitudes A_y and A_x (in equation 3.6 and 3.7) are computed by finding the area under the power spectral density curve. One can treat to the spectrum of a time series as the distribution of variance of the series as a function of frequency. Therefore, the

total area under the curve gives us the variance of the process and there is a square relationship between variance of a sine wave and amplitude of the motion.

$$\sigma^2 = \int_{-\infty}^{+\infty} S(f)df \tag{3.29}$$

$$\sigma^2 = \frac{A^2}{2} \tag{3.30}$$

The magnitudes of the power spectral density for raw data and replicated data may be slightly different. The reason is, in the replicated power spectral density figures, it was taken into account the frequency but not the magnitude. For that reason, the area under the curve and corresponding oscillation frequency has to be same but the magnitude will not necessarily be the same.

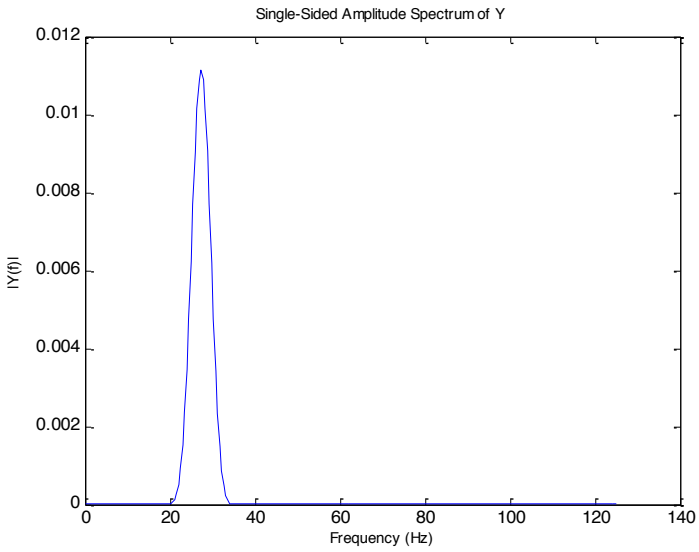

Figure 16 Example Single Sided Amplitude Spectrum from Raw Data for cross-flow (Y) motion (Vr=5.59, Cylinder 2)

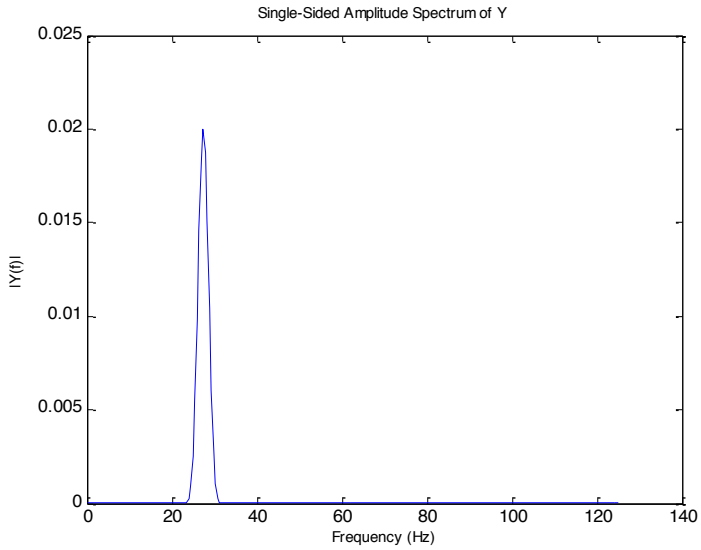

Figure 17 Example Single Sided Amplitude Spectrum from Replicated Data for cross-flow (Y) motion (Vr=5.59, Cylinder 2)

Motion trajectory was plotted for replicated data on top of the raw data. Figure 18 shows an exact match between raw data and replicated data.

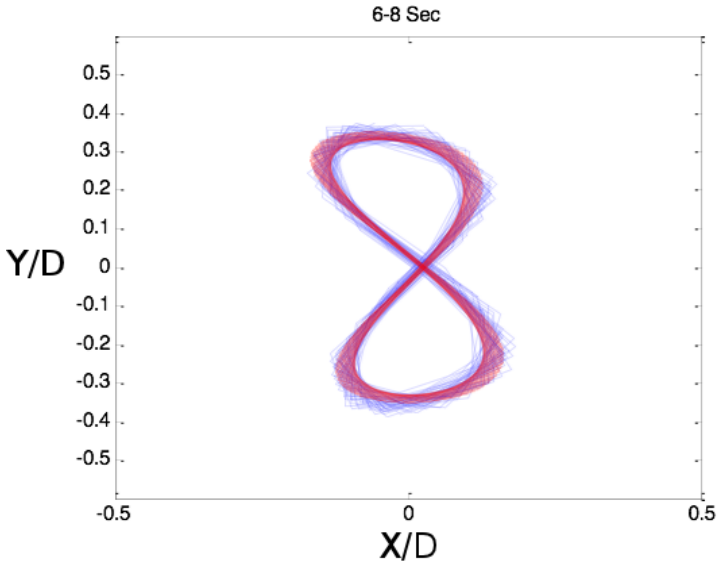

Figure 18 Motion Trajectory at Vr= 5.59 for cylinder 2, blue shape indicates the raw data, and red shape indicates the replicated data

In order to get the equation of motion for other reduced velocity values that needed to be analyzed, this process was repeated. Rigid cylinder experiments were conducted based on the equation of motions (3.6) and (3.7).

3.3.2 Digital Particle Image Velocimetry (DPIV)

Digital particle image velocimetry (DPIV) is a flow visualization technique used to analyze the flow characteristics. Using this method, one can obtain the instantaneous flow velocity field as well as the vorticity field in the flow.

In this section first general information on wake modes will be given and then necessary steps followed during the rigid cylinder experiments will be explained. For detailed information, product manuals such FlowMaster and Davis 8.2 Software from LaVision can be studied.

3.3.2.1 Wake Modes

Flow visualizations were done along with the force measurements using the same high-speed cameras as in flexible cylinder experiments. PIV cameras were placed underneath the tank normal to the light sheet. Green light sheet was set up parallel to the flow field that would be observed. Digital particle image velocimetry (DPIV) method was used to measure the instantaneous flow velocity field across a flat area of a flow field. Flow was seeded with tiny, neutrally buoyant particles with particle diameter of 20 μm as illustrated in Figure 19.

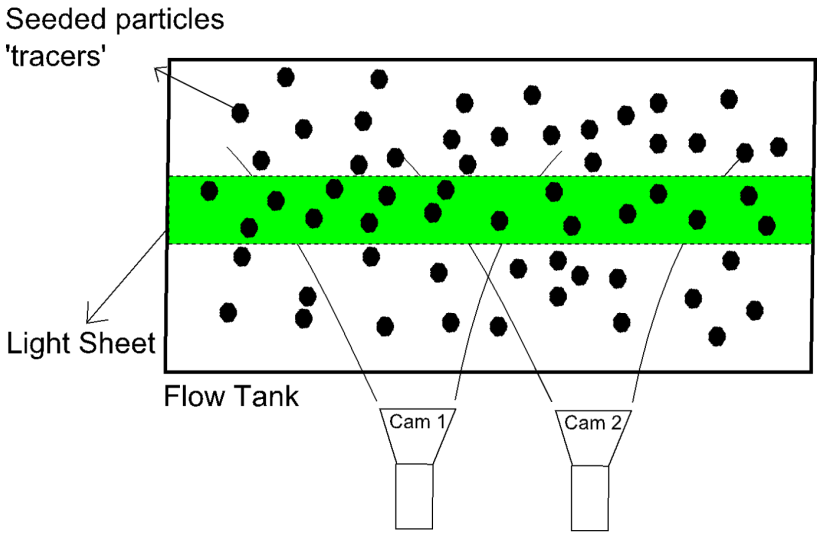

Figure 19 Side view of the tank with seeded particles

For each run, seeded particle motions were captured by the cameras. Vector and vorticity fields were then determined using a standard time series cross-correlation between successive images, using Davis program from LaVision.

Wake modes of a vibrating cylinder helps to understand the forces acting on the cylinder better. A cylinder starts to vibrate when incoming water hits the cylinder, and the vibration of the cylinder changes the wakes behind the cylinder. For that reason, the force associated with the freely vibrating cylinder under water is different than the forces acting on a cylinder in air. It is believed that understanding the wakes pattern under certain conditions helps to understand the nature of the vibration itself because vortex-induced vibrations are strongly dependent on the vortex shedding behind the cylinder.

Williamson and Roshko (1988) and Morse and Williamson (2009) have conducted series of experiments in order to see the wake modes of a cylinder subjected to vortex-induced vibrations where cylinder oscillates only in cross-flow direction (1-DOF system). They created a map describing the vortex shedding regimes. Figure 20 shows

the map of vortex shedding regime. Section (a) illustrates the new version of vortex shedding regimes that they created and section (b) represents the earlier version of map of vortex shedding regime.

The definitions of the wake modes illustrated in Figure 20 can be described as follows:

2S = Two single vortices are shed per cycle of oscillation

2P = Two pairs of vortices are shed per cycle of oscillation

P+S = One pair and one single vortices are shed per cycle of oscillation

$2P_0$ (P*) = Similar to 2P pattern but the secondary vortex is weaker

2T = Two triplet of vortices are shed per cycle of oscillation (showed in DPIV results, Figure 56)

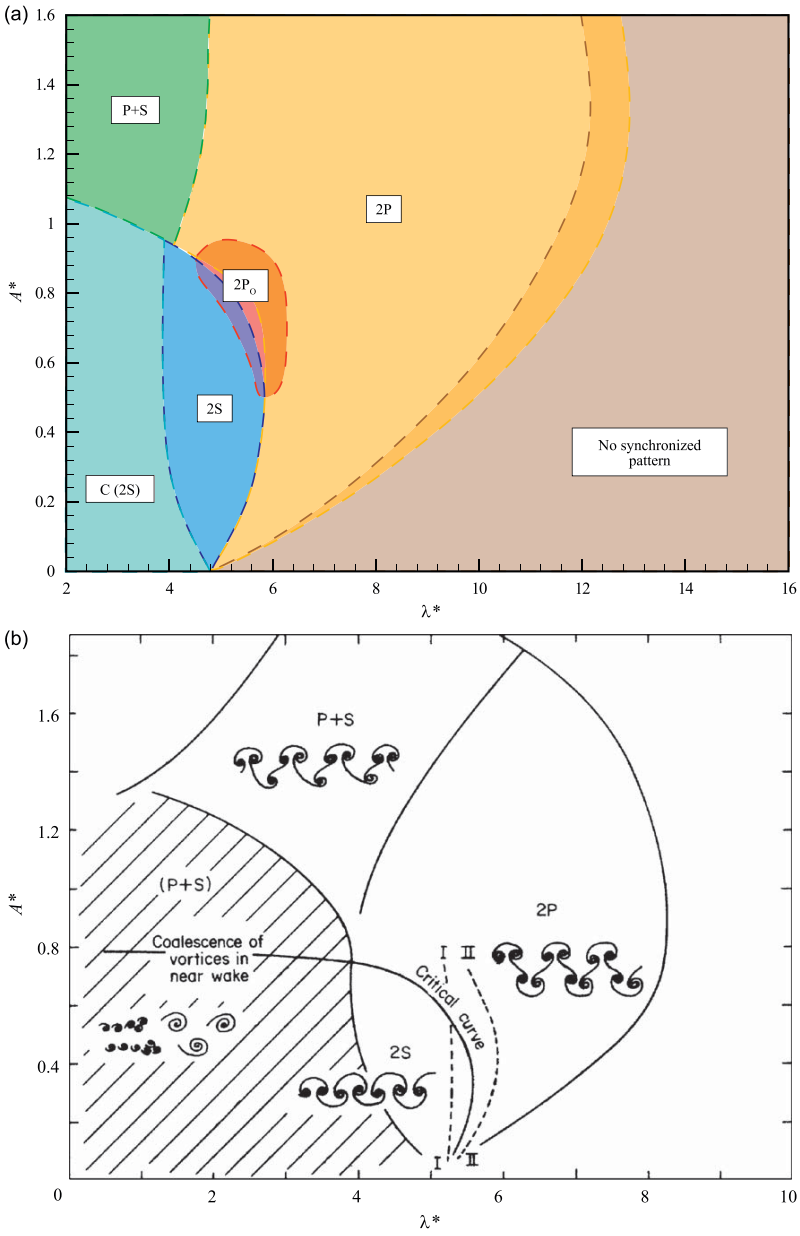

Figure 20 (a) Map of vortex shedding regimes and the mode boundaries identified by Morse and Williamson (2009) (b) previous mode boundaries identified by Williamson and Roshko (1988)

3.3.2.2 PIV Experimental Setup

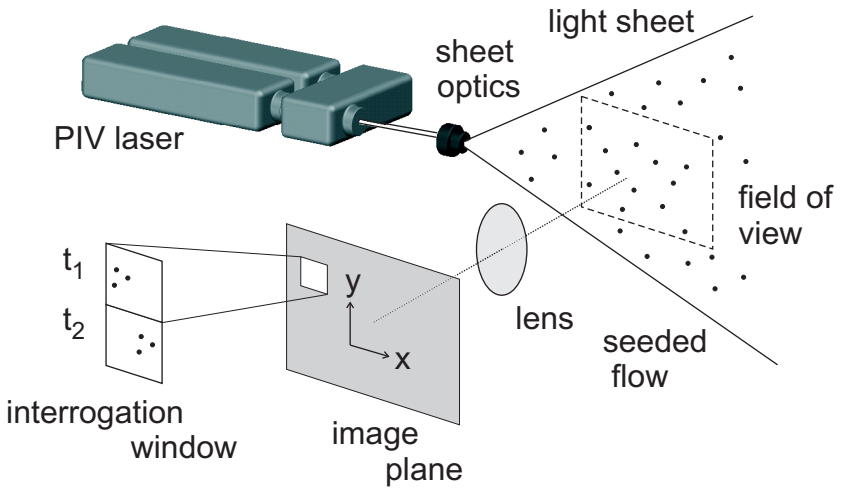

Figure 21 Experimental set of a 2D PIV system (LaVision Manual)

Figure 21 shows the general setup of a 2D PIV system. In the setup, flow is seeded with tiny neutrally buoyant particles called tracers, and light sheet cuts the field of view perpendicular relative to the camera (camera is shown as lens). The camera is positioned perpendicular to the field of view in order to capture the movements of the particles. It is very important that this PIV set up needs to be ensured in the same orientation in each experiment in order to get better results. The light sheet produced by the laser can be adjusted using optics. The ultimate goal of PIV is to measure the velocity vector field in the fluid. PIV accomplishes this goal by taking two images sequentially and calculates the distances traveled between groups of particles within this time. The main assumption of the PIV is that tracers follow the flow in the fluid and forms a pattern so high speed cameras can capture the motion (LaVision Manual).

PIV works based on interrogation window analyzes as shown in Figure 21. In order to calculate the displacement vector in each interrogation window, all particles that move homogeneously in the same direction within the window are selected. Experiments showed that at least 10 particles needed to be in the interrogation window in order to get better results (LaVision Manual). After such particles are selected, statistical correlation techniques can be used.

In order to calculate the displacement vector in each interrogation window and compare the results, basic statistical correlation techniques can be used. As a result, a vector field of the flow can be obtained by performing this process over the entire frame of two images.

The correlation technique used in DAVIS is PIV time series sum of correlation.

PIV time series sum of correlation: This method is very useful if one is interested in the average vector field. In this method, the algorithm computes from each acquired image only the correlation planes using the cross-correlation of individual interrogation windows in order to get determine the velocity field (LaVision Manual).

PIV system used in this study consists of five main modules:

1. Cooler,
2. High speed laser system with light sheet optics,
3. Seeding particles
4. High-speed cameras and
5. DAVIS PIV processing software

Necessary steps for a rigid cylinder PIV experiment in a tow tank;

1. ***Setting up the experiment:*** First of all, depending on the experiment type, necessary experimental set up should be selected. For instance, for a rigid cylinder experiment subjected to vortex-induced vibration, the cylinder has to be placed in the view of the cameras. In the present set up; the cylinder is placed vertically in the tow tank. The laser sheet is aligned to cut just a very small portion of the cylinder and the wake behind it (Figure 21).
2. ***Calibration of the Cameras and Setting up the Camera Characteristics:*** Since the laser sheet will shine over a very small portion of the cylinder height, calibration of the cameras has to be done in the laser sheet field of view. For that purpose, a calibration plate provided by LaVision was used in order to calibrate the cameras. The calibration plate used had an array of small white dots spaced 10 mm apart and the plate was placed horizontally in the field of laser view. The calibration was done using the calibration dialogue in the Davis 8 software. The cameras were positioned perpendicular to the field of view.

   Calibration works based on mark search. First, three start marks should be defined for the mark search and in the next step those marks should be redefined as specified in the instructions field. The program automatically tries to find other marks based on a polynomial fit algorithm and creates a mapping function. After search finishes, this mapping function can be applied to all the other images so one can correct the image for camera angle and lens distortion.

   It should be noted that cameras have max resolution of 2400x1800 pixels with max frame rate of 720 Hz. Maximum frame rate or minimum frame rate that is

allowed in the program depend on the interrogation window size. As mentioned earlier, experiments showed that an ideal interrogation window must contain at least 10 particles and the particles should not move more than one third of the interrogation window between frames (Lavision Manual). The speed of the camera for the rigid cylinder experiments was determined to be 250 Hz, allowing the camera to obtain full resolution images with the max resolution of 2400x1800 pixels.

3. ***Setting up the light sheet:*** Setting up the light sheet is not a separate section than the calibration of the cameras. Depending on the cameras' capability of getting images in a desired distance from the light sheet, suitable height and power of the laser sheet needs to be adjusted. It is a very important step because it is desired to see as much view of field as possible.
4. ***Particle focusing:*** Particle focusing also needs to be done along with the camera calibration.
5. ***Seeding:*** Suitable seeding particle size needs to be selected depending on the PIV experiment. Particles need to be neutrally buoyant and distributed homogeneously in the field of view. In the experiments, flow was seeded with tiny, neutrally buoyant particles with particle diameter of 20 μm.
6. ***Vector calculation:*** Vector calculation is the most important section of the PIV. The processing routine chosen to obtain the general features of the vector field is listed as below;
    a. As vector calculation parameter; 'PIV time series pyramid correlation is selected'.

b. The vector field was computed using a multi-pass sequential cross correlation on interrogation windows. In sequential cross correlation, cross correlation method is applied to the frame pairs (i.e. 0+1, 2+3, 3+4 …) and vector field is calculated based on those frame pairs.

c. In case of a decreasing interrogation window size, initial interrogation window size was selected to be 64x64 and final interrogation window size was selected to be 32x32 based on the observed particle density in the images.

d. Fifty percent overlap was used in defining interrogation windows. Window overlap and the interrogation window size determine the grid size of a vector field (Flowmaster Manual); therefore one can increase the number of calculated vectors by having larger overlap regions.

e. Windows are not weighted in order to increase the speed in the vector field computation and maintain the use of an FFT algorithm.

f. Additional operations can be added to the operation list in the software. In order to smooth the velocity vector field, smoothing operation was also selected after the PIV time series pyramid correlation method.

CHAPTER 4

RESULTS

4.1 Center Point Motion Response

The amplitude of motion in cross-flow and in-line directions observed for the center points of cylinder 1, cylinder 2 and cylinder 3 exhibit a similar response to an elastically mounted rigid cylinder.

4.1.1 Cylinder 1 Experiments

Cylinder 1 experiments were carried out for validation purposes by doing a similar experiment with Dahl (2008). The non-dimensional amplitude response as a function of reduced velocity is compared with the results of Dahl (2008) in Figure 23. Normalized amplitude was defined as the average of the top ten percent of the local maxima from the motion time history, normalized by the diameter of the cylinder. The number of oscillations included approximately equal to 200 cycles for each experimental run, depending on the frequency of oscillations for the 12 seconds of experimental data.

Figure 22 shows the original non-dimensional amplitude plot of Dahl (2008) experiments along with orbit shapes for flexible beam cylinder motions at the midpoint of the beam.

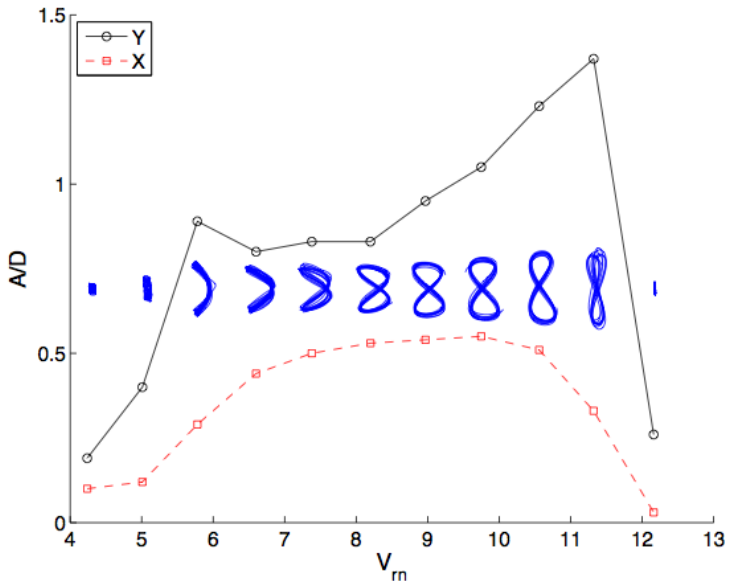

Figure 22 Non-dimensional amplitudes and orbit shapes for flexible beam cylinder motions at the midpoint of the beam (Dahl, 2008)

In Figure 23, red filled circles indicate the non-dimensional cross-flow amplitudes and red filled diamond points represent the non-dimensional amplitudes in in-line direction for cylinder 1. In addition, black filled circles represent the cross-flow non-dimensional amplitudes and black filled diamond points represent the non-dimensional in-line amplitudes for the experiments conducted by Dahl (2008). Cross flow direction is notated as Y and in-line direction is notated as X in the figure.

Two experiments (Dahl (2008) and cylinder 1 experiments) showed almost the same phenomena in that there was a dramatic jump in the beginning between the normalized reduced velocities 4 and 5, and motion amplitudes increased up to ~1.5-~1.6 gradually. The fall in the amplitude responses were observed between the reduced velocities 11 and 12 in Dahl`s study, and around 14 and 16 in the present study.

In addition, it has to be noted that Dahl (2008) reached maximum non-dimensional amplitude of ~1.5; however, in the experiments defined as cylinder 1, it reached to maximum non-dimensional amplitude of ~1.6.

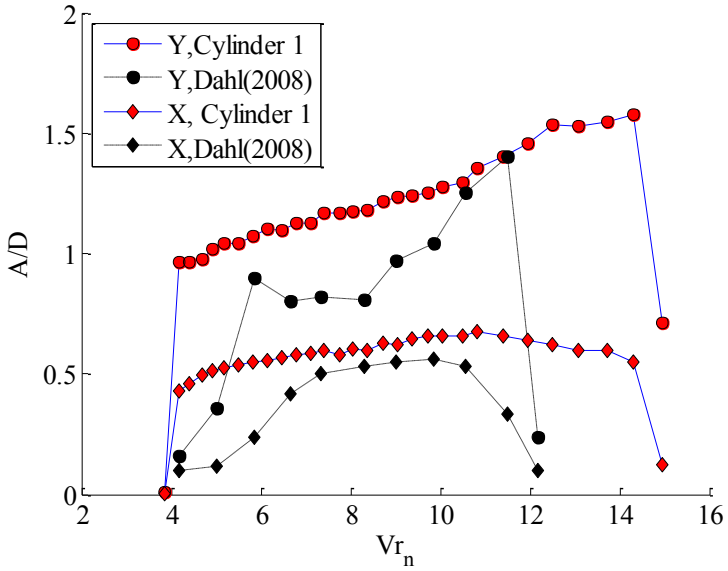

Figure 23 Non-dimensional amplitude response of the center point of flexible cylinder 1 and Dahl (2008) for In-Line (X) and Cross-Flow (Y) directions.

Figure 24 shows experimental results for cylinder 1, but now having true reduced velocity values in x-axes instead of normalized reduced velocities and normalized amplitude values in y-axes. In this figure, there are some overlap regions (for example around Vr= 5.3 and 6.7) where cylinder has different amplitudes with very close reduced velocities to each other. Likewise at Dahl (2008), the amplitude of motion is very small for reduced velocities less than 5, with a dramatic jump to large amplitude motions for reduced velocities greater than 5. Response gradually increases up to the reduced velocity of 6.9 and after that point suddenly falls. The difference in the lock-in range and maximum amplitudes reached between current experiments and Dahl (2008) is possibly due to having different mass ratios (m*) for tested cylinders. In this study,

reduced velocity refers to the true reduced velocity and nominal reduced velocity is not used throughout this study.

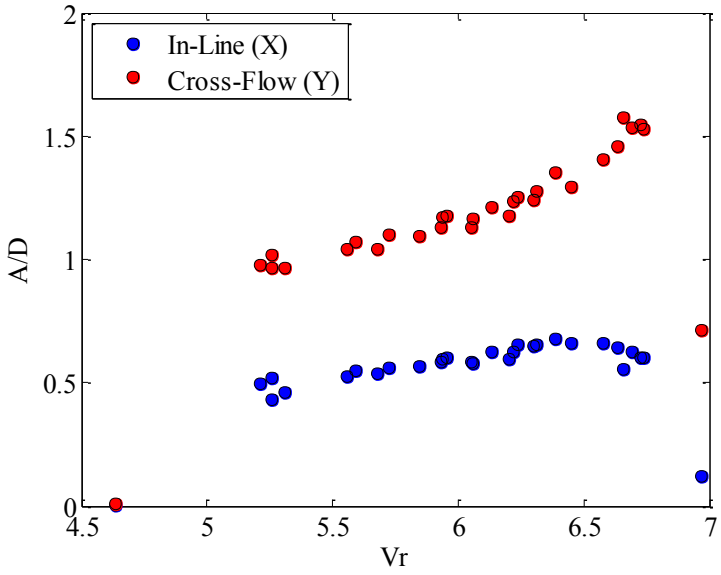

Figure 24 Cylinder 1 case Vr vs. A/D figure for both In-Line (X) and Cross-Flow (Y) direction

Figure 25 shows the Lissajous figures or orbital patterns for the midpoint location from cylinder 1 as a function of increasing reduced velocity. It is important to note that the response of cylinder 1 and the response of similar experiments conducted by Dahl (2008), resembles each other in that both cylinders oscillate primarily with a figure eight pattern over the same reduced velocity values. These orbitals are also very similar to the motions of a 2-DOF rigid cylinder with 2:1 (in-line: cross-flow frequency) ratio as shown in Dahl et al. (2006, 2007, 2008).

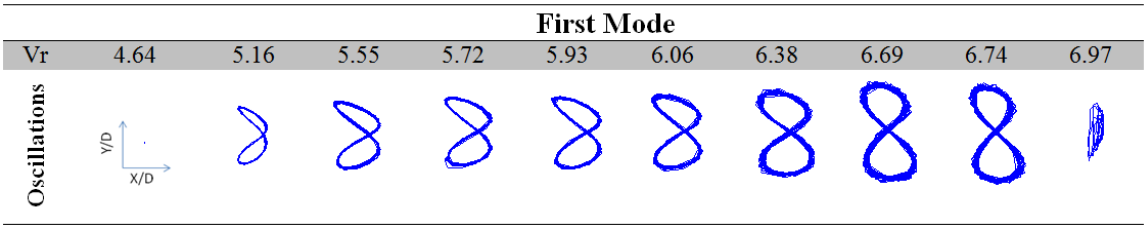

Figure 25 Lissajous (orbital) shapes of the center point of cylinder 1 for tested reduced velocities.

4.1.2 Cylinder 2 Experiments

Different than cylinder 1, cylinder 2 is tuned to oscillate with first mode shape in cross-flow direction and second mode shape in in-line direction. Therefore the orientation of the aluminum beams inside the cylinder and oscillation frequencies associated with the mode shapes are different in both cylinders. On the other hand, both cylinders have very close aspect ratios and mass ratios.

Figure 26 shows the non-dimensional response of the center point of cylinder 2 as a function of reduced velocity. It is observed that Cylinder 2 also oscillates primarily with a figure eight pattern over the reduced velocities between 5 and 6 as showed in Figure 27, and after the reduced velocity ~5.8 irregularities in cylinder motion starts, leading to an irregular motion trajectory. In this particular motion, cylinder motion was adjusted to oscillate first mode shape in cross-flow direction and second mode shape in in-line direction. Instead, it was observed that cylinder moves with a second mode shape in cross-flow with high motion amplitudes and first mode shape in in-line direction with very small motion amplitudes.

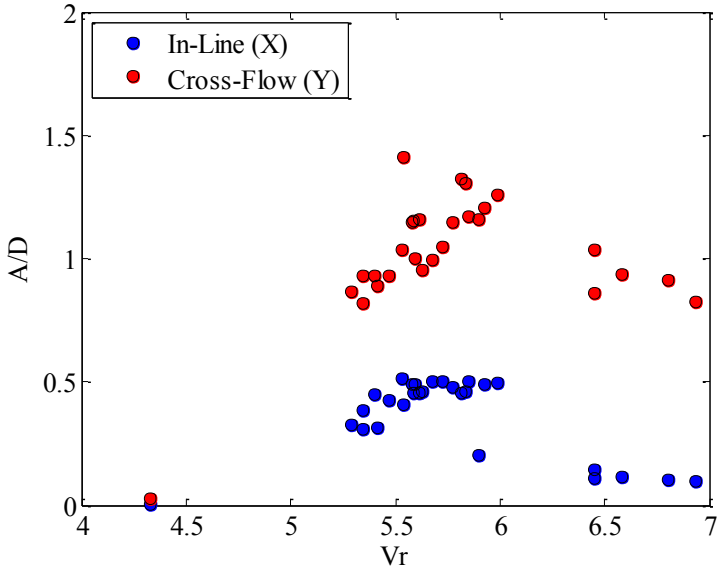

Figure 26 Cylinder 2 case Vr vs. A/D figure for both In-Line (X) and Cross-Flow (Y) direction

Figure 27 shows the orbital shapes of cylinder 2 experiments over the reduced velocities 4 to 7 for the Reynolds numbers between 3,500-10,000.

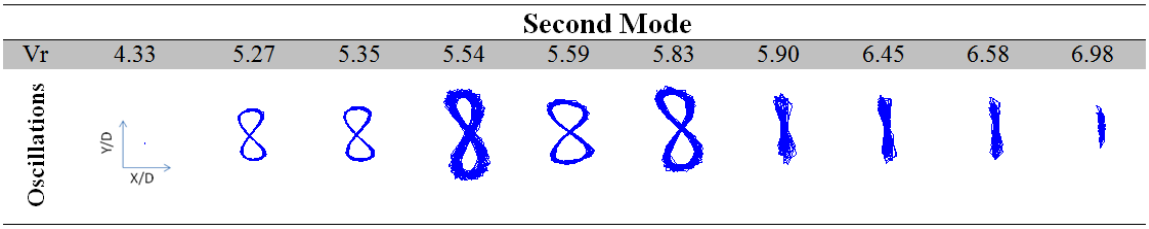

Figure 27 Lissajous (orbital) shapes of the center point of cylinder 2 for tested reduced velocities.

In this study, cylinder 2 experiments are focused to explain the orbital shapes since it is thought cylinder will trouble exciting second mode in the in-line direction leading an irregular orbit shape. For further investigation and a clear picture of the motion; response snapshots were plotted for cylinder 1 and cylinder 2 for selected reduced

velocities. Afterwards, frequency response was examined for each velocity increment for both cylinder 1 and cylinder 2. In the end, scalogram analysis was done to explain further the frequency content of each motion in time.

4.1.3 Cylinder 3 Experiments

Figure 28 shows the non-dimensional response of the center point of cylinder 3 as a function of reduced velocity. From the figure it can be easily observed that there is a dramatic jump in the response amplitudes between the reduced velocity values of 5 and 6. This result is consistent with the study of (Khalak and Williamson (1999), Govardhan and Williamson (2000), Jauvtis and Williamson (2004)) where they also observed a sharp jump in the response amplitudes for low mass ratios ($m^*=2.6$).

It is also observed that for low reduced velocities (lower than 5) cylinder oscillates in in-line direction with higher amplitudes than cross-flow direction. Therefore, larger response is observed in in-line direction than cross-flow direction for those reduced velocities. Between the reduced velocities 5 and 6.5, irregularities in cylinder motion start, leading to two main different cylinder responses as crescent shape and eight shape.

It should be remembered that cylinder motion was adjusted to oscillate first mode shape in cross-flow direction and third mode shape in in-line direction. However, we were unable to reach high enough flow speeds; therefore, second mode shape and third mode shape in in-line direction was not observed for this cylinder case.

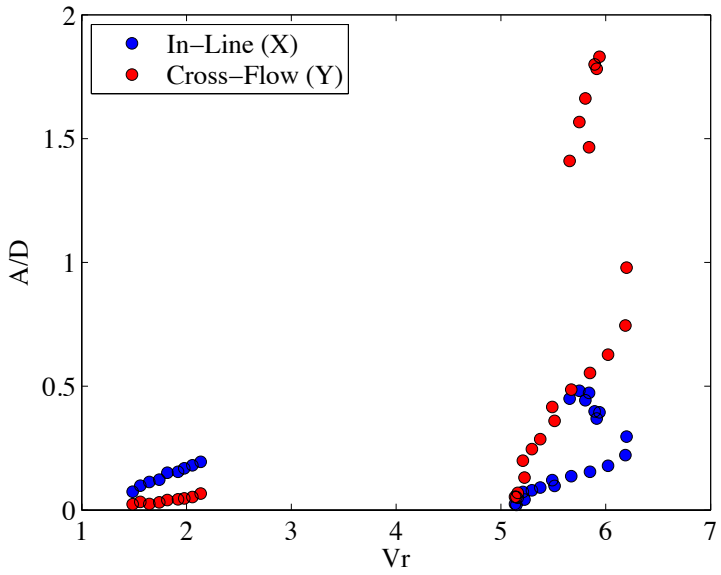

Figure 28 Cylinder 3 case Vr vs. A/D figure for both In-Line (X) and Cross-Flow (Y) direction

Figure 29 shows the orbital shapes of cylinder 3 experiments over the reduced velocities 1.5 to 6.5 for the Reynolds numbers between 2,000-10,000. In this experiments, three main different responses were observed. First, a straight in-line motion was observed at reduced velocities lower than 5 where cross-flow amplitude was very low. Secondly, crescent type cylinder response was observed until the reduced velocity value of 5.5, and finally figure eight and crescent shape responses were observed alternately between the reduced velocity values of 5.5 and 6.2.

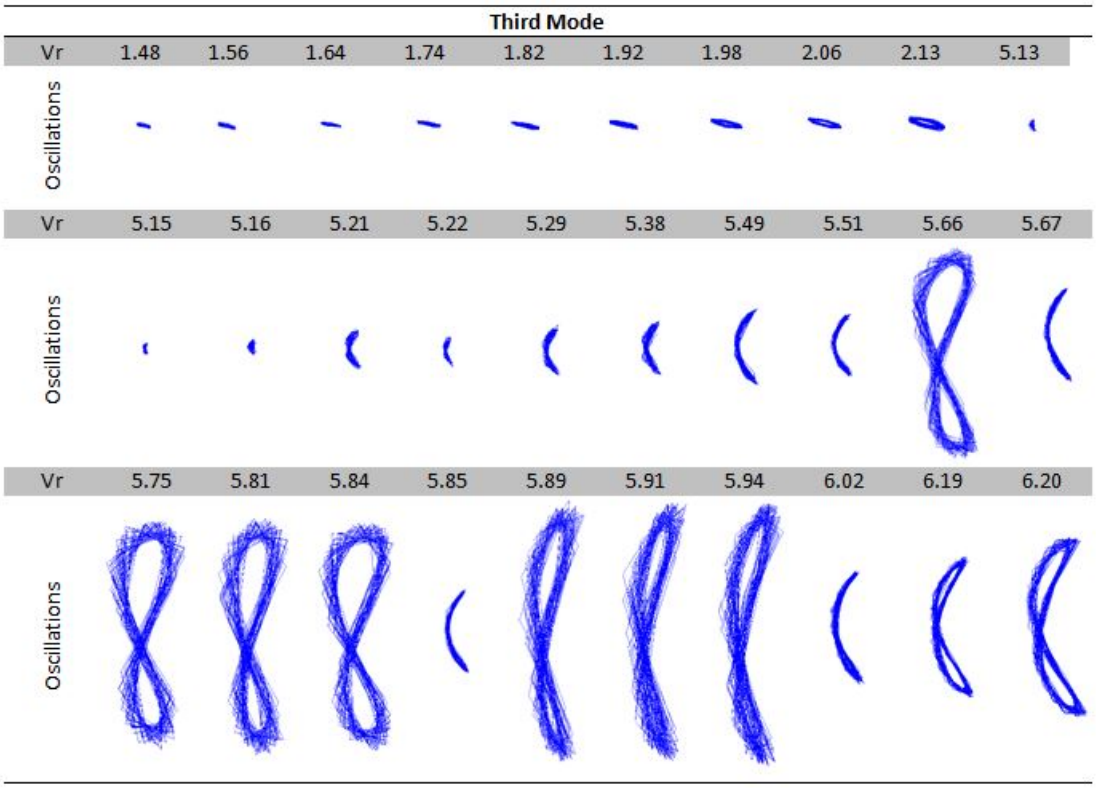

Figure 29 Lissajous (orbital) shapes of the center point of cylinder 3 for tested reduced velocities (Axes normalized by cylinder diameter as in Figure 26 and Figure 28).

In the thesis, cylinder 3 case is not further examined since a full map of response motion was not obtained due to being unable to reach high enough flow speeds in the experiments.

4.2 Response Snapshots

Response snapshots were plotted for the first 20 data points (out of 500 data points where sampling rate was 250 Hz) for cylinder 1, cylinder 2 and cylinder 3 cases. Figures 30, 31, 32, 33, 34 and 35 illustrate the response snapshots of cylinder 1 and cylinder 2 in each direction (cross flow and in-line) for various reduced velocities (See Appendix B for cylinder 3 experiments).

4.2.1 Cylinder 1 Response Snapshot

Cylinder 1 response shows that as the reduced velocity increases, the amplitudes in both in-line and cross-flow direction increases. Also, cylinder has first mode shape in both in-line and cross-flow directions as expected. In addition, motion amplitude increases with very small increments in in-line direction, but with large increments in cross-flow direction as reduced velocity increases.

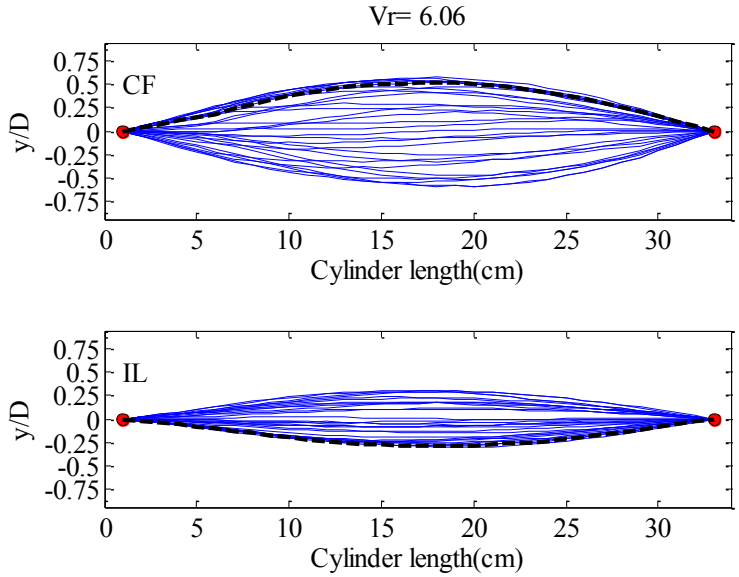

Figure 30 Response Snapshot for cylinder 1 at Vr=6.06. Dashed black line on the response snapshot figures show the initial shape of the cylinder for the selected time interval, i.e. 2 seconds of data (between 6 and 8 sec) selected in a 12 seconds of data. Red circles indicate the end points of the cylinder, and blue lines indicate the cylinder shape in different times.

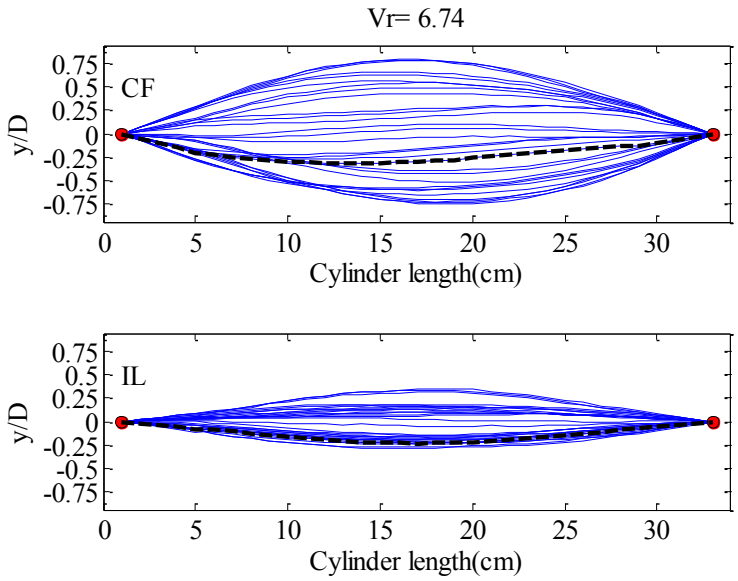

Figure 31 Response Snapshot for cylinder 1 at Vr=6.74. Dashed black line on the response snapshot figures show the initial shape of the cylinder for the selected time interval, i.e. 2 seconds of data (between 6 and 8 sec) selected in a 12 seconds of data. Red circles indicate the end points of the cylinder, and blue lines indicate the cylinder shape in different times.

4.2.2 Cylinder 2 Response Snapshot

When cylinder 2 experiments were examined, it was found that depending on the reduced velocity, the motion of the cylinder tended to exhibit first mode shape in cross-flow& in-line, second mode shape in cross-flow& first mode shape in in-line and some combination of first mode shape and second mode shape in cross-flow& in-line direction. It should be remembered that, in flexible cylinder experiments in vacuum mode shapes used in order to describe the shape of the cylinder, but these are not necessarily the same modes that are being excited.

Figure 32 and 33 show the response snapshots for cylinder 2 for the reduced velocities 5.54 and 5.90. Both figures illustrate that cylinder is primarily oscillating with first mode shape in in-line and cross-flow directions. At reduced velocity 5.54,

there is a significant cross-flow first mode response, and a large in-line first mode response. However, at reduced velocity 5.90, the response motion amplitude in in-line direction decreases, but it has still very high amplitude in cross flow direction. For those reduced velocity values, cylinder is oscillating mainly with figure 8 shape as showed in Figure 27.

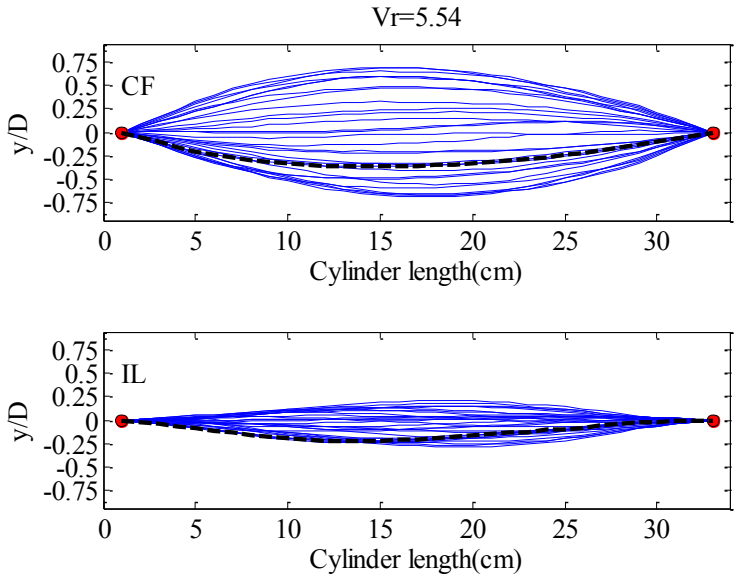

Figure 32 Response Snapshot for second mode shape Vr=5.54. Dashed black line on the response snapshot figures show the initial shape of the cylinder for the selected time interval, i.e. 2 seconds of data (between 6 and 8 sec) selected in a 12 seconds of data. Red circles indicate the end points of the cylinder, and blue lines indicate the cylinder shape in different times.

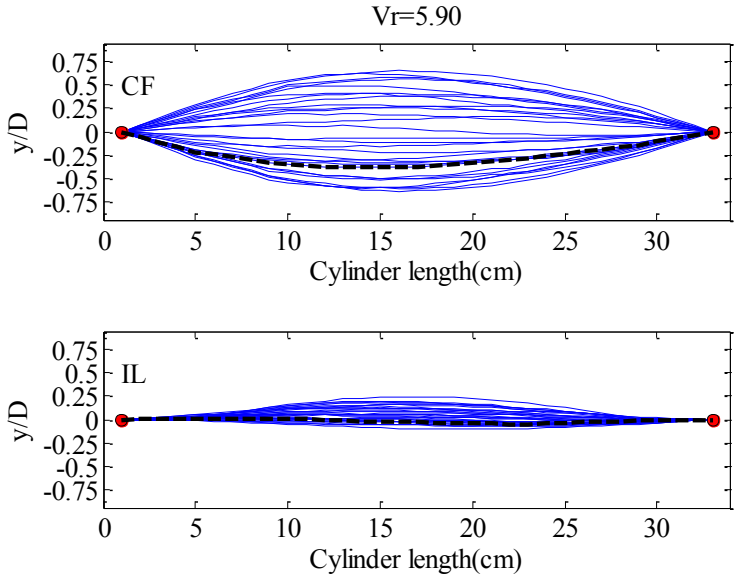

Figure 33 Response Snapshot for second mode shape Vr=5.90. Dashed black line on the response snapshot figures show the initial shape of the cylinder for the selected time interval, i.e. 2 seconds of data (between 6 and 8 sec) selected in a 12 seconds of data. Red circles indicate the end points of the cylinder, and blue lines indicate the cylinder shape in different times.

It should be noted that, reduced velocity 5.9 falls into the transition region (from regular figure 8 to irregular motion) and has the second mode natural frequency in in-line direction but cylinder still oscillates with the first mode shape both in in-line and cross-flow directions. In addition, Figure 27 illustrates that orbital shape of this motion has some irregularities in it and it is not oscillating purely with figure 8 shape. Mode mixing in cross-flow direction in the spatial shape starts after the reduced velocity value of 6. Two different reduced velocity values were examined further after this point.

Figure 34 shows that at reduced velocity 6.45, cylinder has very small amplitude in in-line direction, and has some combination of second mode and first mode in cross-flow direction. Motion trajectory in Figure 27 also shows that cylinder oscillates mostly in cross-flow direction and has irregularities in its trajectory.

Figure 35 represents the response snapshot at the reduced velocity 6.58, and shows that cylinder oscillates purely with second mode shape in cross-flow direction, and moves barely in in-line direction. In comparison with lower reduced velocity values in Figure 27, irregularities in cylinder trajectory become clearer. It is interesting because cylinder 2 motion was calculated to oscillate with first mode shape in cross-flow direction and second mode shape in in-line direction.

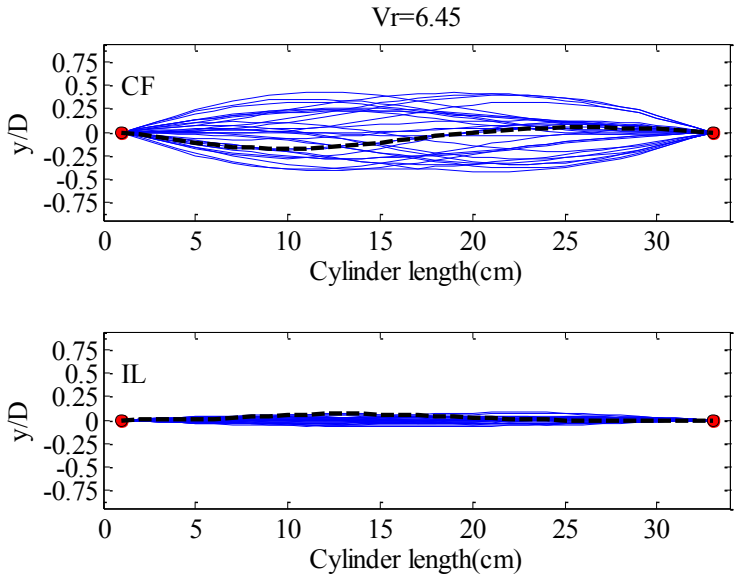

Figure 34 Response Snapshot for second mode shape Vr=6.45. Dashed black line on the response snapshot figures show the initial shape of the cylinder for the selected time interval, i.e. 2 seconds of data (between 6 and 8 sec) selected in a 12 seconds of data. Red circles indicate the end points of the cylinder, and blue lines indicate the cylinder shape in different times.

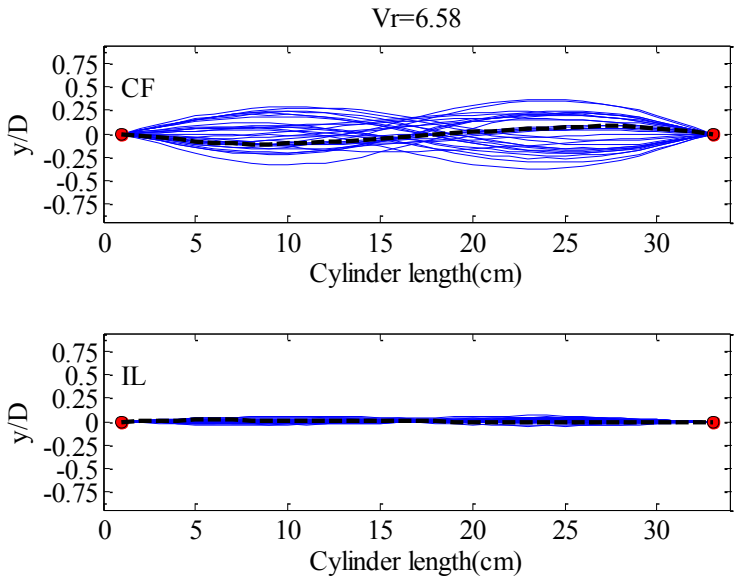

Figure 35 Response Snapshot for second mode shape Vr=6.58. Dashed black line on the response snapshot figures show the initial shape of the cylinder for the selected time interval, i.e. 2 seconds of data (between 6 and 8 sec) selected in a 12 seconds of data. Red circles indicate the end points of the cylinder, and blue lines indicate the cylinder shape in different times.

To truly evaluate the modal response, it is necessary to perform a modal decomposition, which is not included in the scope of this thesis.

4.3 Spanwise Response

Even though a response snapshot is very good to show the cylinder response for a short time period, it does not give enough information about spanwise response in the whole time period, therefore; spanwise response plots were plotted.

Depending on the reduced velocity and the particular modal response of the cylinder, the spanwise motion of the cylinder tends to exhibit a standing wave response or a combination of standing wave with some travelling wave response.

4.3.1 Cylinder 1 Spanwise Response

Figure 36 shows the spanwise response of the cylinder 1 at a reduced velocity of 6.06. In some cases, tracking of the motion of individual points along the length of the cylinder is lost, hence the measured spanwise motions of some points on the cylinder is missing. Figure 36 indicates that at the reduced velocity of 6.06, cylinder 1 has both the cross-flow and in-line motion exhibiting a standing mode shape that is similar to a first mode as expected. At this reduced velocity, the cylinder exhibits an expected response both in cross-flow and in in-line direction similar to a first mode shape. These motions are consistent with the observed regular figure eight shape motion at this reduced velocity.

Figure 37 shows the spanwise response of the cylinder 1 for a higher reduced velocity of 6.74. Figure 37 indicates that at the reduced velocity of 6.74, cylinder 1 is oscillating similar to the oscillation at reduced velocity of 6.06. However, colors in the Figure 37 are thinner which indicates higher oscillation frequencies.

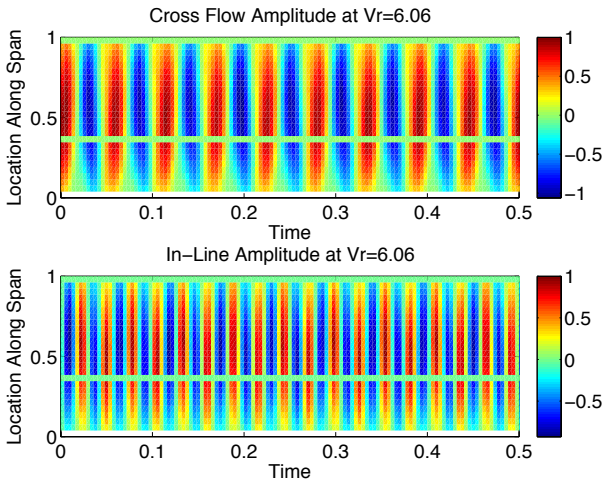

Figure 36 Span wise response of cylinder 1 for V_r=6.06. Colors indicate the magnitude of the amplitude response. Amplitudes indicate an excitation similar to the first mode in both in-line and cross-flow directions, but the dominant frequency is equal in both directions.

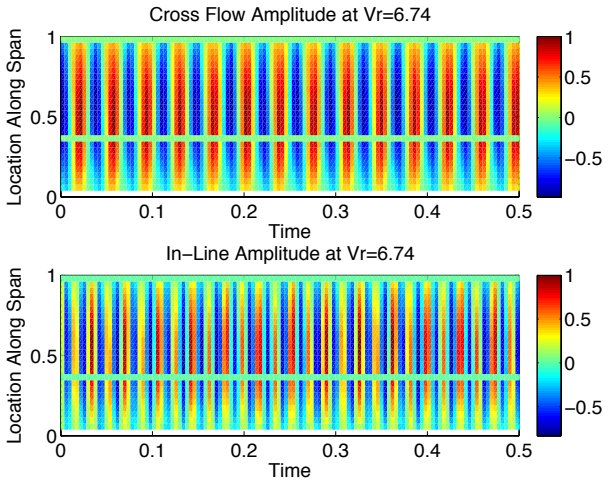

Figure 37 Span wise response of cylinder 1 for V_r=6.74. Colors indicate the magnitude of the amplitude response. Amplitudes indicate an excitation similar to the first mode in both in-line and cross-flow directions, but the dominant frequency is equal in both directions.

4.3.2 Cylinder 2 Spanwise Response

Cylinder 2 displays a strikingly different response than expected in the high-reduced velocities. In the original construction of the experiment, the system at cylinder 2 experiments was tuned to excite the first mode cross-flow, but second mode in-line.

Figure 38 shows the spanwise response of the cylinder 1 at a reduced velocity of 5.54. As observed in cylinder 1 experiments, Figure 38 indicates that at the reduced velocity of 5.54, cylinder 2 has both the cross-flow and in-line motion exhibiting a standing mode shape that is similar to a first mode. This is surprising as one can see that the in-line direction oscillates with twice the frequency of the cross-flow direction. At this reduced velocity, the cylinder exhibits an expected response in cross-flow, similar to a first mode shape; however, in the in-line direction, the cylinder is excited at the second mode frequency, yet takes on a mode shape similar to the first mode. These motions are consistent with the observed regular figure eight shape motion at this reduced velocity.

Figure 39 shows the spanwise response of cylinder 2 at a reduced velocity of 5.90. As shown in Figure 39, the cylinder oscillates primarily similar to first mode with an additional observation similar to second mode shape in cross-flow direction. In the in-line direction cylinder 2 oscillates with very small amplitude variation therefore less color change was observed.

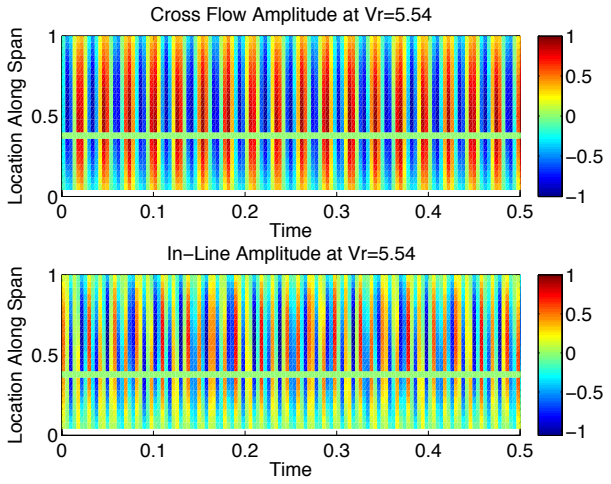

Figure 38 Span wise response of cylinder 2 for V_r=5.54. Colors indicate the magnitude of the amplitude response. Vertical lines of consistent color indicate a standing wave response with a mode shape similar to the first mode in both cross-flow and in-line directions, but the in-line frequency is twice the cross-flow frequency

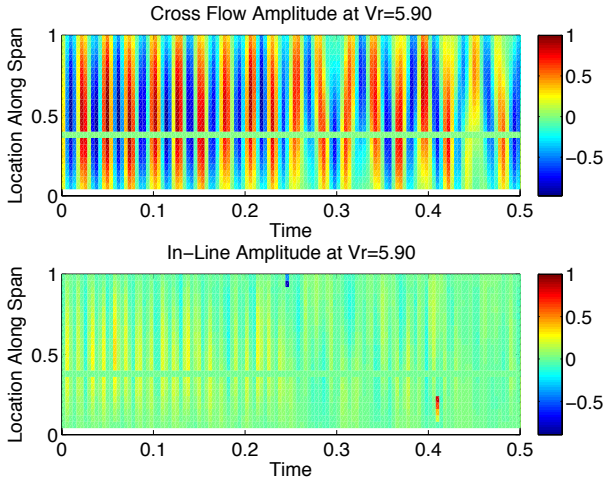

Figure 39 Span wise response of cylinder 2 for V_r=5.90. Colors indicate the magnitude of the amplitude response. Vertical lines of consistent color indicate a standing wave response with a mode shape similar to the first mode in cross-flow direction and very small oscillation in in-line direction, but the in-line frequency is twice the cross-flow frequency

Figure 40 shows the spanwise response of cylinder 2 for a higher reduced velocity of 6.45. As shown in Figure 27, the physical test velocity was regularly increased;

however, the response at a particular reduced velocity moved around significantly. For instance cylinder 2, did not display a response for reduced velocities between 6 and 6.45. Figure 40 shows the first response for the cylinder at the higher reduced velocity. The cross-flow amplitude at reduced velocities higher than 6.45 are less than at lower reduced velocities and the in-line amplitude becomes even smaller as reduced velocity increases. Between the reduced velocity 6.45 and 7, orbital motion is primarily in the cross-flow direction. The shedding frequency has increased with speed, such that the cross-flow direction exhibits an excitation of the second mode. The frequency response was observed to be near 35 Hz, close to the second mode natural frequency in the in-line direction. This is surprising because in the original construction of the experiment, the system was tuned to excite the first mode cross-flow, but second mode in-line. In addition, response snapshots have showed that cylinder 2 oscillates with second mode shape in cross-flow direction for reduced velocities larger than 6.45. However, at reduced velocity 6.45, the cylinder oscillates with some combination of first mode and second mode shape in cross-flow direction and with very small amplitude in in-line direction.

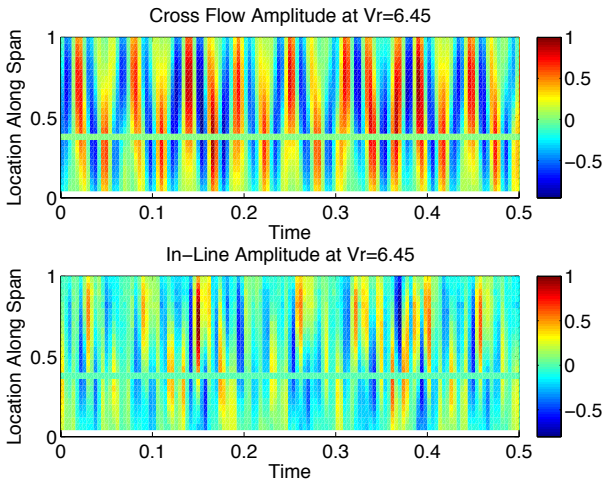

Figure 40 Span wise response of cylinder 2 for V_r=6.45. Colors indicate the magnitude of the amplitude response. Amplitudes indicate an excitation of the second mode in the cross-flow direction.

Figure 41 and 42 show the spanwise response of cylinder 2 for reduced velocity of 6.58 and 6.98. In comparison with response snapshot figures, analysis of the motion during the whole cylinder oscillation period showed a standing wave with some combination of first mode and second mode shape in cross-flow direction with large amplitude response, and in in-line direction with very small amplitude response. On the other hand, at higher reduced velocity of 6.98 cylinder spanwise response analysis showed that cylinder oscillates in both directions with second mode shape. At this motion the frequency response was observed to be near 36 Hz, close to the second mode natural frequency in the cross-flow direction.

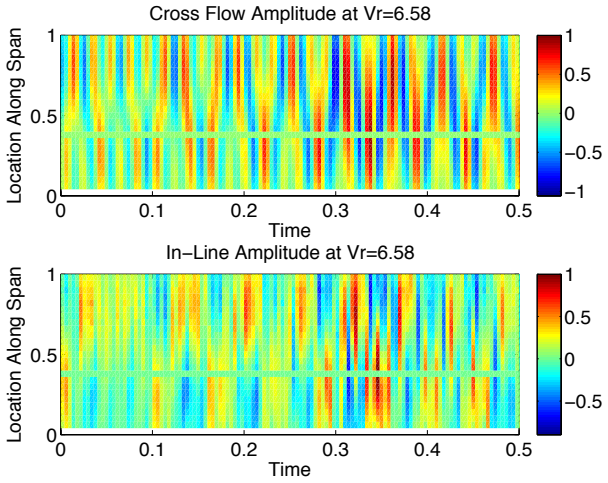

Figure 41 Span wise response of cylinder 2 for V_r=6.58. Colors indicate the magnitude of the amplitude response. Amplitudes indicate an excitation of the second mode in the cross-flow direction.

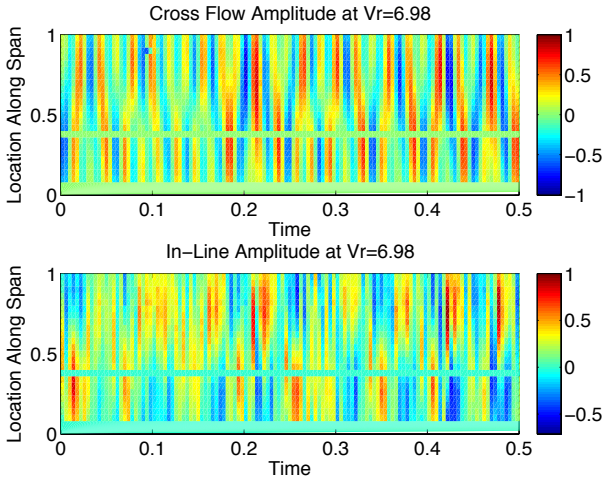

Figure 42 Span wise response of cylinder 1 for V_r=6.98. Colors indicate the magnitude of the amplitude response. Amplitudes indicate an excitation of the second mode in the cross-flow direction.

4.4 Frequency Response Analysis

Frequency response was investigated further for all reduced velocities tested for both Cylinder 1 and Cylinder 2 based on cylinder center point positions. Figure 43 shows the frequency spectra in cross-flow direction for cylinder 1 as a function of reduced velocity, normalized by the first natural frequency of the cylinder. For reduced velocities below 6, a typical condition of lock-in occurs, where the frequency of shedding matches the effective natural frequency (frequency of motion of the structure). Between a reduced velocity of 6 and 6.8, the response frequency begins to grow maintaining a figure eight orbital motion.

Figure 44 shows the frequency spectra in the in-line direction for the same cylinder. The spectrum indicates that the frequency response in the in-line direction continues to grow, maintaining a 2:1(in-line: cross-flow) frequency ratio. In in-line direction, for reduced velocities below 6, cylinder oscillates with twice natural frequency in cross-flow direction, and then gradually increases reaching up to four times natural frequency (in vacuum) in cross-flow ($4xf_{ny}$).

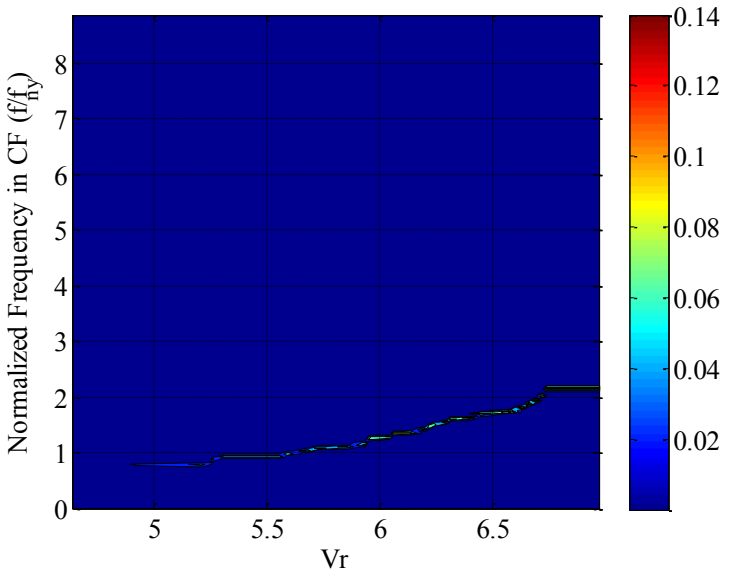

Figure 43 Frequency spectra for first mode cross-flow direction. Colors indicate the magnitude of the dominant frequency.

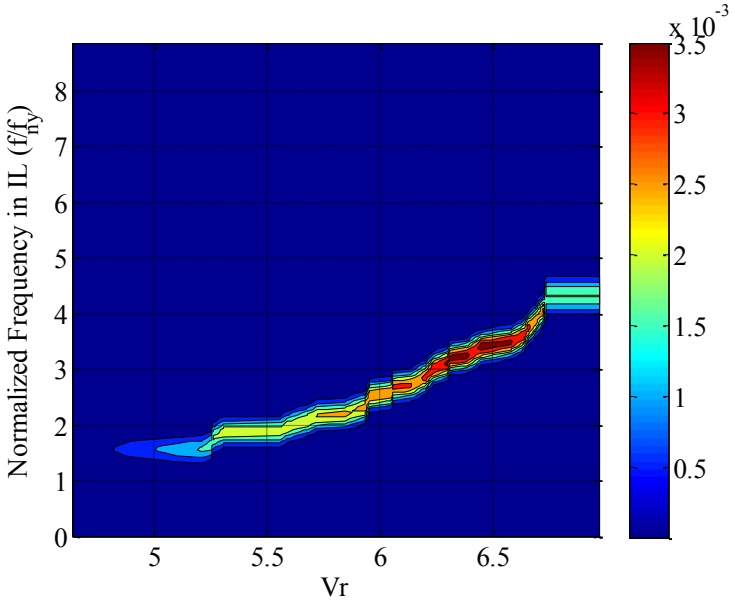

Figure 44 Frequency spectra for first mode in-line direction. Colors indicate the magnitude of the dominant frequency.

Figures 45 and 46 show the response frequency spectra for cross flow and in line directions for cylinder 2. Similar to cylinder 1, in-line dominant frequency is twice the cross-flow dominant frequency for tested reduced velocities. Figure 45 illustrates that

for the reduced velocities between 4.5 and 5.5 in cross flow direction, lock-in occurs where the observed frequency of motion is equal to the natural frequency of the structure. Between reduced velocities 5.5 and 6, both the frequency response in in-line and cross-flow direction continues to grow. After the reduced velocity of 6, the ratio of the oscillation frequency to the natural frequency in cross flow direction stabilizes as reduced velocity increases. In addition, Figure 46 shows that amplitude of the response motion also increases as the reduced velocity increases. It should also be noted that cylinder primarily oscillates with figure 8 shape until the reduced velocity value of 6 and then irregularities in the motion trajectory starts.

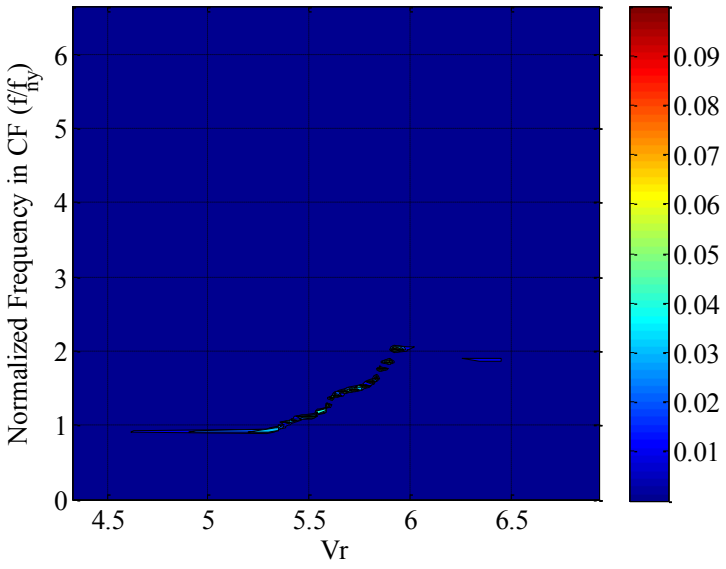

Figure 45 Frequency spectra for second mode cross-flow direction. Colors indicate the magnitude of the dominant frequency.

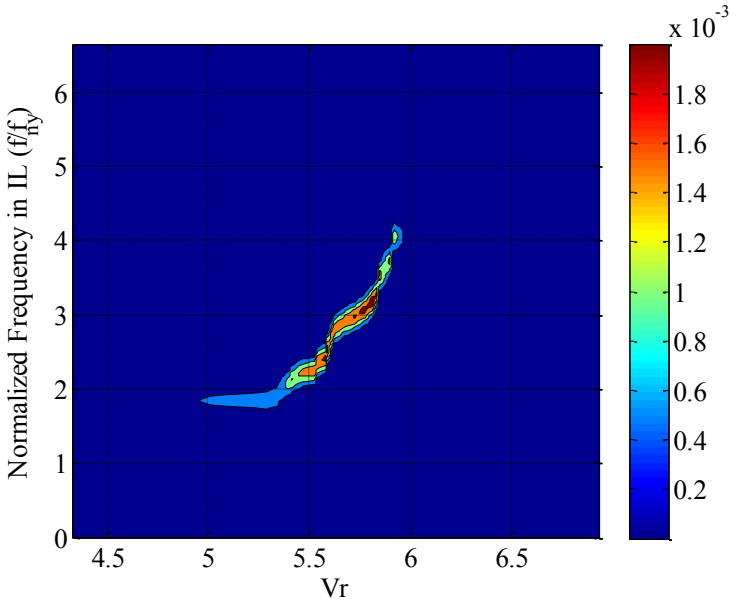

Figure 46 Frequency spectra for second mode in-line direction. Colors indicate the magnitude of the dominant frequency.

4.5 Time Dependent Frequency Analysis (Scalogram)

The frequency content of the motion at specific locations along the length of the cylinder for both cross-flow and in-line direction is shown in the Figures 47, 48, 49 and 50. Locations on the cylinder were chosen to be at L/4,L/2 and 3L/4. In addition to the scalogram plot, the power spectral density was illustrated on the left hand side of the scalogram for each analysis to show the dominant forces contributing to the motion. In addition, each raw signal was plotted on top of the scalogram figure to show the raw data trend over time.

Figure 47 shows the scalogram at the reduced velocity 6.74 for cylinder 1 where cylinder primarily oscillates with figure eight motion. Instantaneous frequency content of both in-line and cross-flow motions show relatively steady first harmonic components as a function of time.

Cross-Flow Direction

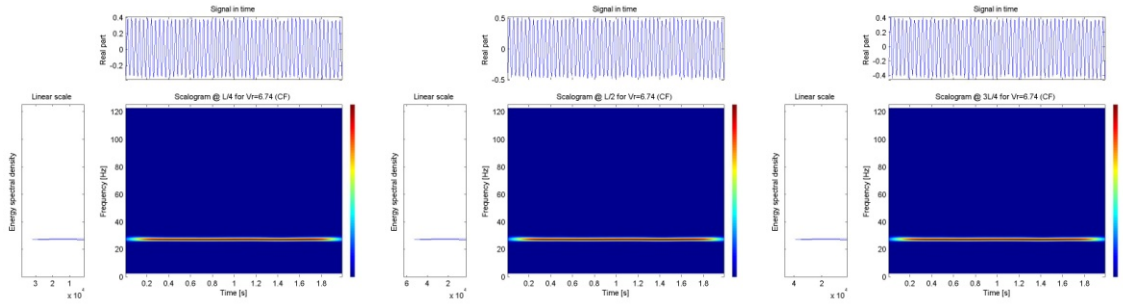

(a) $f/f_{ny}=2$, Vr=6.74 (b) $f/f_{ny}=2$, Vr=6.74 (c) $f/f_{ny}=2$, Vr=6.74

In-Line Direction

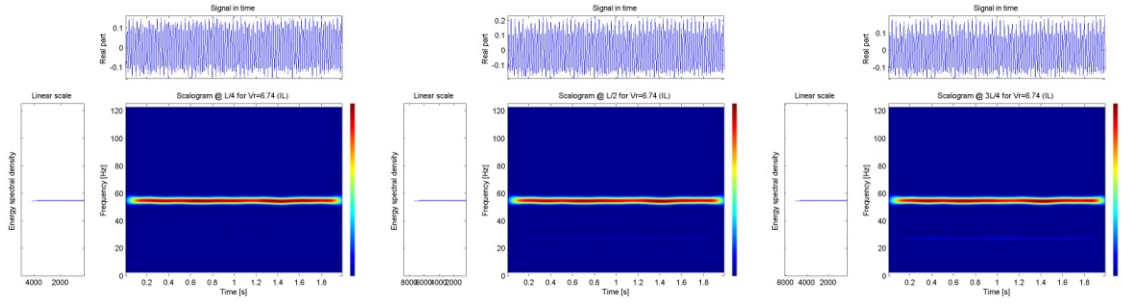

(d) $f/f_{nx}=4$, Vr=6.74 (e) $f/f_{nx}=4$, Vr=6.74 (f) $f/f_{nx}=4$, Vr=6.74

Figure 47 Cylinder 1, Scalogram showing instantaneous frequency components at Vr=6.74 for CF and IL directions. Colors indicate the magnitude of the dominant frequency.

Figure 48 shows the scalogram at the reduced velocity 5.54 for cylinder 2 where cylinder also primarily oscillates with figure eight motion. Instantaneous frequency content of both in-line and cross-flow motions show relatively steady first harmonic components as a function of time.

Cross-Flow Direction

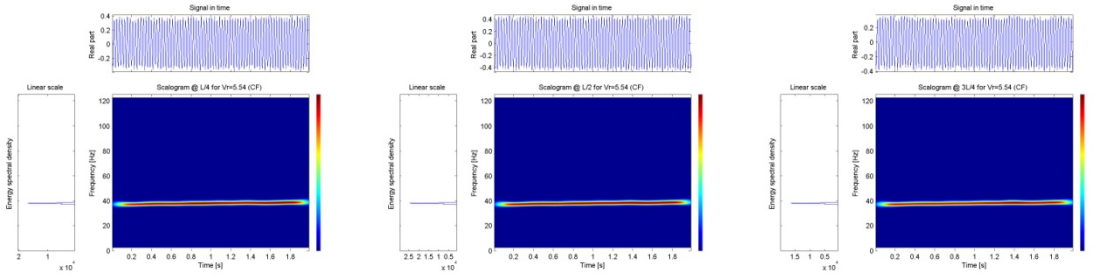

(a) $f/f_{ny}=1$, Vr=5.54 (b) $f/f_{ny}=1$, Vr=5.54 (c) $f/f_{ny}=1$, Vr=5.54

In-Line Direction

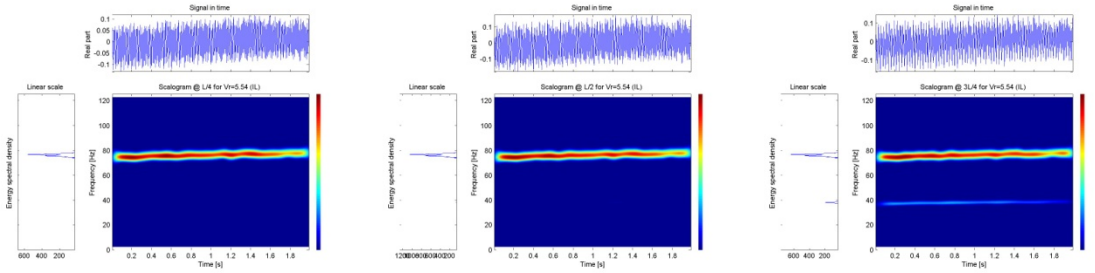

(d) $f/f_{nx}=2$, Vr=5.54 (e) $f/f_{nx}=2$, Vr=5.54 (f) $f/f_{nx}=2$, Vr=5.54

Figure 48 Cylinder 2, Scalogram showing instantaneous frequency components at Vr=5.54 for CF and IL directions. Colors indicate the magnitude of the dominant frequency.

At the reduced velocity of 6.45 cylinder starts to have second mode shape in cross-flow direction with very large amplitude and first mode shape in in-line direction with relatively smaller amplitude.

Figure 49 illustrates the scalogram at the reduced velocity 6.45 for cylinder 2 for both in-line and cross-flow directions along the length of the cylinder. In this particular motion, cylinder oscillates with sum combination of first mode and second mode shape in cross-flow direction with a large response amplitude, and first mode shape in in-line direction with a very small response amplitude. The power spectral density in the in-line direction shows that at center point of the cylinder, drag is dominated by its fourth harmonic, with a small contribution from the second harmonic. However, locations @L/4 and @3L/4, drag is dominated with its first

harmonic, and with a small contribution from fourth harmonic. On the other hand, for the same reduced velocity in cross-flow direction, lift is dominated with its second harmonic along the length of the cylinder.

Cross-Flow Direction

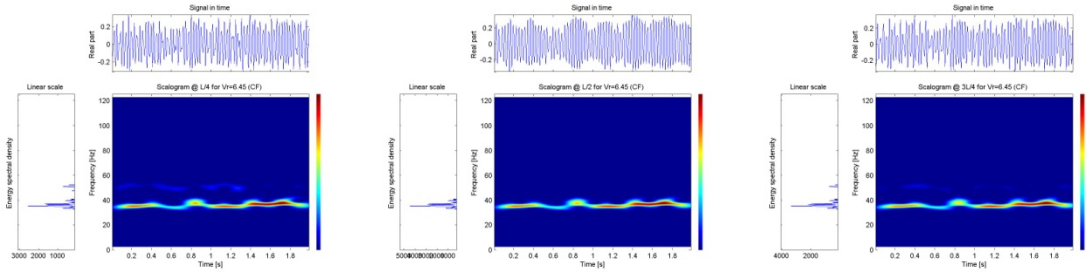

(a) $f/f_{ny}=2$, Vr=6.45 (b) $f/f_{ny}=2$, Vr=6.45 (c) $f/f_{ny}=2$, Vr=6.45

In-Line Direction

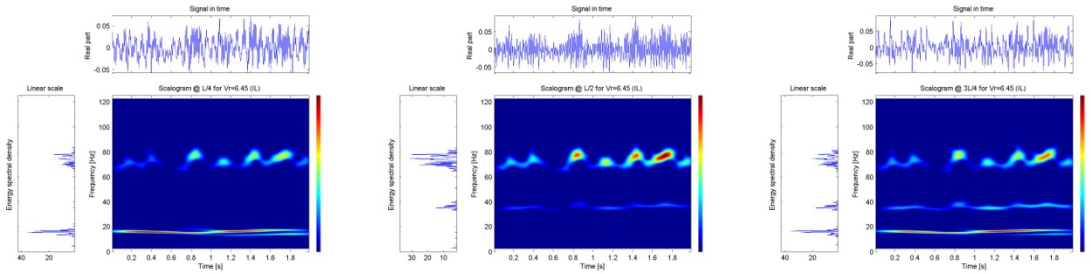

(d) $f/f_{nx}=1$, Vr=6.45 (e) $f/f_{nx}=4$, Vr=6.45 (f) $f/f_{nx}=1$, Vr=6.45

Figure 49 Cylinder 2, Scalogram showing instantaneous frequency components at Vr=6.45 for CF and IL directions. Colors indicate the magnitude of the dominant frequency.

At reduced velocity 6.58 (Figure 50) the cylinder purely oscillates with second mode shape in cross-flow direction with large response amplitude and first mode shape in in-line direction with very small response amplitude. Scalogram in cross flow direction shows relatively steady second harmonic components as a function of time with a small contribution from the third harmonic at cylinder locations L/4 and 3L/4. However, scalogram graph for in-line motion illustrates that fourth harmonic component is dominant at the center of the cylinder, but first harmonic component is dominant at cylinder locations L/4 and 3L/4.

Cross-Flow Direction

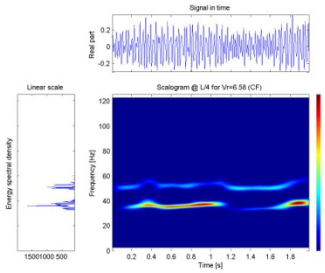

(a) $f/f_{ny}=2$, Vr=6.58

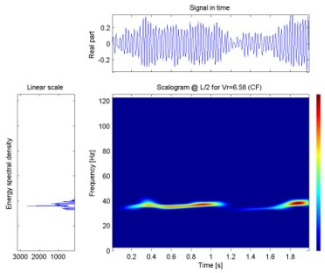

(b) $f/f_{ny}=2$, Vr=6.58

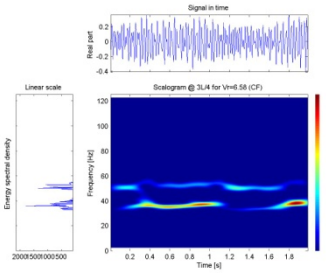

(c) $f/f_{ny}=2$, Vr=6.58

In-Line Direction

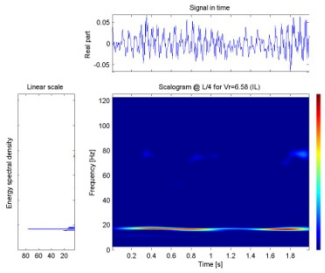

(d) $f/f_{ny}=1$, Vr=6.58

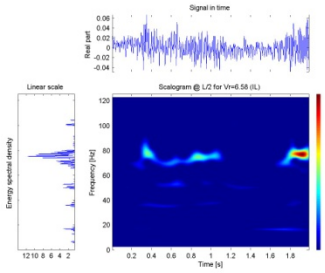

(e) $f/f_{ny}=4$, Vr=6.58

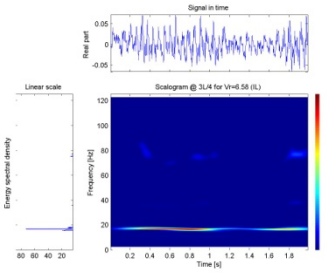

(f) $f/f_{ny}=1$, Vr=6.58

Figure 50 Cylinder 2, Scalogram showing instantaneous frequency components at Vr=6.58 for CF and IL directions. Colors indicate the magnitude of the dominant frequency.

In-line frequency component appears to cause second mode shape in cross-flow direction since frequency component in cross-flow direction is stable in time. The same phenomenon was observed at reduced velocity 6.45 where cylinder oscillates purely first mode in in-line direction and some combination of first mode and second mode in cross-flow direction. As this particular motion (Vr=6.45) contains the combination of two different modal responses (first mode and second mode), it has stronger fourth harmonic component at the center of the cylinder in in-line direction than reduced velocity 6.58. Yet still first harmonic components in the motion are dominant at locations L/4 and 3L/4 which may cause the second mode shape component in the motion.

4.6 Hydrodynamic Forces And Added Mass

In order to explain the unexpected results of cylinder 2 motion at higher reduced velocities, hydrodynamic forces needed to be investigated. For that reason, a rigid cylinder mounted on a force transducer was forced to move in small flow visualization tank with the exact motions observed for the center point of the flexible cylinder for a variety of runs. These experiments were carried out for various reduced velocities for both cylinder 1 and cylinder 2.

Force coefficients were calculated from force data obtained from those experiments. Calculated force coefficients are reported in Table 1 (cylinder 1) and Table 2 (cylinder 2).

Table 2 Computed Force Coefficients for three runs from forced motions replicating the response of cylinder 1.

		Run 1	Run 2	Run 3
V_r		5.16	6.06	6.74
C_{La}		-0.08	-0.08	-0.01
C_{my}		0.038	0.041	0.005
C_{mx}		0.066	0.056	0.051
C_{Lv}		-0.18	-0.018	-0.07
C_{Dv}		0.017	0.006	0.007
A_y*		0.91	1.17	1.53
A_x*		0.34	0.58	0.60
f (Hz)	In-line	20	36.14	54.70
	Cross-flow	9.8	18.07	27.35
Re		2030	4400	7400

Table 3 Computed Force Coefficients for three runs from forced motions replicating the response of cylinder 2.

		Run 1	Run 2	Run 3
V_r		5.54	5.59	5.83
C_{La}		-0.07	-0.075	0.0016
C_{my}		0.025	0.033	0
C_{mx}		-0.20	-0.0625	-0.095
C_{Lv}		0.005	0.0061	-0.39
C_{Dv}		-0.15	-0.039	0.039
A_y*		1.41	1.15	1.31
A_x*		0.41	0.46	0.46
f (Hz)	In-line	76.67	54.70	66.4
	Cross-flow	38.09	27.35	33.2
Re		8500	6200	7800

In table 2 and table 3, all motions correspond to figure eight motions for different reduced velocities. In table 2, the motions were selected in such a manner that the oscillation would occur just before the transition region where transition occurs from first mode to second mode in cross-flow direction for cylinder 2.

For cylinder 2 case, Table 3 shows that as Reynolds number increases frequency in both directions and amplitude in cross-flow direction (A_y*) also increase. On the other hand, amplitude in in-line direction does not increase along with Reynolds number. In contrast to cylinder 2 case, Table 2 (cylinder 1) shows that as Reynolds number increases, corresponding reduced velocity, amplitudes in in-line and cross-flow direction, as well as the frequency in both directions increase.

4.7 Flow Visualizations

A preliminary investigation of the wake is performed to indicate how the wake changes with figure eight motions of the cylinder.

4.7.1 Validation of DPIV Experiments

In order to validate the experiments and set-up the processing routine; two different flow visualization experiments were replicated from Morse and Williamson (2009) as shown in Figure 51. The replicated motions:

1. 2S mode regime is replicated at A*=0.5 and Vr=5.0 (Figure 51, c)
2. 2P mode regime is replicated at A*=0.6 and Vr=6.4 (Figure 51, d)

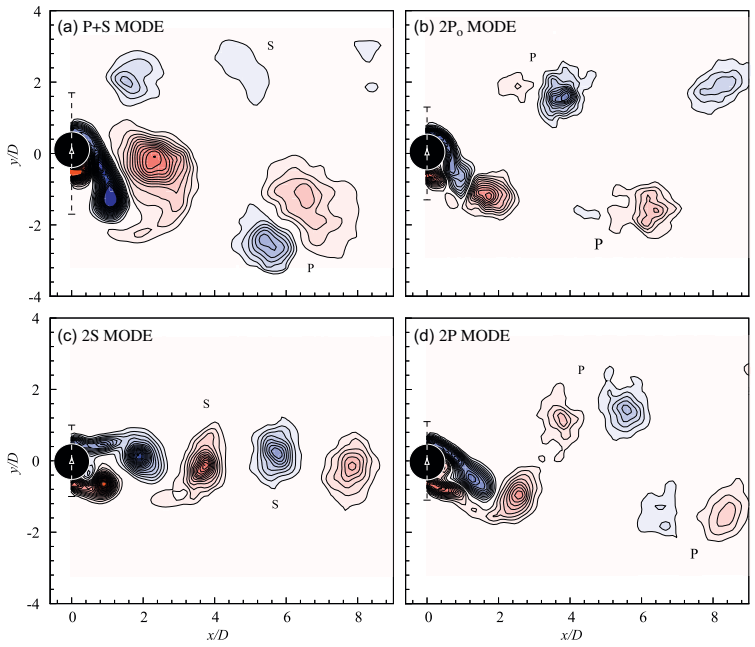

Figure 51 Vorticity fields for each of the main vortex shedding modes P+S, 2S, 2P and 2Po. Cylinder is moving right to left. (c) and (d) shows the original wake modes of replicated motions defined by Morse and Williamson (2009)

DPIV method in the horizontal plane provides a clear picture of two distinct shedding modes along the cylinder where cylinder is moving right to left.

Figure 52 shows the wake mode at non-dimensional amplitude of 0.5 and reduced velocity value of 5.0. Results are similar to the results of Morse and Williamson (2009) where the resulting 2S pattern can be clearly observed. Similarly, Figure 53 shows the wake mode at non-dimensional amplitude of 0.6 and reduced velocity value of 6.4 with a resulting 2P wake pattern similar to Morse and Williamson (2009). In these figures colors indicate the power of the vortices, and different colors (blue and red) indicate the vortices in opposite directions.

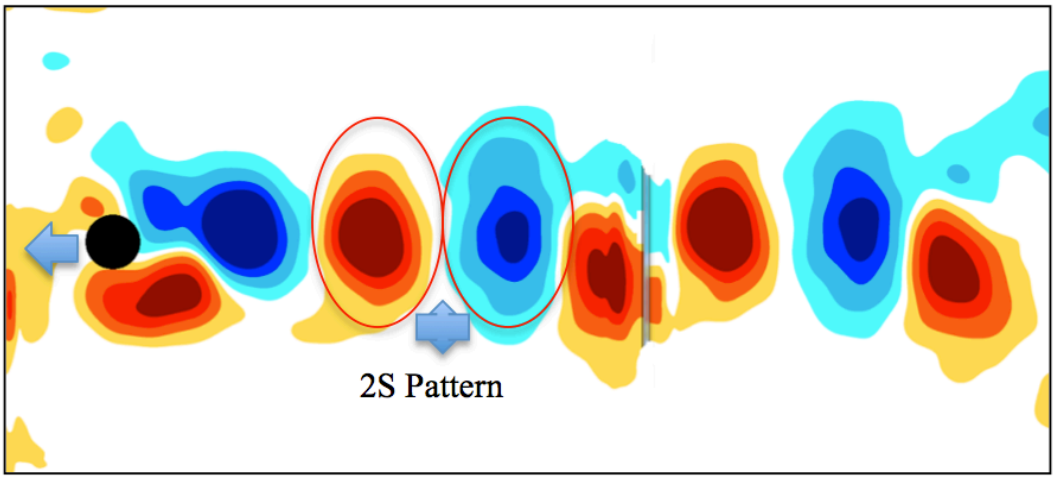

Figure 52 Replicated 2S Pattern. Colors show vorticity.

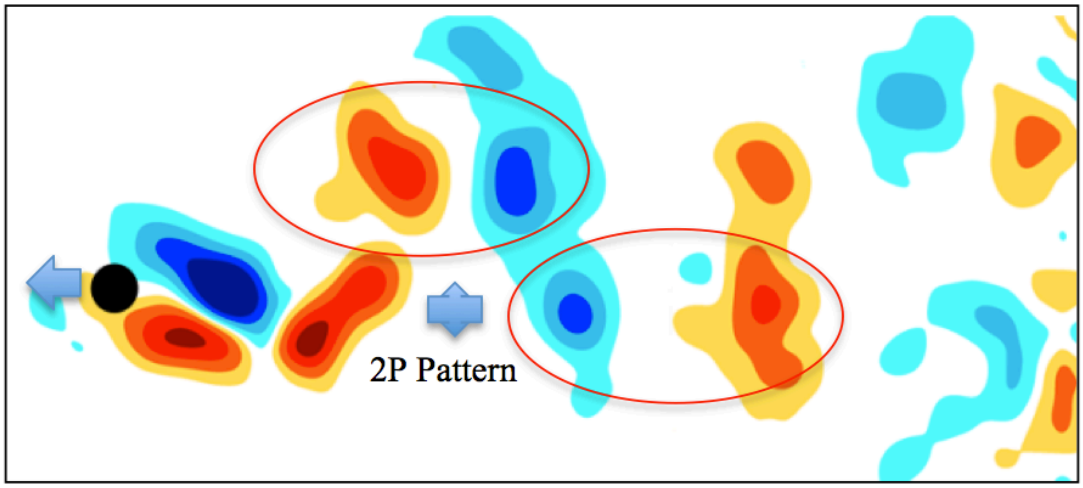

Figure 53 Replicated 2P Pattern. Colors show vorticity.

4.7.2 Cylinder 1 Flow Visualizations

Three flow visualization experiments have been conducted for increasing reduced velocity values where cylinder is moving left to right in those experiments. Figures show the snapshot in the wake of the cylinder for the same three reduced velocities for which forces were calculated. The figures between 54 and 56 show that there is periodic vortex shedding to each side of the cylinder and symmetry in the wake is conserved as the response amplitude increases.

Figure 54 shows the wake pattern behind the cylinder 1 at reduced velocity value of 5.16 and non-dimensional amplitude of 0.91. In this motion cylinder oscillates with traditional figure eight motion. It was observed that the wake pattern associated with the cylinder motion resembles 2S wake mode as denoted by Williamson and Roshko (1988).

Figure 55 shows the flow visualization at reduced velocity value 6.06 and non-dimensional amplitude 1.17 where cylinder oscillates also with figure eight motion. The resulting wake mode does not resemble any of the wake modes presented in Williamson and Roshko (1988) and Morse and Williamson (2009).

Figure 56 shows that, when the cylinder oscillates with non-dimensional amplitude 1.53 at reduced velocity 6.74, wake pattern resembles to 2T mode, where two triplet of vortices shed per cycle of oscillation.

In conclusion, there is a clear transition to the wake as reduced velocity increases and the response of the cylinder changes from the figure eight shape to straight-line shape.

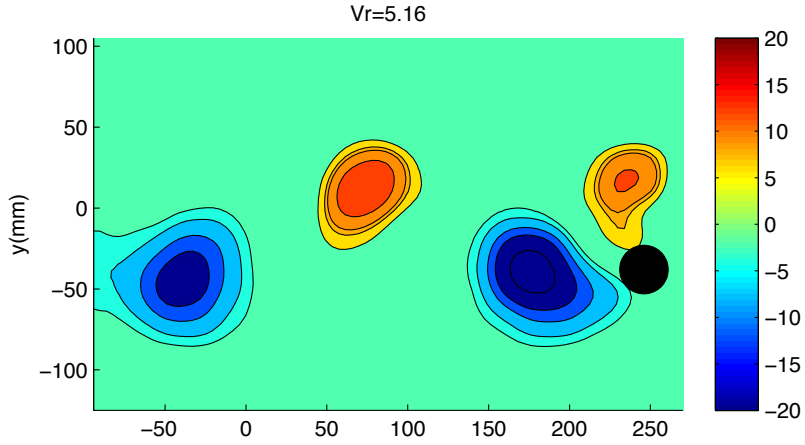

Figure 54 Wake pattern at Vr=5.16, A*=0.91. Colors show vorticity.

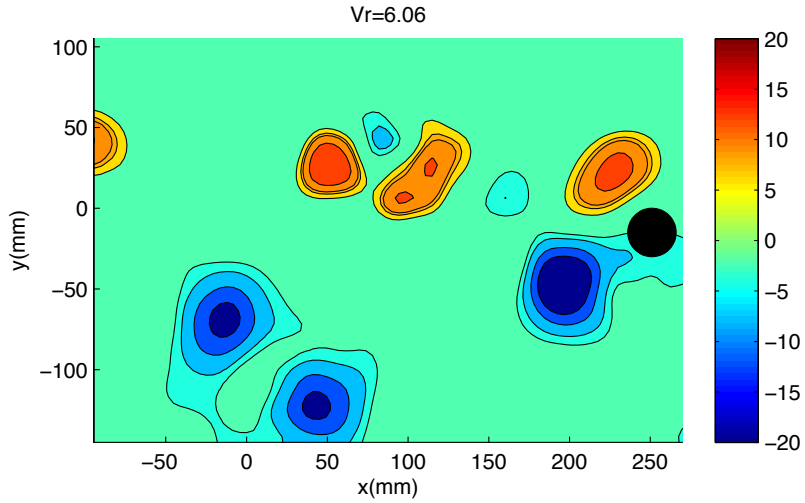

Figure 55 Wake pattern at Vr=6.06, A*=1.17. Colors show vorticity.

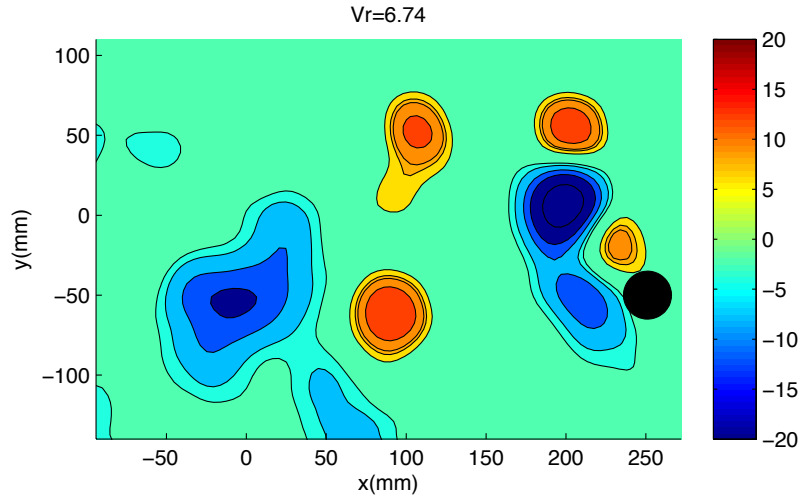

Figure 56 Wake pattern at Vr=6.74, A*=1.53. Colors show vorticity.

4.7.3 Cylinder 2 Flow Visualizations

Figures 57, 58, and 59 show the wake modes of cylinder 2 for the same three reduced velocities for which forces were calculated.

In particular, wake mode at reduced velocity 5.54 resembles 2Po mode as shown in Figure 57. In this particular motion, two pair of vortices shed per cycle as denoted by Williamson and Roshko (1988) where one vortex is stronger than its counterpart in the opposite direction. It should be noted that cylinder motion at reduced velocity 5.54 is the motion right before cylinder trajectory becomes irregular. Therefore it was anticipated that with the observed symmetric motion of the figure eight shape, that the wake would display symmetry as well.

With the same assumption such that figure eight motion produces regular wake pattern behind the cylinder, it was expected to have regular motions for the other reduced velocities as well. However, in addition to the previous wake mode, it was observed in Figure 58 that vortices did not separate from each other and generated long tails that connect the vortices and at highest reduced velocity of 5.84 more irregularities in the wake was observed as shown in Figure 59.

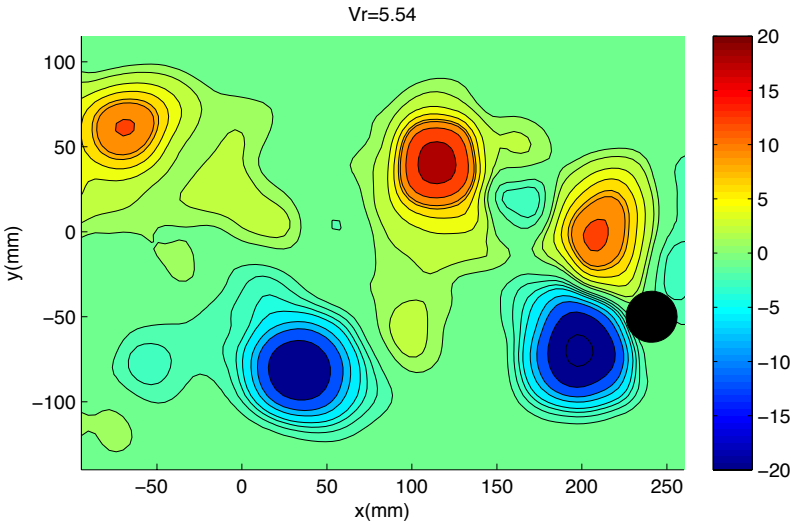

Figure 57 Wake pattern at Vr=5.54, A*=1.41. Colors show vorticity.

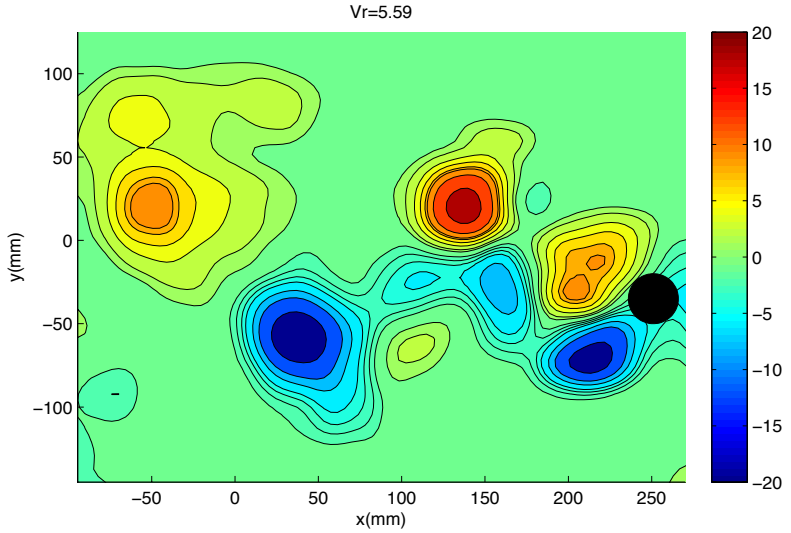

Figure 58 Wake pattern at Vr=5.59, A*=1.15. Colors show vorticity.

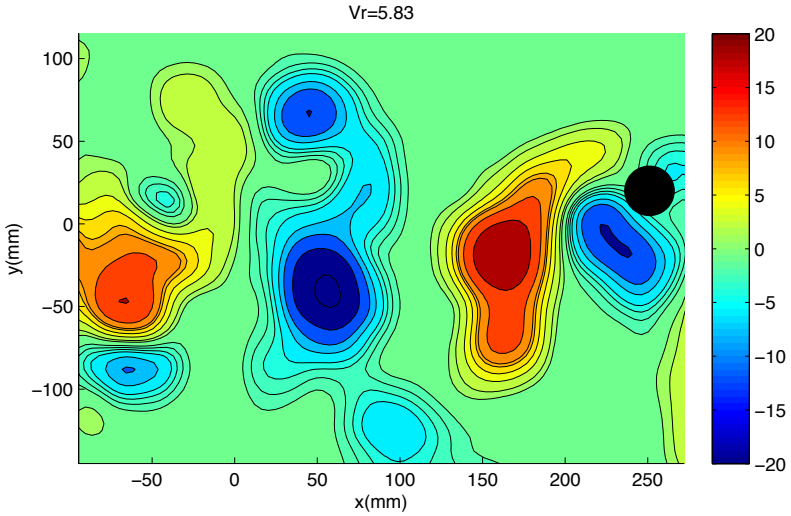

Figure 59 Wake pattern at Vr=5.83, A*=1.31. Colors show vorticity.

To summarize, orbital shapes observed in different cylinder experiments led to interesting results such that:

1. Cylinder 1 experiments done for validation with Dahl (2008), and results showed a delay in reduced velocities possibly because of having different mass ratios.
2. Vr-A* figure for cylinder 1 (Figure 23) indicates that cylinder amplitude response is gradually increasing without any drop but for a free vibration it is expected to have fluctuations in the response amplitudes.
3. Low mass ratio flexible cylinder experiments showed higher amplitude responses than low mass ratio rigid cylinder experiments done by (Dahl et al. (2006), Kang et al. (2013), Huera-Huerta et al. (2014)).
4. Cylinder adjusted to have second mode shape in in-line direction and first mode shape in cross-flow direction moves with first mode in-line and second mode cross-flow direction. In other words, first mode shape with second mode frequency was obtained.
5. At cylinder 2 experiments, added mass coefficient in in-line direction was found to decrease as cylinder trajectory in in-line direction changed from first mode to second mode (mode mixing). Interestingly added mass coefficient in cross-flow direction was not effected much.
6. Fluctuating drag in phase with velocity (C_{dv}) at cylinder 2 experiments are consistent with a possible forced oscillation in the in-line direction.
7. Scalogram analysis (cylinder 1 and 2) for selected reduced velocities confirmed the irregularities in in-line direction along the length of the cylinder.

8. Different from one degree of freedom vortex map, flow visualizations of cylinder 1 and cylinder 2 experiments showed that results are shifted in the direction of increasing added mass and normalized amplitude values.
9. In the flow visualizations of cylinder 1 experiments periodic vortex shedding is obtained which is consistent with observed orbital patterns.
10. In cylinder 2 flow visualizations, it was anticipated that with the observed symmetric motion of the figure eight shape the wake would display symmetry as well. However, it is shown that asymmetry in the wake increases as the reduced velocity increases.

CHAPTER 5

DISCUSSION

Cylinder 1 experiments were designed to have 1-1 mode shape (first mode in-line and first mode cross-flow direction) by keeping the in-line to cross flow frequency ratio 2:1. Cylinder responses for linearly increasing incoming fluid velocities compare well with the previous studies Dahl et al. (2006, 2007, 2010). In all these experiments the cylinder was moving primarily with figure eight shape even though the response amplitudes were different. The mass ratio range in the experiments Dahl et al (2006) conducted was between 3 and 6, Reynolds number ranged from 11,000 to 60,000, and aspect ratio was 26. However, in the present study the mass ratio is reported as being close to ~1. It is thought that having very small mass ratios (close to critical mass ratio ~0.5) may alter the cylinder response amplitude. In addition, it is interesting that the results of the experiments conducted by Dahl et al (2006) look like more free vibration experiments in that cylinder response amplitudes do not increase linearly as flow speed increases; likewise in this study it was expected to have amplitude variations. However, it was observed that cylinder 1 response amplitudes increased linearly as flow speed increased. It is also thought to be the effect of mass ratio difference between those two experiments. The results of the cylinder 1 experiments indicate that when the same odd mode is excited in each direction for the beam, it results in large response motions.

In the case of cylinder 2, it was expected that it would have an irregular response since cylinder will have trouble exciting the in-line mode due to the fact that the

experiments were designed to have second mode shape in in-line and first mode shape in cross flow direction. Instead, it was observed that when cylinder reached the second mode frequency, surprisingly it oscillated in in-line direction with second mode frequency that matches the second mode frequency in in-line direction; however, modal shape looked like a first mode. The most important question here is: Why is it exciting the first mode shape instead of the second mode shape in in-line direction when second mode frequency is excited?

Vandiver and Jong (1987) conducted cable strumming experiments at Castine, Maine in 1981 and from an icebreaker in 1983 in order to study the vibration characteristics of long flexible cylinders subjected to vortex-induced oscillation. They obtained similar results to the cylinder 2 results that were obtained in this study. For example, in one case they found that although the drag force fluctuations were at the natural frequency of the fourth in-line mode, the dominant modal force corresponded to the third mode. Vandiver and Jong (1987) explain this phenomenon saying:

> Under lock-in conditions the shedding of vortices over the entire cylinder is essentially simultaneous, independent of the cross-flow mode shape. Regardless of the symmetry of the cross-flow mode shape with respect to the center of the cylinder, the in-line drag force fluctuations are symmetrically distributed. Therefore, the in-line modal force for all even-numbered modes is zero.

This explanation and findings prove the idea that cylinder 2 oscillation is a forced oscillation rather than a free vibration where cylinder behaves like a forced oscillation

so that it takes on the first mode forcing the first mode and move with the particular frequency. In this case, that frequency is the frequency of the second mode shape.

An illustration of this case can be seen in Figure 60 which also resembles the cylinder 2 case in this study where the drag force fluctuations are at the natural frequency of the second in-line mode (an anti-symmetric mode), the dominant modal force corresponds to the first mode (a symmetric mode). In other words, in cylinder 2 experiments it is observed that when the cylinder reaches the second mode frequency, it oscillates in in-line direction with first mode frequency that matches the second mode frequency in in-line direction; however, modal shape looks like a first mode.

In Figure 60, applying a uniformly distributed harmonic loading with zero damping along the entire length of the cylinder reveals following results: (i) First mode is obtained when first mode is desired to excite in in-line direction (a.1 and b.1 in Figure 60), (ii) a new mode which is similar to first mode is obtained when second mode is desired to excite in in-line direction (a.2 and b.2 in Figure 60), and finally (iii) third mode is obtained when third mode is desired to excite in in-line direction (a.3 and b.3 in Figure 60).

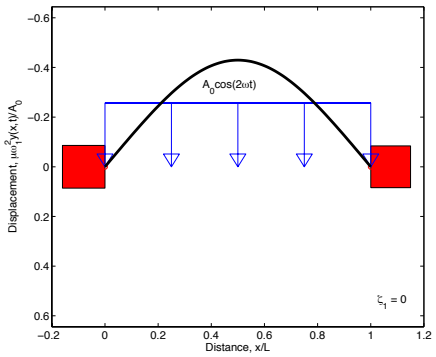

a 1 First mode shape applied with uniform load along the length of the cylinder (n=1)

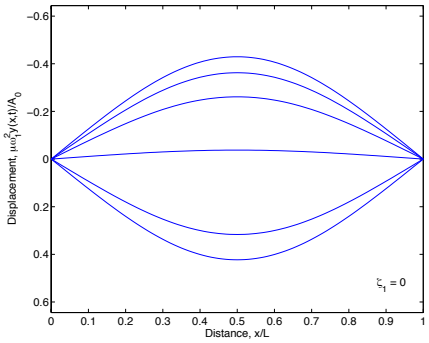

b 1 Response snapshot of the first mode case

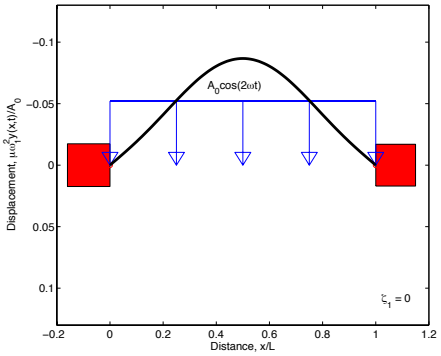

a 2 Second mode shape applied with uniform load along the length of the cylinder (n=4)

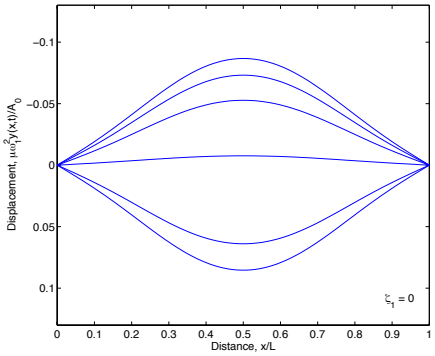

b 2 Response snapshot of the second mode case

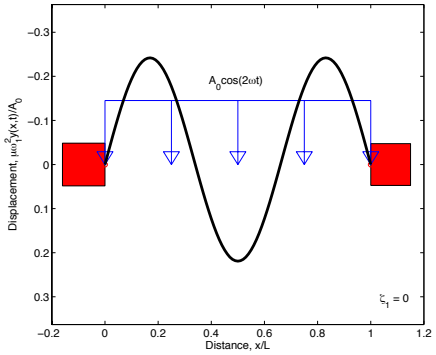

a 3 Third mode shape applied with uniform load along the length of the cylinder (n=9)

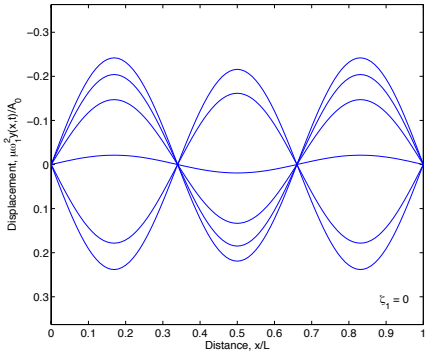

b 3 Response snapshot of the third mode case

Figure 60 An illustration of cylinder response of 1-3 modes applying uniformly distributed harmonic loading along the entire length of the cylinder.

However, these illustrations are not fully representative of these experiments. Because, this is assuming that in-line motions are completely uncoupled from cross-flow motions; in reality they are not. So, second mode in in-line direction may not even exist for the system that we have because the modal shape of a simply supported beam is typically defined for a structure oscillating with harmonic motion in a vacuum; in a dense fluid like water, added mass can alter the oscillating frequency and may cause the change in vortices. In other words, the fluid and structure together define the oscillation modes.

In order to see the possible contributions of hydrodynamic forces to the wake, force measurements have been done along with the rigid cylinder experiments. Force measurements for cylinder 1 showed that, added mass coefficients in both directions are close to zero ($C_{mx} \approx 0, C_{my} \approx 0$) which means the contribution of the added mass to the system is neglible for the single point at the center. Therefore, no correlation can be made for increasing Reynolds number or reduced velocity values.

In addition, some scatter appears in the response of cylinder 2 near a reduced velocity of 5.6, 5.8 and 6.5. This scatter may be attributed to multiple structural mode excitation or multiple wake mode excitation, where the wake may exhibit high or low amplitude excitations depending on the formation of the wake (Morse and Williamson, 2009). Wake visualizations were not performed for all these particular runs, so conclusive arguments about the scatter of the response in this region may not be made without further study of the wake.

In vortex-induced vibration, fluid forces will cause excitation or dissipation of motion depending on the flow of power in the system. If the system has very little

damping, C_{lv} (refers to lift coefficient in phase with velocity) and C_{dv} (refers to drag coefficient in phase with velocity) values should be close to zero in a free vibrating system and be positive. In other words, the energy through fluid forcing must balance energy due to damping, resulting in a steady-amplitude periodic oscillation. In addition, if C_{dv} is large and positive that implies that fluid is providing energy to the cylinder to make it vibrate. On the other hand, C_{dv} is large and negative implies that there is coupling between in-line and cross-flow direction and system is similar to forced motion system. Force coefficient table (Table 3) showed that for cylinder 2 case, there was a large negative C_{dv} value with ~-0.15 in comparison with other cases examined. This result supports the theory that because of the coupling between in-line and cross-flow motion, the cylinder vibrates. It was also found that at higher Reynolds number value of ~8500, added mass in cross-flow direction was found to be close to zero but added mass in in-line direction was found to be large and negative. Scalogram analysis also showed some irregularities at this motion, such that in some cases cylinder 2 was not oscillating with constant frequency in in-line direction during the oscillation period. Therefore, the result of the scalogram plots also support the idea that added mass in in-line direction alters the cylinder 2 oscillation frequency, and forces the cylinder to vibrate in cross-flow direction with second mode shape. In other words, it can be said that cylinder 2 oscillating in cross flow direction is driving the excitation in in-line direction.

Although the force measurements show that there can be a significant variation in the added mass in the in-line direction and the wake visualization shows that there is a particular wake pattern associated with the cylinder's motions, these experiments were

only performed for the midpoint motions of the cylinder. It is necessary to expand the visualization and force measurement along the length of the cylinder to show whether there is a phase shift in vortex shedding to accommodate an alteration in the fluid forcing that would allow for the observed mode shape. It is important to note that since the structure is oscillating in water, there is no necessity that the structure vibrates with the same mode shape as in a vacuum since we must consider that the mode consists of both the structural motions and fluid motions in the wake, hence it may be necessary to characterize the mode of the vibration by both the shape of the structure and the form of the wake.

Cylinder 3 experiments were designed to have 1-3 mode shape (first mode cross-flow and third mode in-line direction) by keeping the in-line to cross-flow frequency ratio 2:1. As expected, the design of another symmetric mode in the in-line direction caused regular and periodic patterns along the length of the cylinder for each flow speed tested. In addition, Figure 28 showed that there was a dramatic jump in the response amplitude values between the reduced velocity values of 5 and 6. These results are consistent with the study of (Khalak and Williamson (1999), Govardhan and Williamson (2000), Jauvtis and Williamson (2004)) where they also observed a sharp jump in the response amplitudes for low mass ratios (m*=2.6).

Finally, in flow visualization experiments, the wake was observed for center point of the cylinder for selected reduced velocity values. Cylinder 1 experiments clearly indicate that as reduced velocity increases vortex regime transfers from 2S wake mode to 2T. In the case of cylinder 2, at Vr= 5.54, wake pattern looks like a 2P* pattern, and as the reduced velocity increases instabilities are observed in the wake. These results

are different from equivalent one-degree of freedom system VIV results, and, therefore, it is impossible to make a relevant comparison with the literature.

CHAPTER 6

CONCLUSIONS AND RECOMMENDED FUTURE WORK

6.1 Conclusions

This study illustrates the complex nature of vortex-induced vibrations for flexible bodies. The original purpose of this experiment was to evaluate the effect of mode shape on the vibration of the structure; however, the results show that it is difficult to isolate this effect as the cylinder can easily be excited with different combinations of modes. It is shown that for the low-mode number beams tested, there are three primary responses possible for the cylinder when trying to excite the first mode in the cross-flow direction and first mode in the in-line direction (cylinder 1), first mode in the cross-flow direction and the second mode in the in-line direction (cylinder 2), and first mode in the cross-flow direction and the third mode in the in-line direction (cylinder 3). The first response consists of an expected excitation of the first mode cross-flow with an excitation of the first mode frequency in in-line direction; however, non-dimensional amplitude response showed a linear relationship between reduced velocity and non-dimensional amplitude different than literature.

The second response (cylinder 2) consists of an expected excitation of the first mode cross-flow with an excitation of the second mode frequency in in-line direction; however, the structural shape resembles the first mode shape. Vandiver and Jong (1987) explain this phenomenon saying if a taut cylinder oscillates with sinusoidal mode shape under lock-in conditions, and since the in-line drag force fluctuations are symmetrically distributed along the entire length of the cylinder, the in-line modal

force for all even-numbered modes is zero. The response in this case is characteristic of a figure eight response of the cylinder.

In cylinder 3 experiments, two different responses as crescent and figure eight patterns were obtained. In this case, higher flow speeds could not be reached so third mode shape in the in-line direction could not be obtained.

Independent force measurements of cylinder 1 and cylinder 2 confirm that the figure eight motion is capable of producing hydrodynamic forces to allow structural vibration in this form. Therefore, the situation is found to be a result of a forced oscillation rather than a free vibration. In addition, large added mass change in in-line direction right before spatial mode change from first mode to second mode also supports the idea that added mass may alter the oscillation frequency and change the spatial shape.

The wake visualization of cylinder 2 indicates that this mode of vibration is consistent with an asymmetric wake shedding pattern. Further studies are necessary to evaluate how the transition to each response is defined. In addition, since added mass may change along the length of the cylinder, wake pattern needs to be observed three dimensionally.

6.2 Recommended future work

1. Investigating the fluid forces along the span length for each cylinder case will give more information about the cylinder modal response and certainly provide more insight into the nature of the two-degree-of-freedom vortex induced vibration.
2. In addition, flow visualization experiments should also be conducted three dimensionally because added mass may change along the length of cylinder.
3. Investigating additional modes also help to understand the effect of mode shape, and cylinder responses at higher modes will possibly be interesting (actual physical structures in the ocean have large mode numbers).
4. Because of the limitations of the experimental setup, higher Reynolds numbers could not be examined. It is necessary to extend the experiments for higher Reynolds numbers.
5. Creating a two-degrees-of-freedom map of vortex regime will certainly help to understand the nature of the VIV.

APPENDICES

APPENDIX A

A.1 Recirculating Flow Channel Flow Speeds

Flow speed was measured using flow meter with and without the assembly placed in the water channel.

Motor Hz	Flow velocity without the assembly (m/s)	Flow velocity with the assembly (m/s)
1	0,01	0,01
2	0,0275	0,04
3	0,05	0,06
4	0,06625	0,08
5	0,08	0,1
6	0,1	0,12
7	0,12	0,15
8	0,13375	0,175
9	0,15	0,2
10	0,17	0,225
11	0,1875	0,25
12	0,2025	0,273
13	0,22	0,295
14	0,24	0,32
15	0,2525	0,345
16	0,27375	0,375
17	0,2925	0,395
18	0,30875	0,42
19	0,325	0,44
20	0,345	0,465
21	0,3625	0,493
22	0,38125	0,52
23	0,3975	0,55
24	0,4175	0,58
25	0,43875	0,607
26	0,45875	0,638
27	0,47875	0,663
28	0,4975	0,695
29	0,51625	0,72
30	0,53625	0,75
31	0,555	0,78
32	0,57375	0,81

33	0,5925	0,84
34	0,6125	0,87
35	0,6325	0,90
36	0,65125	0,94
37	0,675	0,97
38	0,69375	1,02
39	0,71375	1,07
40	0,73375	1,12
41	0,755	1,17
42	0,775	1,23
43	0,7975	1,28
44	0,8175	1,34
45	0,84125	1,39
46	0,86375	1,44
47	0,885	1,48
48	0,90625	1,51
49	0,93375	1,54
50	0,9575	1,57
51	0,98125	-
52	1,00375	-
53	1,03	-
54	1,05375	-
55	1,075	-
56	1,09875	-
57	1,1225	-
58	1,14	-
59	1,16	-
60	1,1775	-

APPENDIX B

B.1 Cylinder 1 Response Snapshots

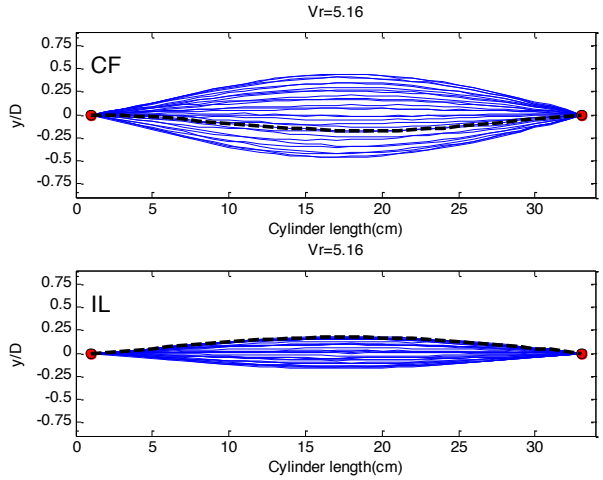

Figure B.1. 1 Response Snapshot at Vr=5.16 in CF and IL

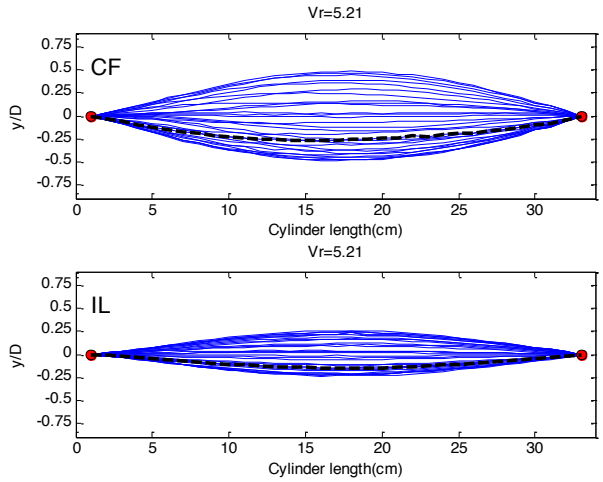

Figure B.1. 2 Response Snapshot at Vr=5.21 in CF and IL

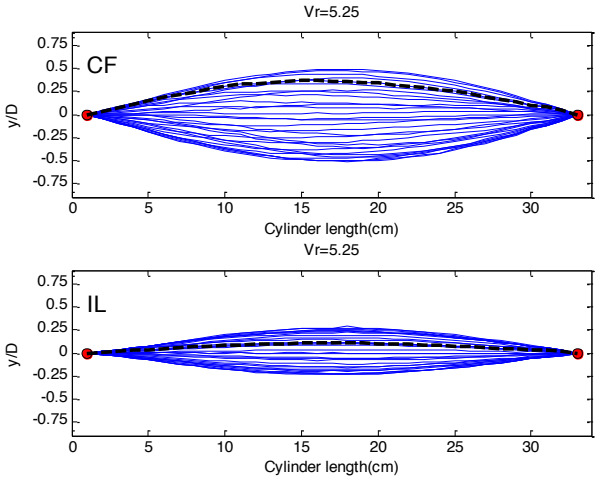

Figure B.1. 3 Response Snapshot at Vr=5.25 in CF and IL

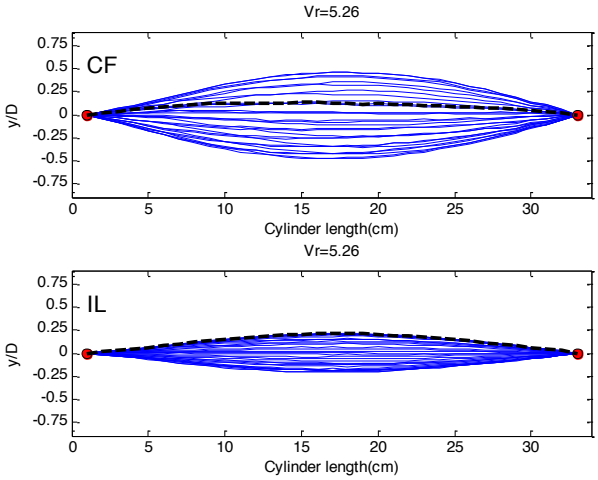

Figure B.1. 4 Response Snapshot at Vr=5.26 in CF and IL

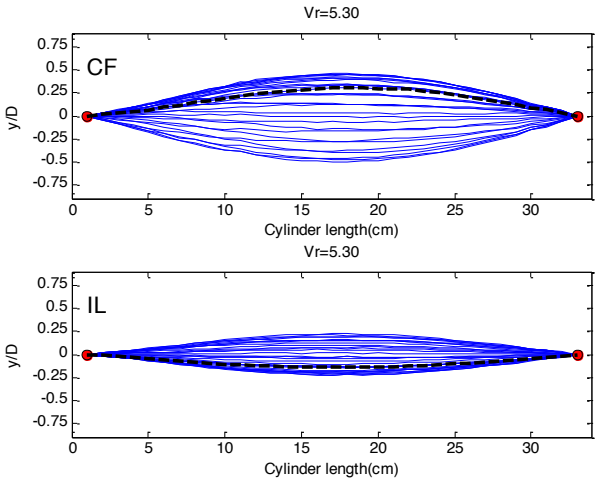

Figure B.1. 5 Response Snapshot at Vr=5.30 in CF and IL

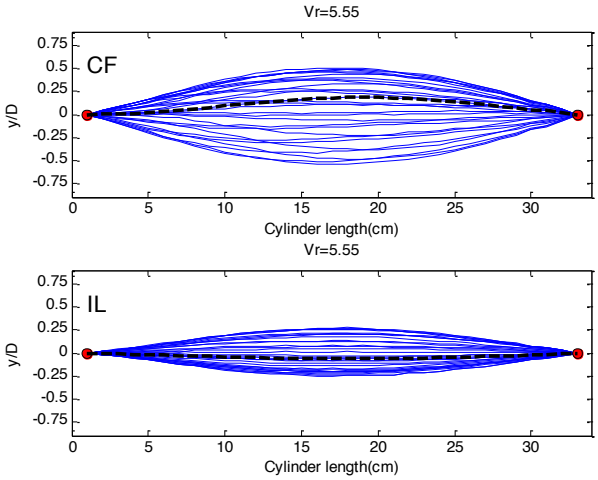

Figure B.1. 6 Response Snapshot at Vr=5.55 in CF and IL

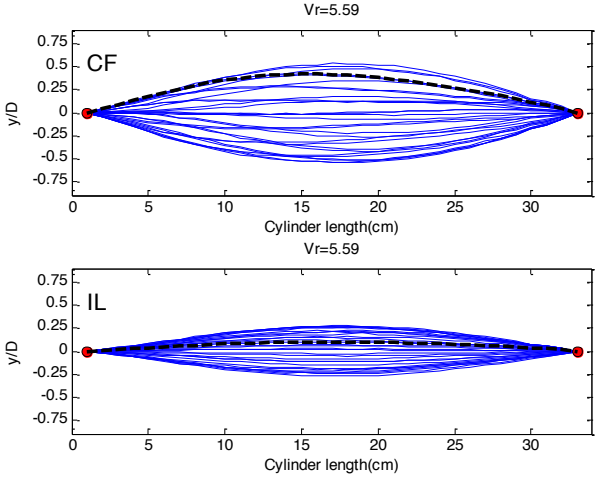

Figure B.1. 7 Response Snapshot at Vr=5.59 in CF and IL

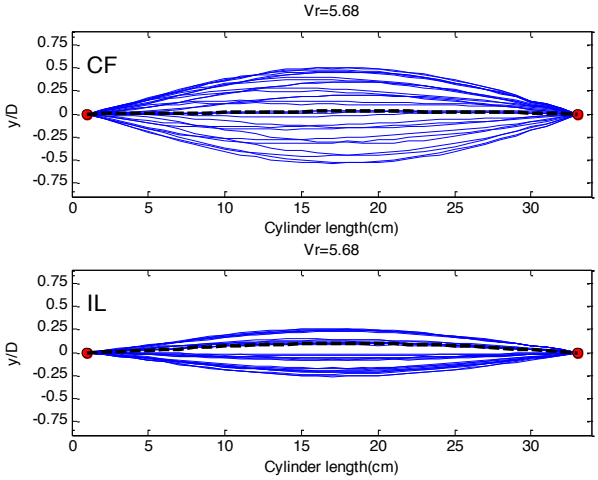

Figure B.1. 8 Response Snapshot at Vr=5.68 in CF and IL

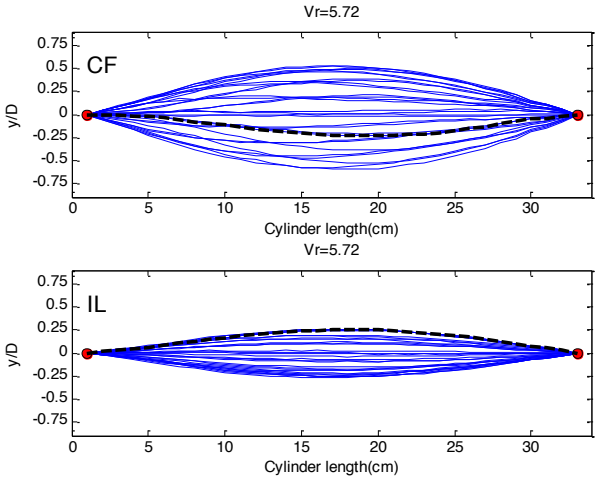

Figure B.1. 9 Response Snapshot at Vr=5.72 in CF and IL

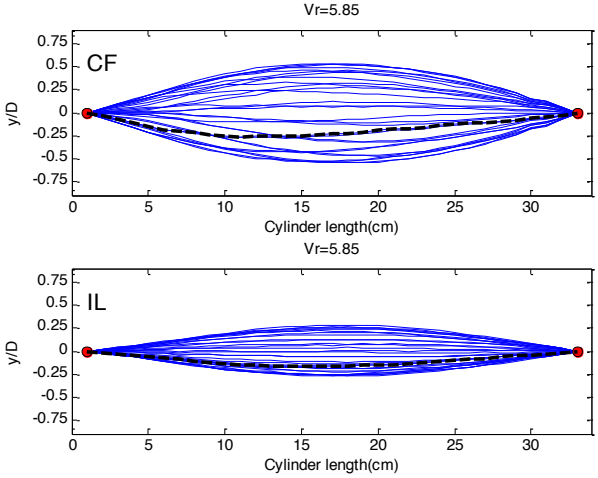

Figure B.1. 10 Response Snapshot at Vr=5.85 in CF and IL

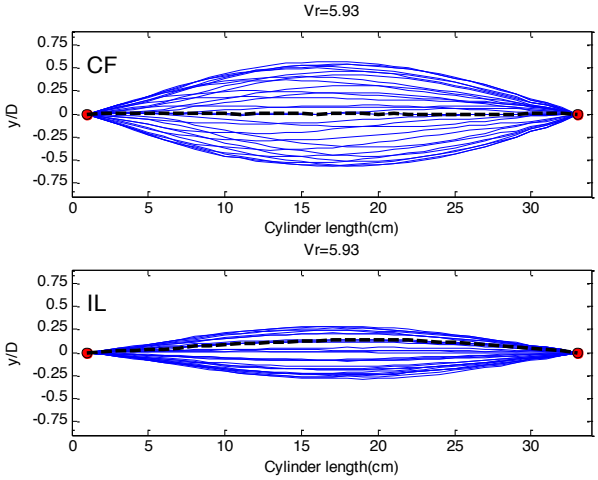

Figure B.1. 11 Response Snapshot at Vr=5.93 in CF and IL

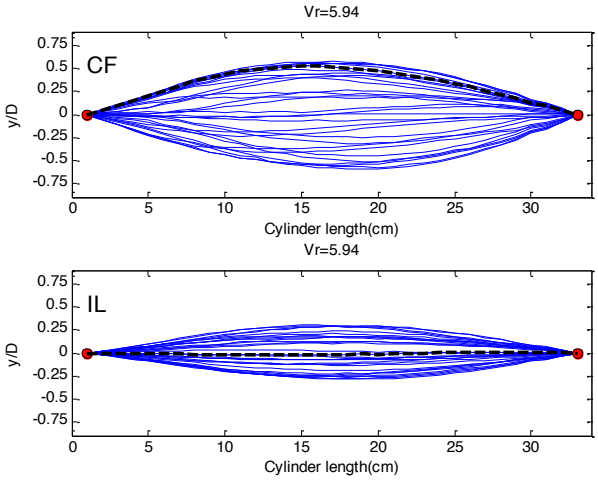

Figure B.1. 12 Response Snapshot at Vr=5.94 in CF and IL

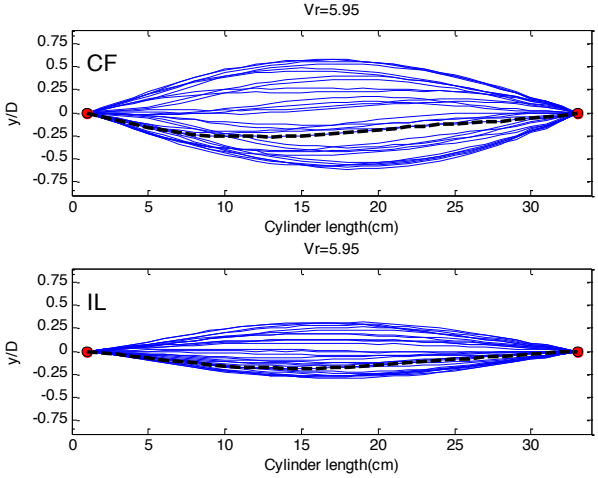

Figure B.1. 13 Response Snapshot at Vr=5.95 in CF and IL

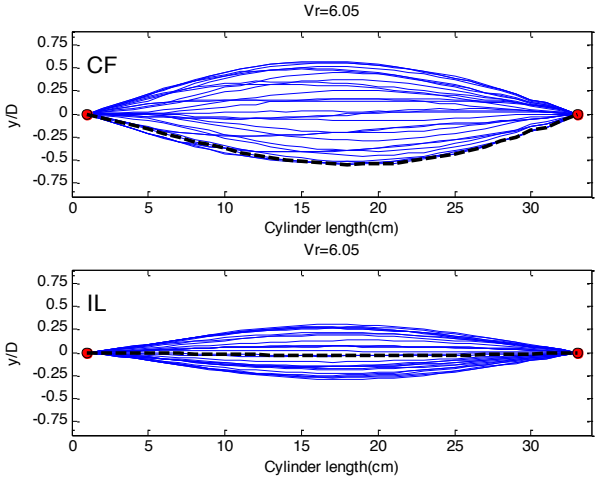

Figure B.1. 14 Response Snapshot at Vr=6.05 in CF and IL

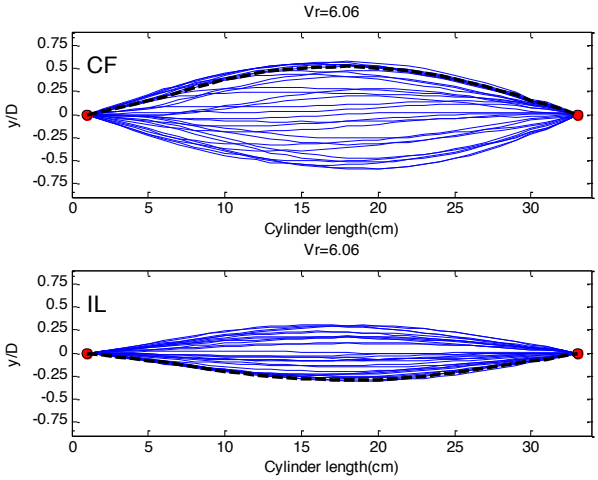

Figure B.1. 15 Response Snapshot at Vr=6.06 in CF and IL

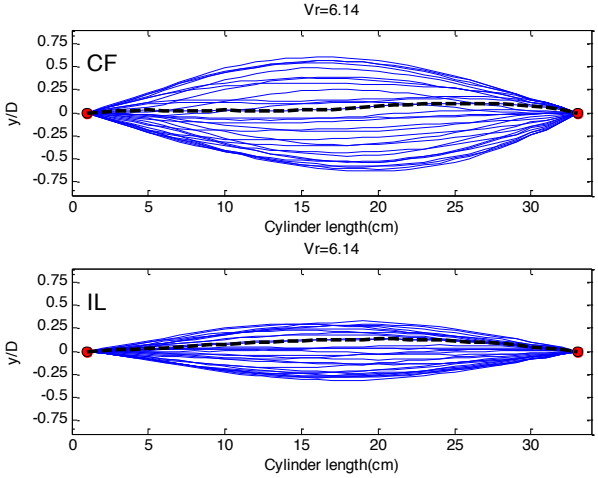

Figure B.1. 16 Response Snapshot at Vr=6.14 in CF and IL

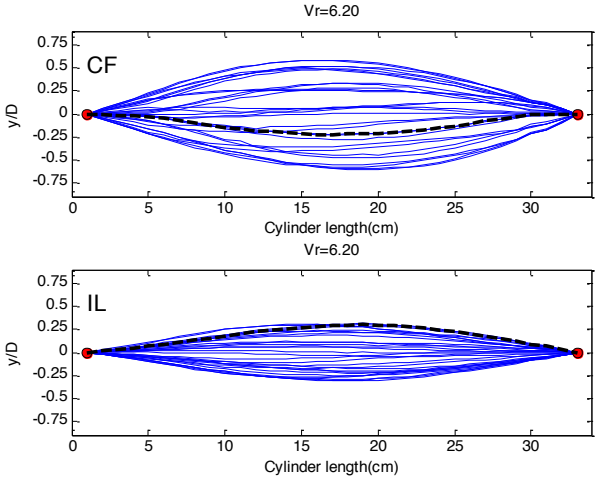

Figure B.1. 17 Response Snapshot at Vr=6.20 in CF and IL

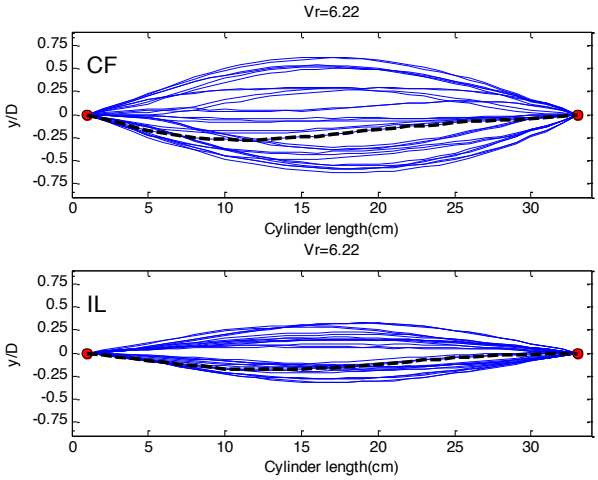

Figure B.1. 18 Response Snapshot at Vr=6.22 in CF and IL

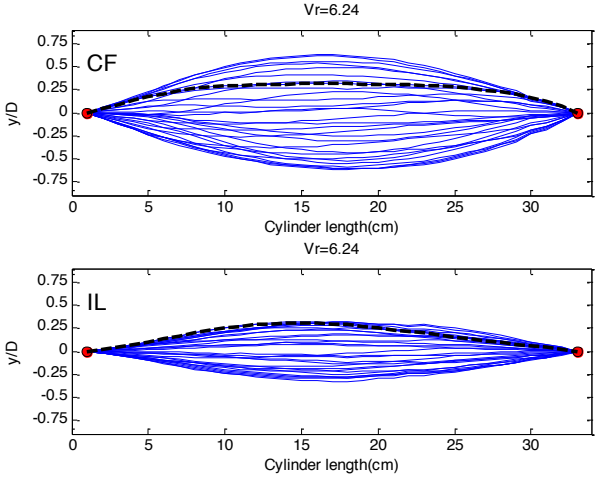

Figure B.1. 19 Response Snapshot at Vr=6.24 in CF and IL

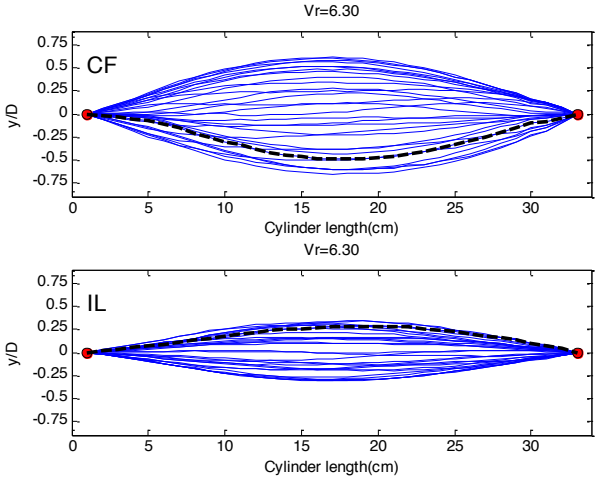

Figure B.1. 20 Response Snapshot at Vr=6.30 in CF and IL

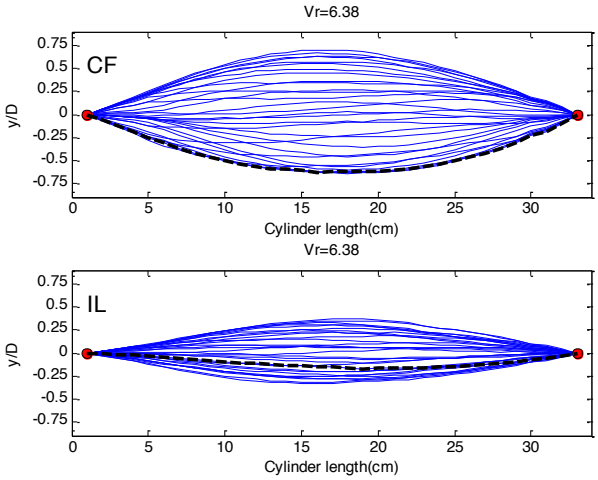

Figure B.1. 21 Response Snapshot at Vr=6.38 in CF and IL

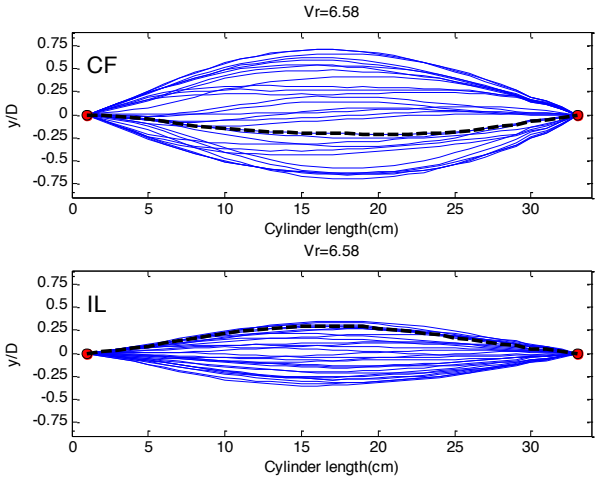

Figure B.1. 22 Response Snapshot at Vr=6.58 in CF and IL

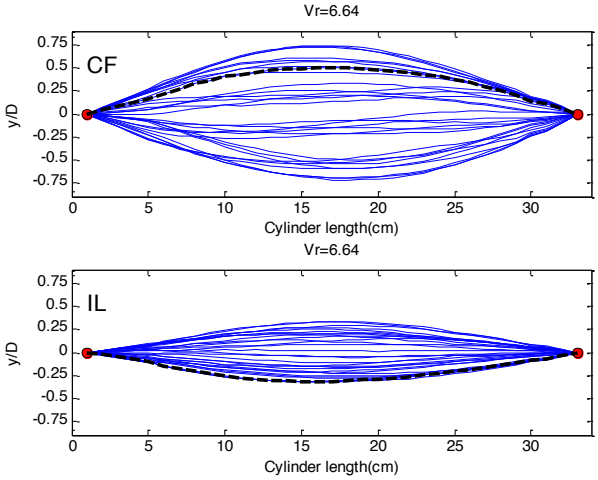

Figure B.1. 23 Response Snapshot at Vr=6.64 in CF and IL

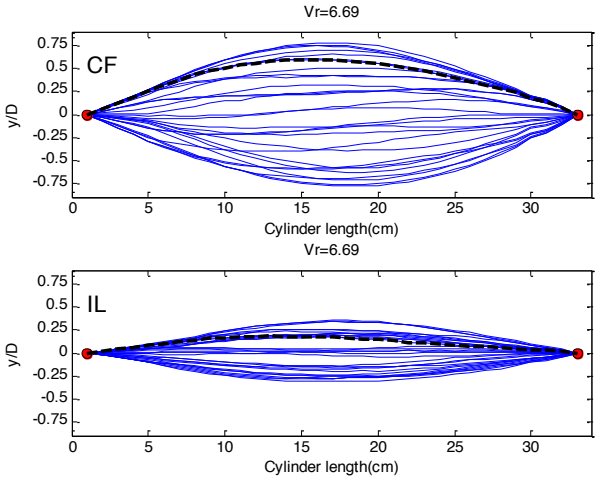

Figure B.1. 24 Response Snapshot at Vr=6.69 in CF and IL

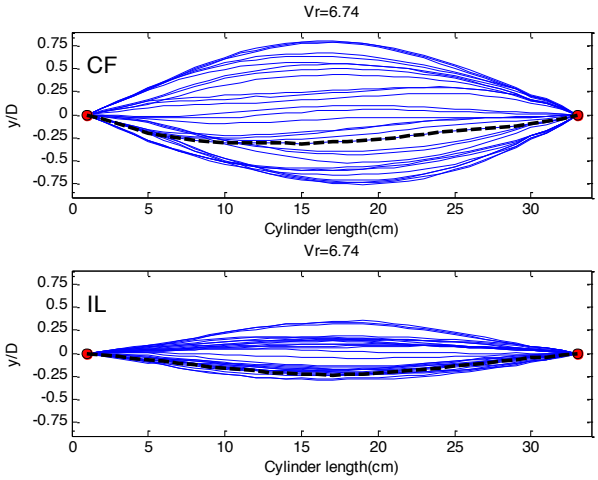

Figure B.1. 25 Response Snapshot at Vr=6.74 in CF and IL

B.2 Cylinder 2 Response Snapshots

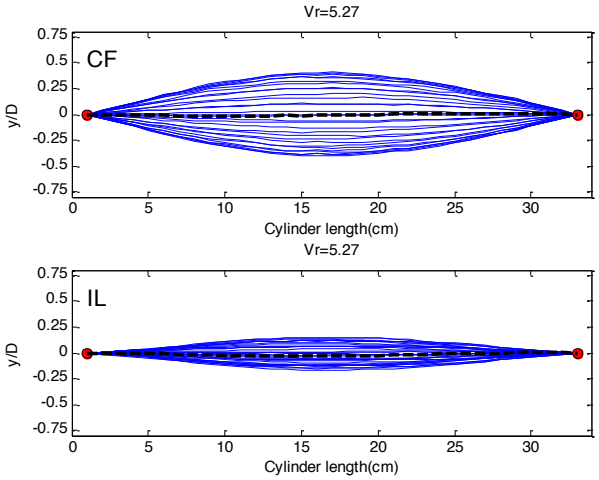

Figure B.2. 1 Response Snapshot at Vr=5.27 in CF and IL

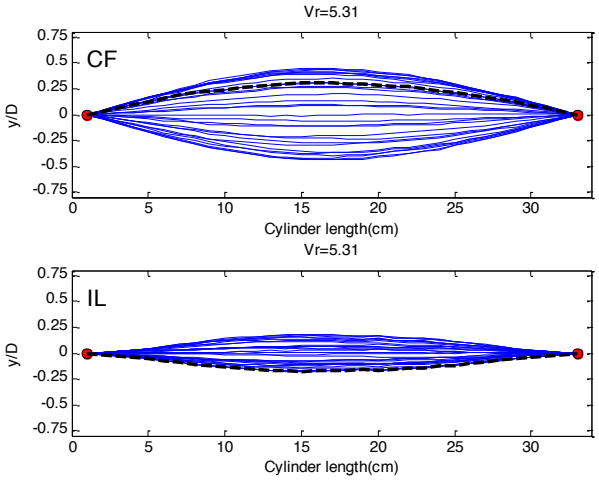

Figure B.2. 2 Response Snapshot at Vr=5.31 in CF and IL

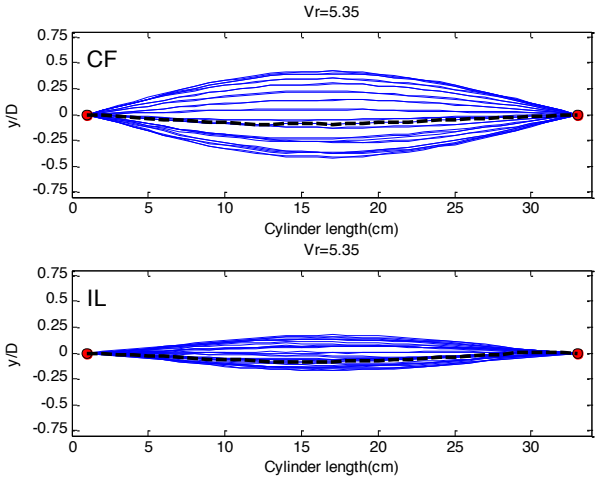

Figure B.2. 3 Response Snapshot at Vr=5.35 in CF and IL

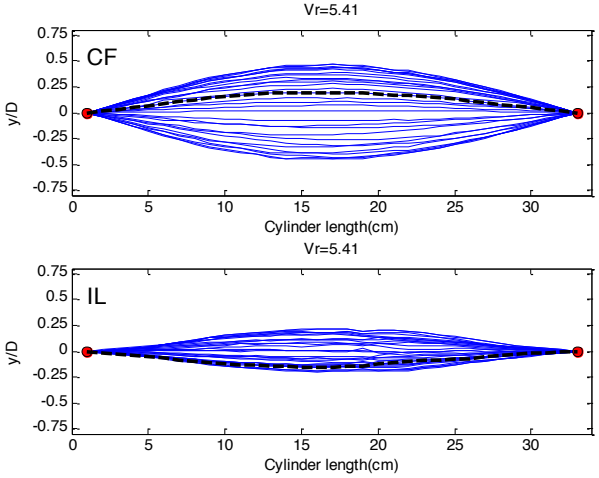

Figure B.2. 4 Response Snapshot at Vr=5.41 in CF and IL

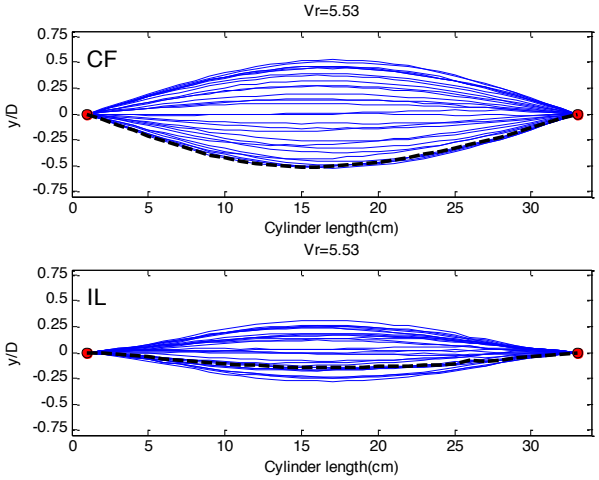

Figure B.2. 5 Response Snapshot at Vr=5.53 in CF and IL

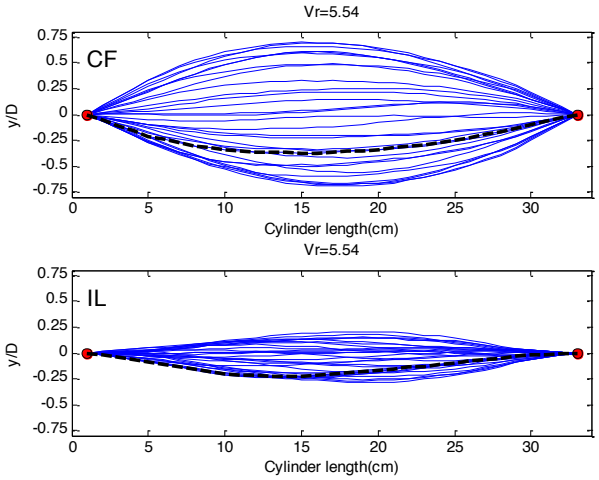

Figure B.2. 6 Response Snapshot at Vr=5.54 in CF and IL

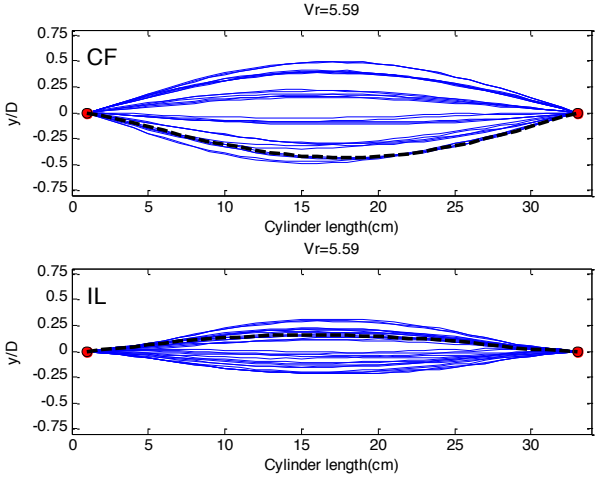

Figure B.2. 7 Response Snapshot at Vr=5.59 in CF and IL

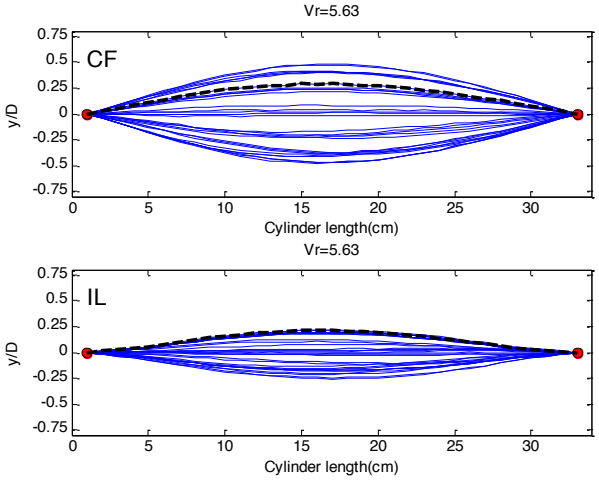

Figure B.2. 8 Response Snapshot at Vr=5.63 in CF and IL

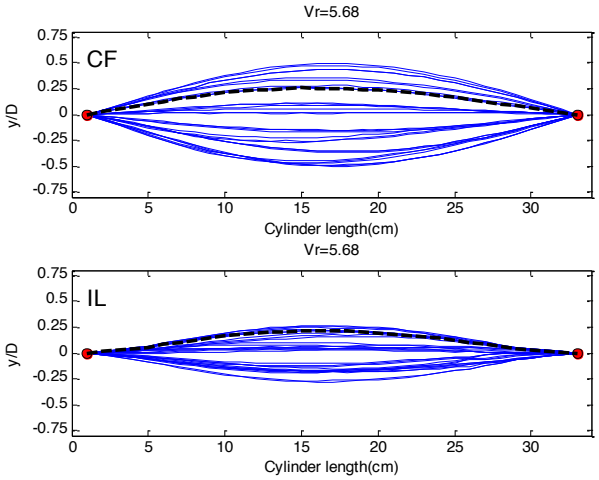

Figure B.2. 9 Response Snapshot at Vr=5.68 in CF and IL

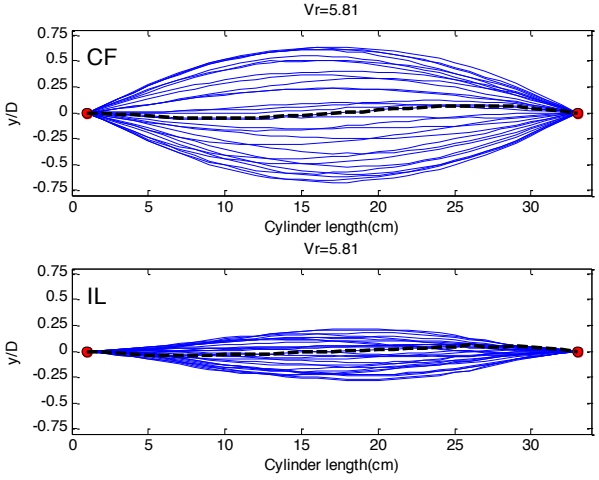

Figure B.2. 10 Response Snapshot at Vr=5.81 in CF and IL

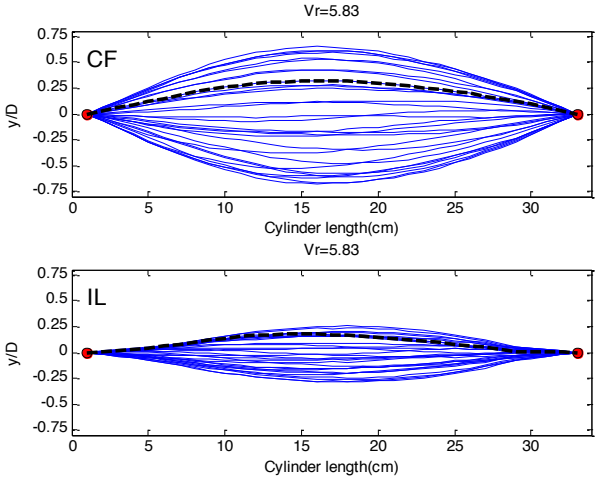

Figure B.2. 11 Response Snapshot at Vr=5.83 in CF and IL

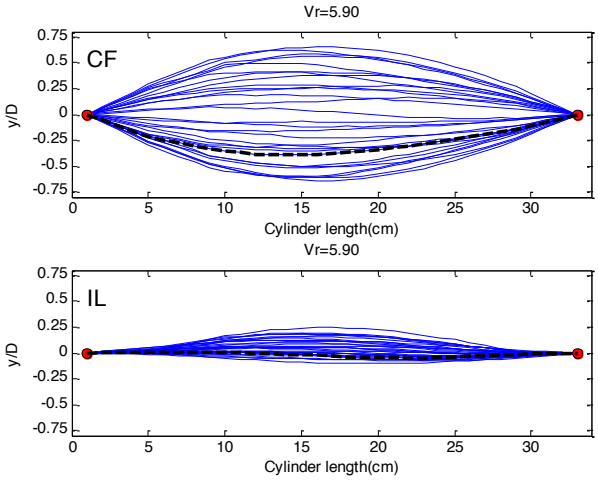

Figure B.2. 12 Response Snapshot at Vr=5.90 in CF and IL

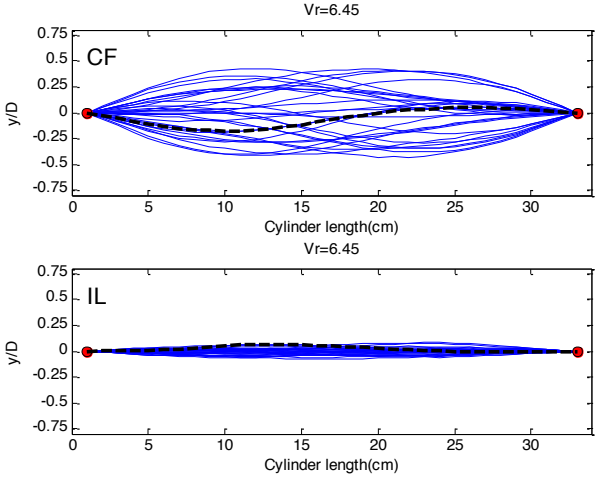

Figure B.2. 13 Response Snapshot at Vr=6.45 in CF and IL

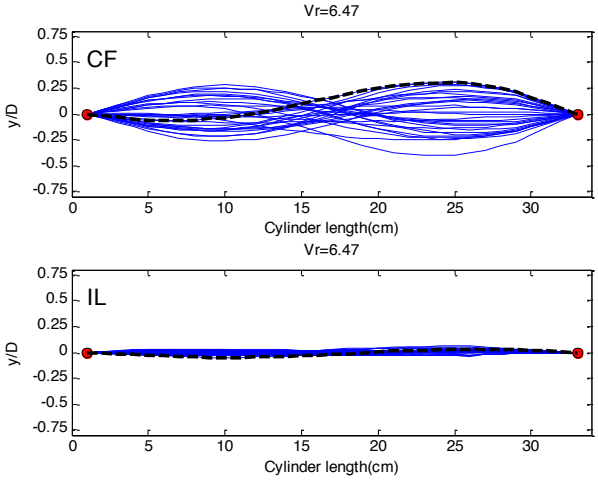

Figure B.2. 14 Response Snapshot at Vr=6.47 in CF and IL

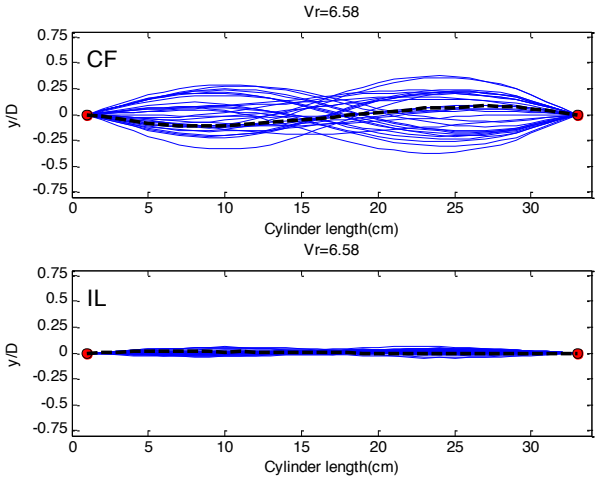

Figure B.2. 15 Response Snapshot at Vr=6.58 in CF and IL

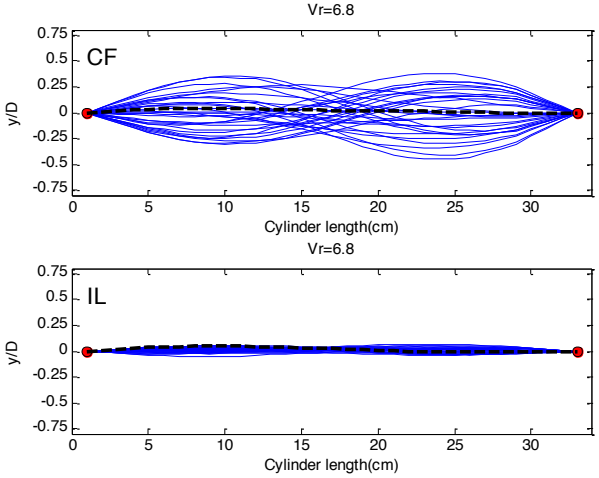

Figure B.2. 16 Response Snapshot at Vr=6.8 in CF and IL

B.3 Cylinder 3 Response Snapshots

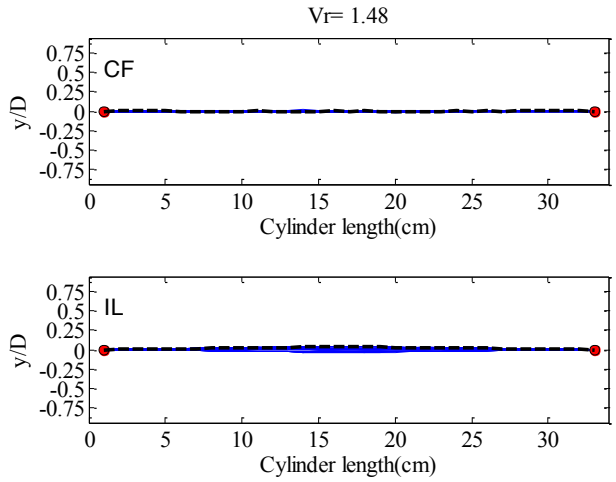

Figure B.3. 1 Response Snapshot at Vr=1.48 in CF and IL

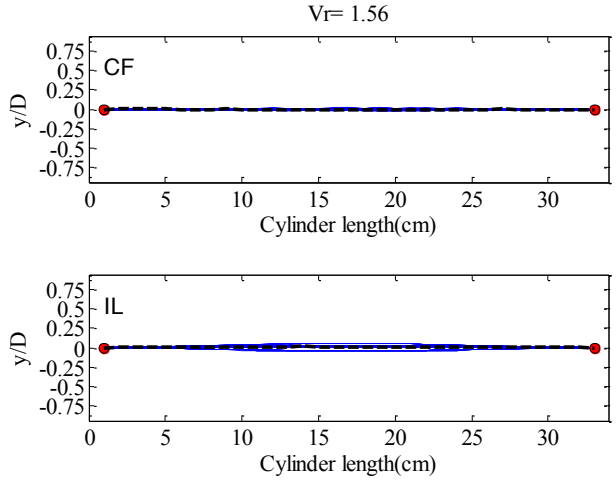

Figure B.3. 2 Response Snapshot at Vr=1.56 in CF and IL

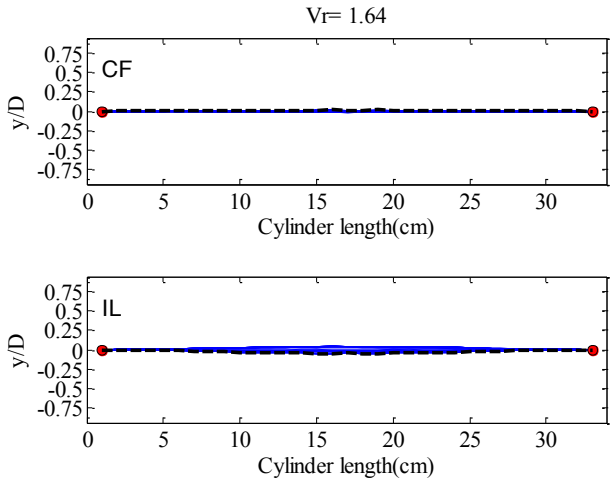

Figure B.3. 3 Response Snapshot at Vr=1.64 in CF and IL

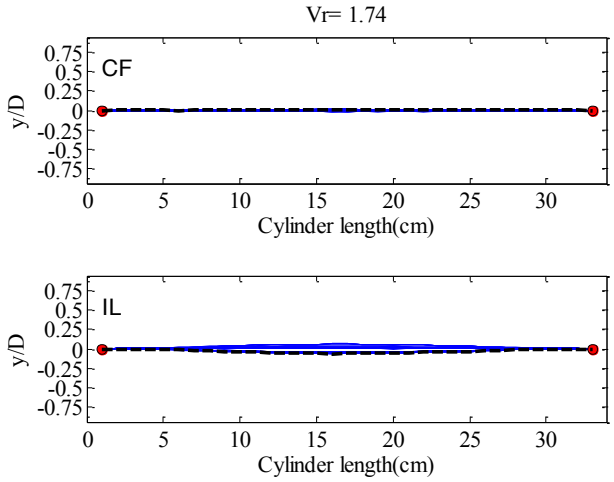

Figure B.3. 4 Response Snapshot at Vr=1.74 in CF and IL

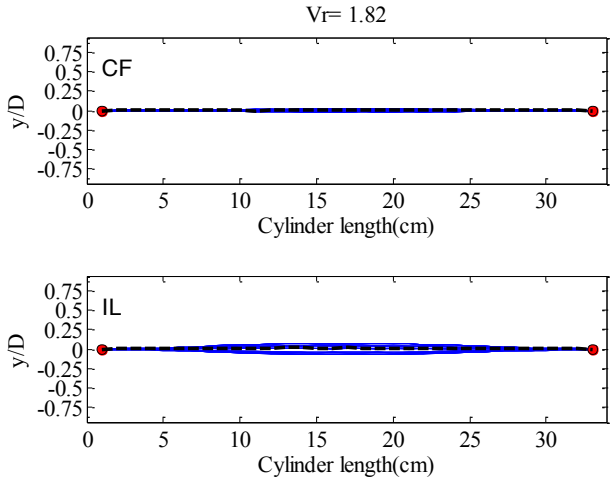

Figure B.3. 5 Response Snapshot at Vr=1.82 in CF and IL

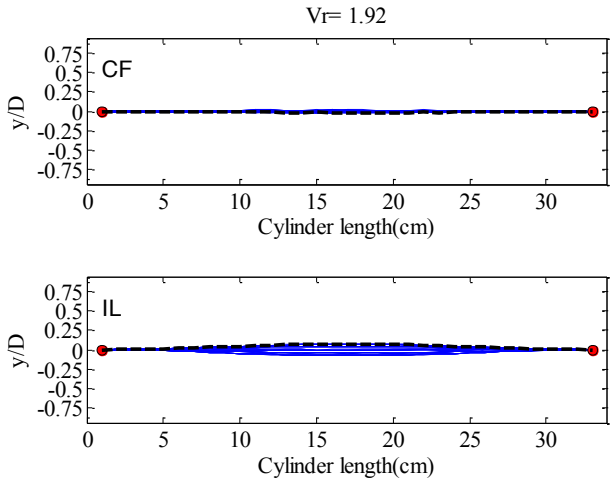

Figure B.3. 6 Response Snapshot at Vr=1.92 in CF and IL

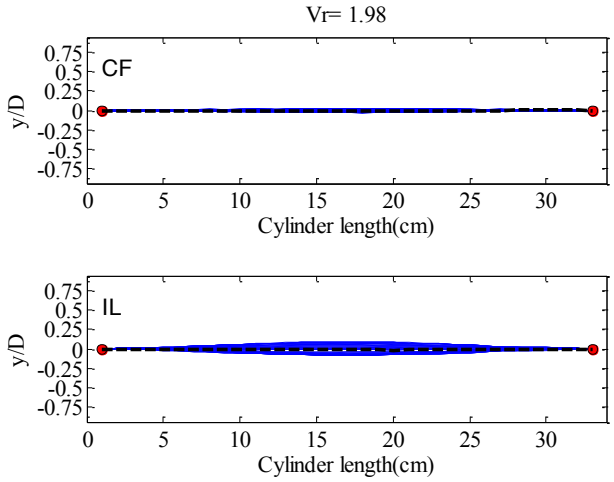

Figure B.3. 7 Response Snapshot at Vr=1.98 in CF and IL

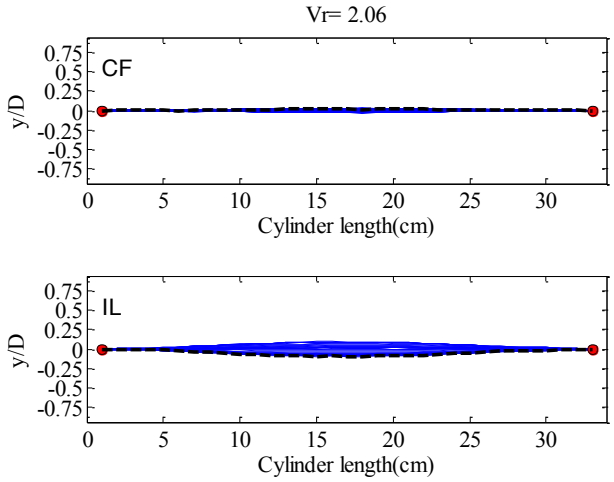

Figure B.3. 8 Response Snapshot at Vr=2.06 in CF and IL

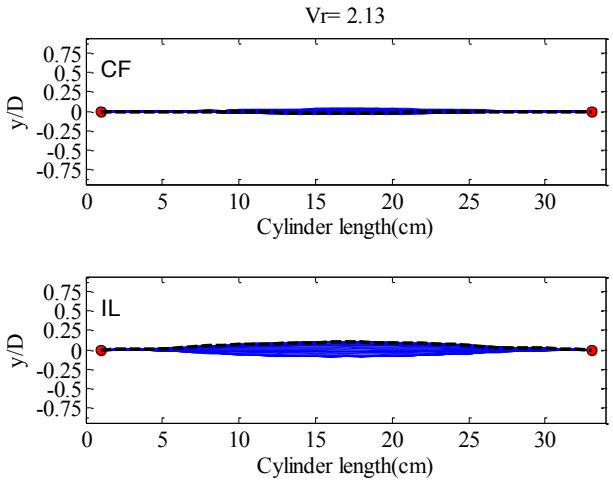

Figure B.3. 9 Response Snapshot at Vr=2.13 in CF and IL

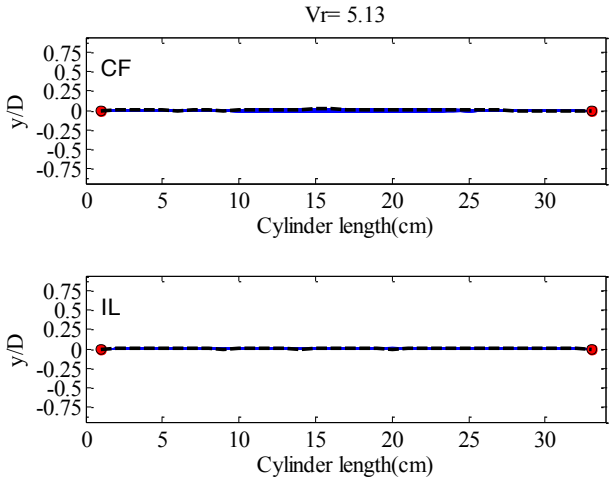

Figure B.3. 10 Response Snapshot at Vr=5.13 in CF and IL

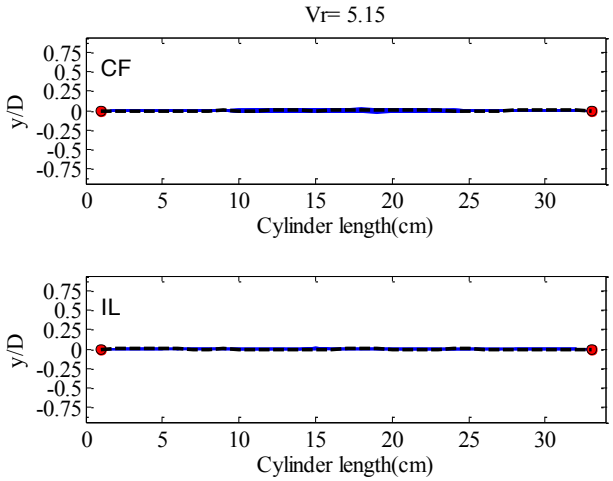

Figure B.3. 11 Response Snapshot at Vr=5.15 in CF and IL

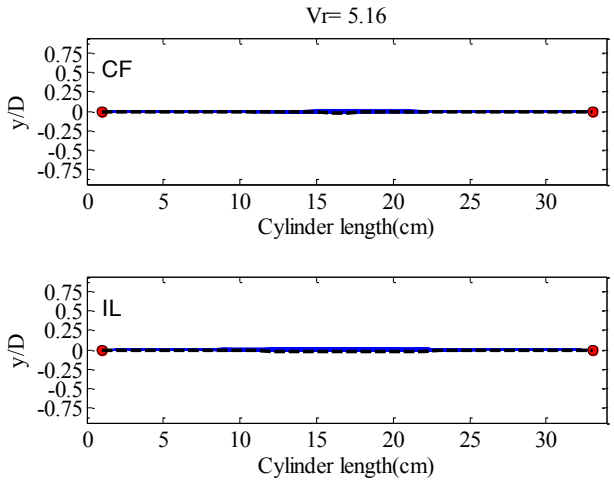

Figure B.3. 12 Response Snapshot at Vr=5.16 in CF and IL

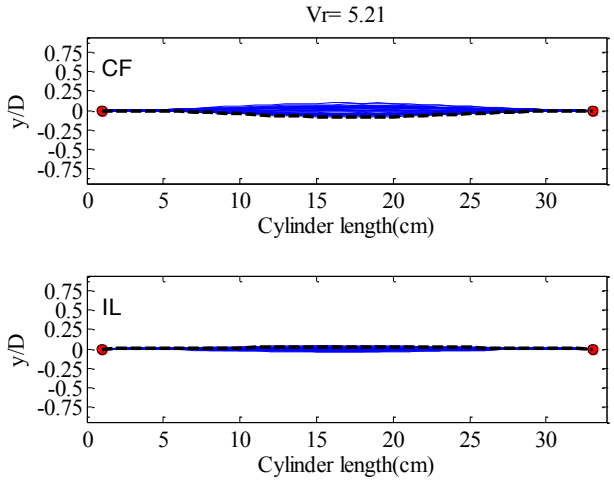

Figure B.3. 13 Response Snapshot at Vr=5.21 in CF and IL

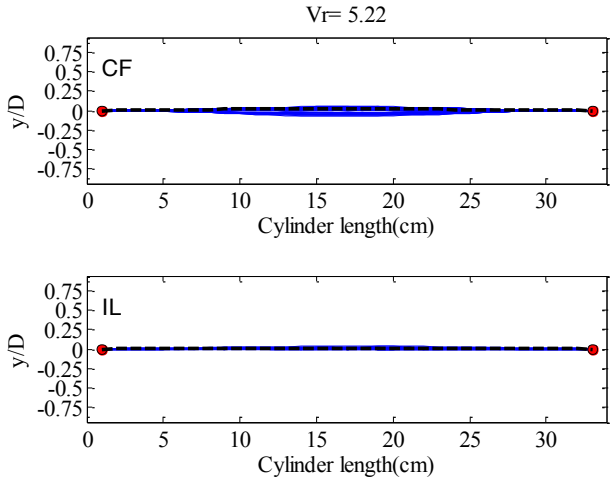

Figure B.3. 14 Response Snapshot at Vr=5.22 in CF and IL

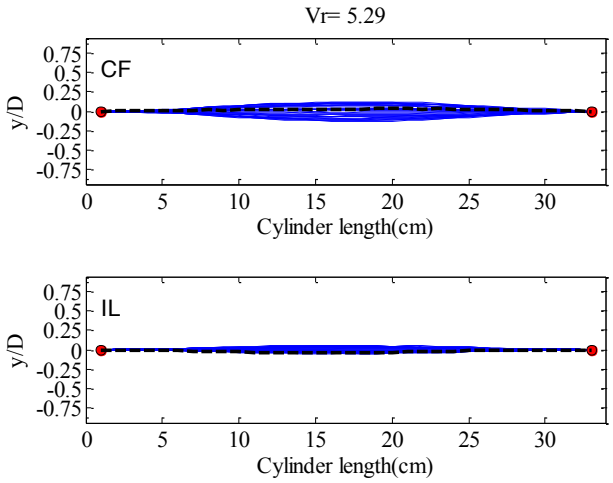

Figure B.3. 15 Response Snapshot at Vr=5.29 in CF and IL

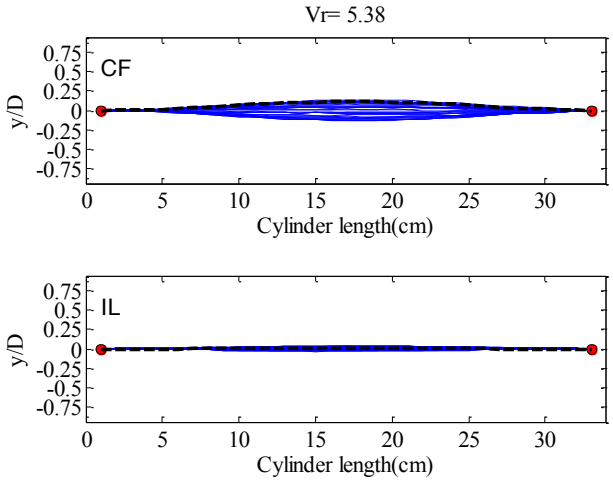

Figure B.3. 16 Response Snapshot at Vr=5.38 in CF and IL

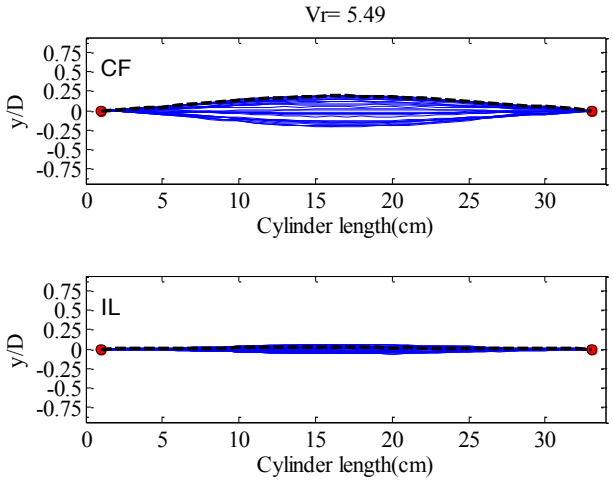

Figure B.3. 17 Response Snapshot at Vr=5.49 in CF and IL

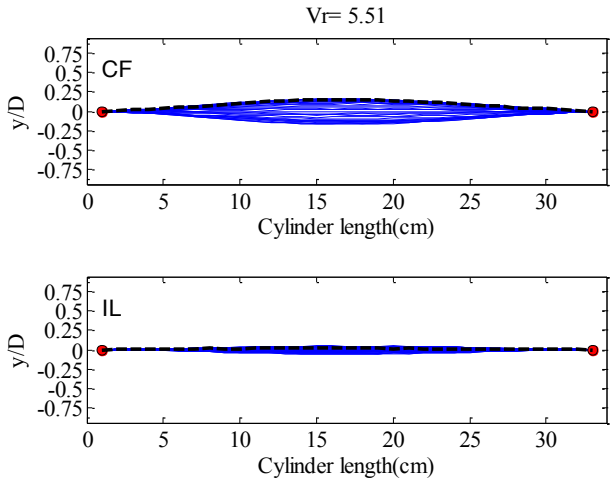

Figure B.3. 18 Response Snapshot at Vr=5.51 in CF and IL

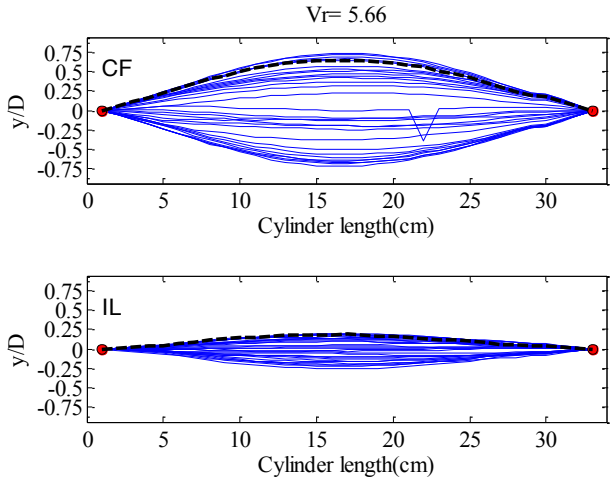

Figure B.3. 19 Response Snapshot at Vr=5.66 in CF and IL

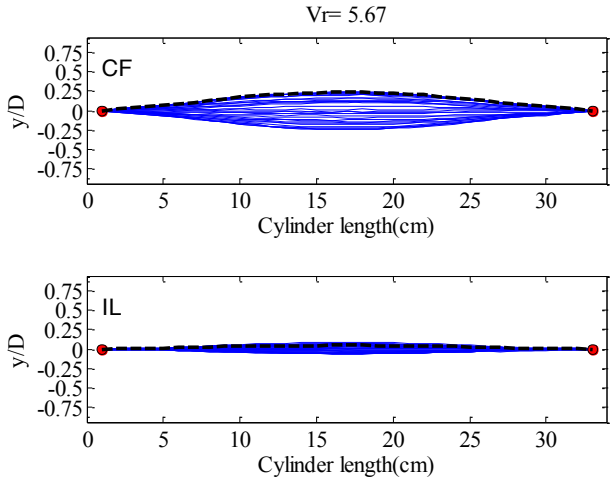

Figure B.3. 20 Response Snapshot at Vr=5.67 in CF and IL

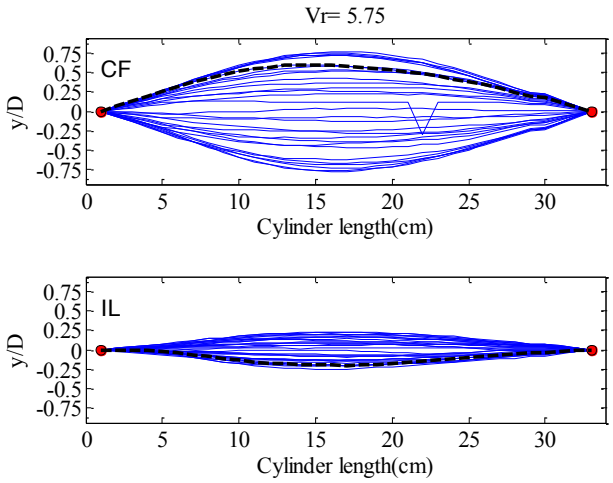

Figure B.3. 21 Response Snapshot at Vr=5.75 in CF and IL

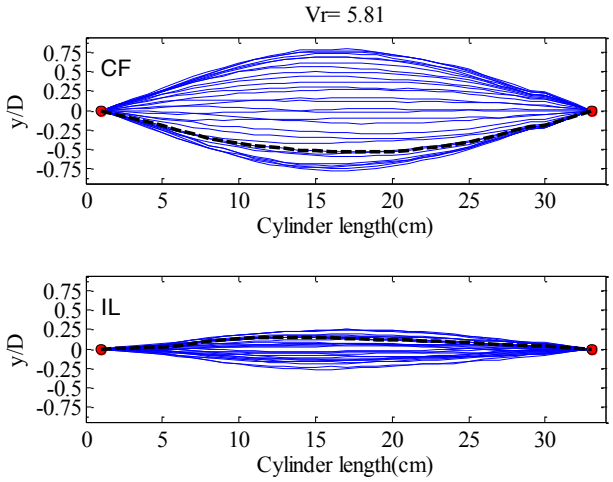

Figure B.3. 22 Response Snapshot at Vr=5.81 in CF and IL

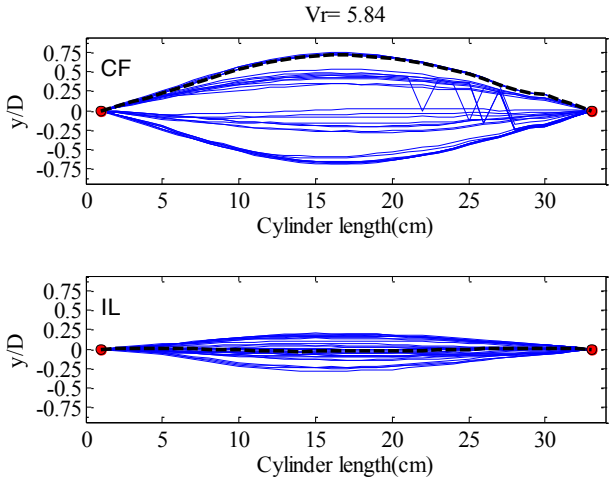

Figure B.3. 23 Response Snapshot at Vr=5.84 in CF and IL

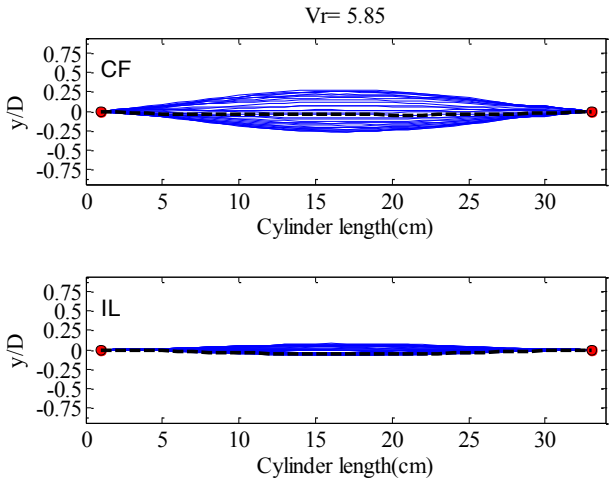

Figure B.3. 24 Response Snapshot at Vr=5.85 in CF and IL

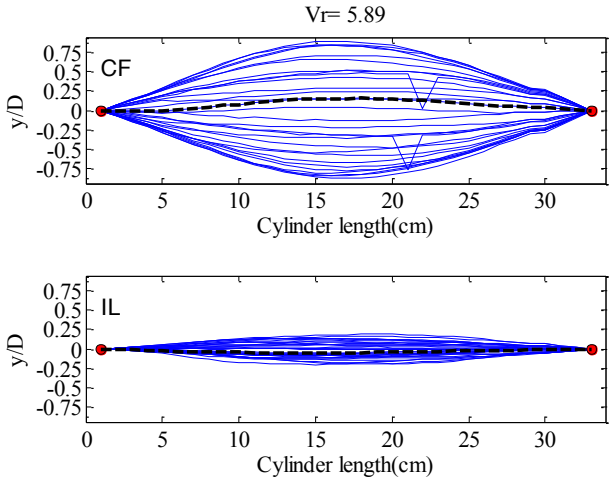

Figure B.3. 25 Response Snapshot at Vr=5.89 in CF and IL

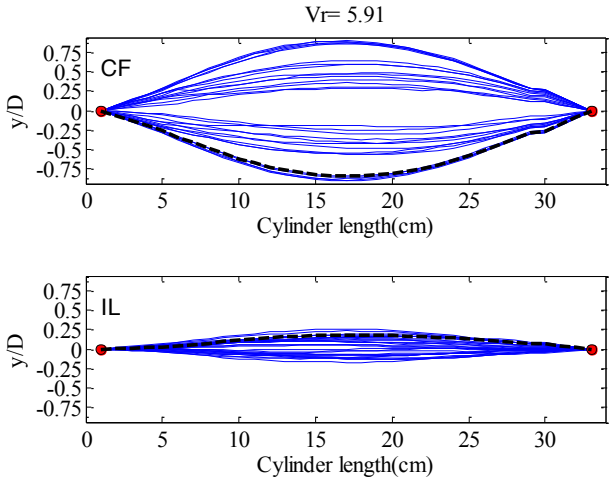

Figure B.3. 26 Response Snapshot at Vr=5.91 in CF and IL

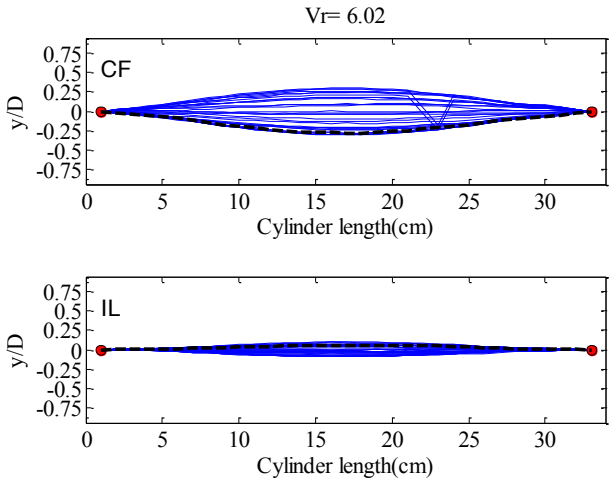

Figure B.3. 27 Response Snapshot at Vr=6.02 in CF and IL

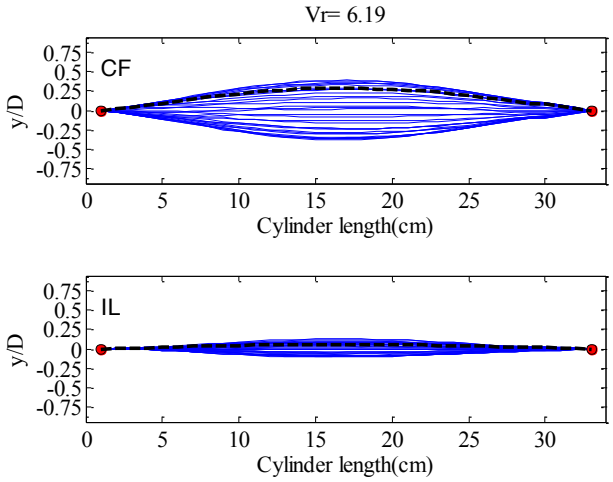

Figure B.3. 28 Response Snapshot at Vr=6.19 in CF and IL

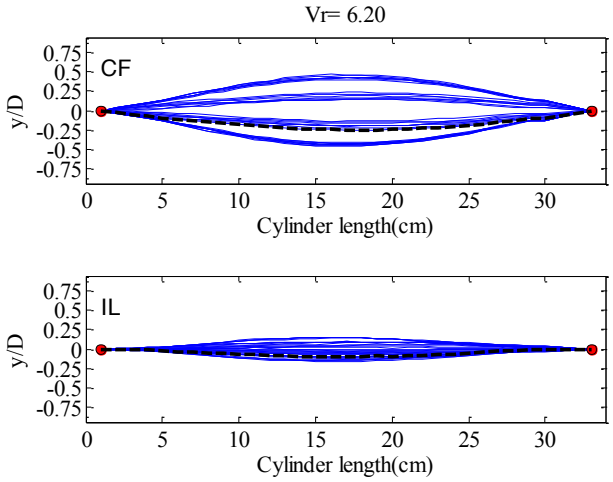

Figure B.3. 29 Response Snapshot at Vr=6.20 in CF and IL

BIBLIOGRAPHY

Achenbach, R., and Heinecke, E., (1981) "On vortex shedding from smooth and rough cylinders in the range of Reynolds numbers 6 x 103 to 5 x 106," *Journal of Fluid Mechanics,* 109, pp: 239-251.

Bearman, P.W. (2011). Circular cylinder wakes and vortex-induced vibrations. Journal of Fluids and Structures, 27:648-658.

Boashash, B., (2003) "Time frequency signal analysis and processing: A comprehensive reference", 1st edn. Elsevier

Chaplin, J.R., Bearman, P.W., Huera-Huerta, F.J., Pattenden, R., (2005) "Laboratory measurements of vortex-induced vibrations of a vertical tension riser in a stepped current," *Journal of Fluids and Structures,* 21(1), pp: 3-24

Dahl, J. M., (2008) "Vortex-induced vibration of a circular cylinder with combined in-line and cross-flow motion," Ph.D. dissertation, Massachusetts Institute of Technology

Dahl, J.M., Hover, F.S., and Triantafyllou, M.S. (2006) "Two-degree-of-freedom vortex-induced vibrations using force assisted apparatus." *Journal of Fluids and Structures*, 22:807-818.

Dahl, J.M., Hover, F.S., Triantafyllou, M.S., Dong, S., Karniadakis, G.E., "Resonant vibrations of bluff bodies cause multivortex shedding and high frequency forces." *Physical Review Letters*, vol.99, n 14, 2007, article 144503.

Dahl, J.M., Hover F.S., and Triantafyllou M.S., (2008) "High Harmonic Forces and Predicted Vibrations from Forced In-line and Cross-flow Cylinder Motions."

Proceedings of the Eighteenth (2008) International Offshore and Polar Engineering Conference, Vancouver, BC, Canada

Dahl, J.M., Hover, F.S., Triantafyllou, M.S., and Oakley, O.H. (2010). Dual resonance in vortex-induced vibrations at subcritical and supercritical Reynolds numbers. *Journal of Fluid Mechanics*, vol. 643, p 395-424.

Green, S.I., (1995) "Fluid Vortices," *Fluid Mechanics and Its Applications*, Vol.30.

Hammache, M. and Gharib, M., (1991)"An experimental study of the parallel and oblique vortex shedding from circular cylinders," *Journal of Fluid Mechanics*, 232, pp: 567:590.

Huera-Huarte, F.J., Bangash, Z.A., Gonzales, L.M. (2014) "Towing tank experiments on the vortex-induced vibrations of low mass ratio long flexible cylinders," *Journal of Fluids and Structures*, Volume 48, pp: 81-92.

Jauvtis, N., and Williamson, C.H.K. (2004). "The effect of two degrees of freedom on vortex-induced vibration at low mass and damping." *Journal of Fluid Mechanics*, 509:23-62.

Kang, Z., Jia, L. (2013). "An experiment study of a cylinder`s two degree of freedom VIV trajectories." *Journal of Ocean Engineering*, 70:129-140.

LaVision. (2013) *"DaVis Flowmaster Software Manual*." LaVision GmbH, Goettingen, Germany.

LaVision. (2013) "*DaVis 8.2 Software Manual*." LaVision GmbH, Goettingen, Germany.

Lie, H., Kaasen, K.E. (2006) "Modal analysis from a large-scale viv model test of a riser in linearly sheared flow," *Journal of Fluids and Structures*, 22, pp: 557,575.

Lienhard, J.H. (1966) "Synopsis of Lift, Drag and Vortex Frequency Data for Rigid Circular Cylinders." *Research Division Bulletin 300*, Washington State University, College of Engineering

Marcollo, H., Eassom, A., Fontaine, E., Tognarelli, M., Beynet, P., Constantinides, Y., and Oakley, O.H. (2011). "Traveling wave response in full-scale drilling riser VIV measurements." *Proceedings of the ASME 2011 30th International Conference on Ocean, Offshore and Arctic Engineering*. Rotterdam, The Netherlands.

Modarres-Sadeghi, Y., Chasparis, F., Triantafyllou, M.S., Tognarelli, M., and Beynet, P. (2011). "Chaotic response is a generic feauture of vortex-induced vibrations of flexible risers." *Journal of Sound and Vibration*, vol.220, pp. 2565-2579.

Moe, G., and Wu, Z.-J. (1990). "The left force on a cylinder vibrating in a current." *ASME Journal of Offshore Mechanics and Arctic Engineering,* vol. 112, pp. 297-303.

Morse, T.L., Williamson, C.H.K. (2009) "Fluid forcing, wake modes, and transitions for a cylinder undergoing controlled oscillations." *Journal of Fluids and Structures*, pp. 697:712.

Mukundan, H., (2008) "Vortex-Induced Vibration of Marine Risers: Motion and Force Reconstruction from Field and Experimental Data," Ph.D. dissertation, Massachusetts Institute of Technology.

Newman, J.N. (1977). "Marine Hydrodynamics." The MIT Press, Cambridge, M.A.

Passano, E., Larsen, C.M., and Wu J. (2010). "VIV of free spanning pipelines: Comparison of response from semi-empirical code to model tests." *Proceedings of the ASME 201029th International Conference on Ocean, Offshore and Arctic Engineering*. Shanghai, China.

ProAnalyst. (2006). "*ProAnalyst Motion Analysis Software User Guide*", Xcitex, Inc., Cambridge, Massachusetts, USA

Sarpkaya, T. (1979). "Vortex induced oscillations." *Journal of Applied Mechanics*, 46:241-258.

Sarpkaya, T. (1995). "Hydrodynamic damping, flow-induced oscillations, and biharmonic response," *ASME Journal of Offshore Mechanics and Arctic Engineering*, vol. 117, pp. 232-238

Sarpkaya, T. (2004). "A critical review of the intrinsic nature of vortex-induced vibrations." *Journal of Fluids and Structures*, 19:389-447.

Smogeli O. (2002). "Design and evaluation of a force-feedback control system for VIV experiments." NTNU and MIT.

Srinil, N., Zanganeh, H., Day, A. (2013). " Two-degree-of-freedom VIV of circular cylinder with variable natural frequency ratio: Experimental and numerical investigations," *Ocean Engineering*, 73, pp: 179:194

Trim, A.D., Braaten, H., Lie, H. and Tognarelli, M.A. (2005). "Experimental investigation of vortex-induced vibration of long marine risers." *Journal of Fluids and Structures*, 21:335-361.

Van Dyke, M. (2002). " An Album of Fluid Motions." *Parabolic Press*, Inc., Stanford, CA.

Vandiver, J.K., and Jong, J. -Y. (1987). "The relationship between in-line and cross-flow vortex-induced vibration of cylinders." *Journal of Fluids and Structures*, 1:381-399.

Vandiver, J.K., Marcollo, H., Swithenbank S., and Jhingran V. (2005). "High mode number vortex-induced vibration field experiments." *Offshore Technology Conference,* Paper Number 17383, Houston, Texas.

Williamson, C.H.K., and Roshko, A. (1988). "Vortex formation in the wake of an oscillating cylinder." *Journal of Fluids and Structures*, 2:355-381.

Williamson, C.H.K., and Govardhan, R. (2004). "Vortex-induced vibrations." *Annual Review of Fluid Mechanics*, 36:413-455.

Williamson, C.H.K., Govardhan, R. (2008). "A brief review of recent results in vortex-induced vibrations," *Journal of Wind Engineering*, pp: 713-735.